Collective phenomena in networks of spiking neurons with synaptic delays

Federico Devalle

TESI DOCTORAL UPF / 2019

DIRECTORS DE LA TESI:

Dr. Ernest Montbrió[1], Prof. Dr. Aneta Stefanovska[2],

[1]Department of Information and Communication Technologies, Universitat Pompeu Fabra, Spain
[2]Department of Physics, Lancaster University, United Kingdom

Acknowledgements

First and foremost, thank you so much Ernest. Your guidance and help along the way have been invaluable. Thank you so much for always dedicating your time to my doubts and questions, and for helping me developing ideas. For being very passionate about research, and showing me how to take the first steps in the scientific world. Thank you for having such an honest, friendly and direct relation to your students, I often had the feeling I was chatting with a friend more than with my supervisor. Thank you also for all the enriching discussions we had over lunch at Sopa.

Thank you Aneta and Peter for being kind and welcoming during my year in Lancaster. Thank you Aneta for the stimulating scientific discussions, and for giving me an original and different perspective on the research I was carrying out. Thank you Peter for your kindness and your constant will to help. Thank you also for your valuable advises while we were organizing the AMCOS conference.
My gratitude goes to the reviewer of this thesis, thank you very much for reading the dissertation and accepting evaluating this work.

I am thankful to Diego Pazó and Alex Roxin, for the fruitful collaborations of these years. Diego, thank you so much for you hospitality in Santander, every time I visited you always made me feel at home. Thank you for your help and patience discussing results and reading and correcting my drafts. Thank you also for giving me feedback on part of this thesis. Alex, thanks a lot for all the insightful scientific discussion, and for discussing science so clearly. Thank you also for raising interest in me in more modelling-oriented works.

Of course, a warm thanks goes to the whole COSMOS family. These three years have been a wonderful experience. Thanks to all the COSMOS PIs for their inspiring presence. A particular thanks to Arkady Pikovsky, Antonio Politi and Misha Rosenblum for the effort in organizing and coordinating the project. Antonio, thank you also for your hospitality in Aberdeen and for the fruitful discussions on synchronization and time delays. Ralph Andrzejak, thank you for your hospitality in the Nonlinear time series analysis group meetings and for you effort in helping the local Barcelona ESRs. Thank you Andreas Daffertshofer for the insightful scientific discussions. A special thanks is for Caroline, for your constant

efforts helping the whole COSMOS team.

Thanks to all the COSMOS students: since the first time we gathered in Florence I felt like we were going to be a family more than colleagues. Thank you Max and Basti for the great time we had in Lancaster, in and outside the University. My year there would have not been the same without you. Thanks also Basti for inviting me to your defense in Amsterdam.

Thank you Marc and Nico for being such good summer adventures companions! Marc, thanks also for being such a fun flatmate, and for your jokes. Most of all for showing me the coolest and hidden spots of Barcelona. Thanks Nico also for the amazing surfing holidays, and for the pool games and dinners at the Bobbin during my stay at Aberdeen.

Irene, a special thank you goes to you. From the very beginning, we have constantly helped each other in settling in Barcelona to start this phd adventure. Thank you for sharing all the better and worse moments of this journey, being always there ready to help and give a wise advise. Thank you for the many many many rehearsals of talks, poster presentations, and for bearing me under the stressfull pre-conference days :) You have been like a sister! Ma soprattutto, per vedere sempre il meglio delle persone, e per la tua costante voglia di cambiare in positivo le cose.

Ola, thank you for your creativity and your positive energy. And for always trying to involve me in outdoor activities! ;) Thank you also for proofreading part of this thesis.

Txema and David, thank you so much for welcoming me at the UPF in our small but very united group. My first year in Barcelona I immediately felt at home, and this is thank to you! Your honest and true friendship helped a lot. Txema, thank you very much also for all the coding tricks you taught me, and for all the help you gave me formatting this thesis. You are the definition of what it means to be a good person.

A big hug and thanks go to all the friends and colleagues I have met in these years in Barcelona. Thank you to the NTSA group for creating such a nice office atmosphere: Petroula, Giulia, Cristina, Minia, Irene, Marc, Angela.
Petroula, thank you for your help settling down my first days in Barcelona.
Giulia and Marc, thanks for all the fun coffee breaks.
Thank you Mario for coming in in the office the very first week of work to welcome me, and make me feel at home.
Elena and Akke, thank you for the amazing trip to Cadaques and for all the parties we enjoyed together.

Thanks Kosta for your friendship and calm presence.

Thanks to my officemates and friends from the Ciutadella campus. Thanks Ane, Manel, Konstantina, David Blair, and Marc. You made me feel very welcomed after coming back from Lancaster.
Manel, thank you for your free and joyful spirit.
Laura, thanks for your smiles and for being always positive.
Vicente, thank you for being so much fun, and for sharing with me the (stressful) last days before the deposit of this thesis. Your whatsapp audios have helped a lot! :)
Thanks also to all people in Gustavo's group, Josephina, Andrea, Victor, Matthieu, Jessica, Gorka, Vaish, Sophie, and everyone else for the nice lab atmosphere. And to Gustavo himself, for coordinating the group!

Thanks to all my Lancaster's friends and colleagues. Thanks to Ticci, Will, Vamsi, Ola, Max, Basti, Gemma, Miro, Yunus, Mattheus, Jakub, for the joyful uni atmosphere.
Thanks to Liviana, Silvia, Pietro, Giulia, Dani, Jean, Angelo, Venusia, Cristina, for all the fun BBQs and nights out in Lancaster, it has been so much fun.

Grazie ai FIsici Che Attraggono, Gio, Calde, Luca, Gare e Torre, per le rimpatriate a Barcellona e i ritrovi a Torino. Grazie a Vale, che mi ha aiutato a prendere la decisione di iniziare questo dottorato.
Grazie a tutta la mia famiglia per avermi sempre supportato in tutte le mie scelte. Grazie mamma e papà, per essere sempre presenti, e aiutarmi e capirmi sempre. Grazie nonno per avermi insegnato tanto.
Y sobre todo a ti, Luci, por todo lo que eres, por toda la ayuda que me has dado y me das, por acompañarme en la parte mas dificil de este viaje, y por todos los que vendran.

This project has received funding from the European Union's Horizon 2020 research and innovation programme under the Marie Sklodowska-Curie grant agreement No 642563.

Abstract

A prominent feature of the dynamics of large neuronal networks are the synchrony-driven collective oscillations generated by the interplay between synaptic coupling and synaptic delays. This thesis investigates the emergence of delay-induced oscillations in networks of heterogeneous spiking neurons. Building on recent theoretical advances in exact mean field reductions for neuronal networks, this work explores the dynamics and bifurcations of an exact firing rate model with various forms of synaptic delays. In parallel, the results obtained using the novel firing rate model are compared with extensive numerical simulations of large networks of spiking neurons, which confirm the existence of numerous synchrony-based oscillatory states. Some of these states are novel and display complex forms of partial synchronization and collective chaos. Given the well-known limitation of traditional firing rate models to describe synchrony-based oscillations, previous studies greatly overlooked many of the oscillatory states found here. Therefore, this thesis provides a unique exploration of the oscillatory scenarios found in neuronal networks due to the presence of delays, and may substantially extend the mathematical tools available for modeling the plethora of oscillations detected in electrical recordings of brain activity.

Keywords: mathematical neuroscience, oscillations, synaptic kinetics, time delays, synchronization, neural population, firing rate, population model, spiking neurons, quadratic integrate-and-fire, coupled oscillators, mean-field, Wilson-Cowan model.

Resum

Una característica fonamental de la dinàmica d'una xarxa neuronal és l'emergència d'oscil·lacions degudes a sincronització. L'origen d'aquestes oscil·lacions és molt sovint degut les interaccions sinàptiques i als seus retards temporals inherents. Aquesta tesi analitza la emergència d'oscil·lacions produïdes per retards sinàptics en xarxes neuronals heterogènies. A partir de troballes recents en teories de camp mig per xarxes neuronals, aquest treball explora la dinàmica i les bifurcacions d'un model de *rate* amb diferents tipus de retards sinàptics. En paral·lel els resultats obtinguts mitjançant el nou model de rate són comparats amb simulacions numèriques de grans xarxes neuronals. Aquestes simulacions confirmen l'existència de nombrosos estats oscil·latoris produïts per sincronització. Alguns d'aquests estats són nous i mostren formes complexes de sincronització parcial i de caos col·lectiu. Gran part d'aquestes oscil·lacions han estat àmpliament ignorades a la literatura, degut a la limitació dels models tradicionals de rate per descriure estats amb un alt nivell de sincronització. Així doncs aquesta tesi ofereix una exploració única dels possibles escenaris oscil·latoris en xarxes neuronals amb retards sinàptics, i amplia significativament les eines matemàtiques disponibles per a la modelització de la gran diversitat d'oscil·lacions neuronals presents en les mesures elèctriques de l'activitat cerebral.

Contents

List of Figures

Introduction

The brain is a fascinating and intriguing functional structure, arguably the most complex organ of the human body. It drives our behavior and, at the same time, it regulates, controls and oversees the functioning of our body. The characterization of brain anatomical and physiological properties continually requires the joint effort of researchers from diverse fields of science.

The pioneering experiments of Santiago Ramon y Cajal in the late XIX century first identified the brain as a network of discrete unitary cells (the *neurons*), that interconnect among each other at clefts called synapses. Together with Camillo Golgi, who earlier developed the staining technique used in Cajal's experiments, Ramon y Cajal was awarded the Nobel prize in medicine in 1906. His discoveries established the fundamentals of the theory known as *Neuron doctrine*, which is still the base of modern neuroscience.

From a physiological standpoint, electricity was known to play a fundamental role in the functioning of the nervous system since Galvani's experiments on the sciatic nerve of frogs in the late XVIII century. Galvani's discovery of "animal electricity" lead later on to the discovery of the action potential, and to the conduction properties of the nervous system. The action potentials constitute the fundamental chunks of information that neurons exchange. These spike-like events coordinate the cooperative action of myriades of neurons, determining the substrate for the complex tasks that our brain needs to accomplish. Understanding the mechanisms of such complex and sophisticated machine continually

required the joint effort of experimental and theoretical research. Experimental evidence inspires new theories, that in turn help designing new experimental paradigms, on which theoretical predictions shall be tested. The cardinal tool employed in theoretical neuroscience is mathematical modeling. Mathematical models have been for centuries a key element of physical sciences, providing an invaluable tool for testing theories and make predictions about the behavior of a given physical system. An early attempt of building a neurophysiologically relevant mathematical model is attributed to Lapicque (Lapique, 1907). In the early XX century, Lapique built a simple phenomenological model of a neuron, now commonly known as integrate-and-fire neuron, to describe nerve excitation. A detailed comprehension and description of action potential generation, came in the mid XX century: in 1952, Hodgkin and Huxley published their studies on the conduction properties of the squid giant axon, presenting the first mathematical model accurately describing the physiological processes leading to action potential generation (Hodgkin and Huxley, 1952). The Hodgkin-Huxley model can still be considered the canonical model to describe single neurons dynamics. Although with different degrees of biophysical detail, the integrate-and-fire and the Hodgkin-Huxley model both describe single neurons dynamics.

In parallel, researchers developed a different type of descriptions, usually called firing rate models. Firing rate models are phenomenological descriptions of the collective, coarse-grained activity of large populations of neurons (Wilson and Cowan, 1972; Freeman, 1975). This type of description is particularly desirable in neuroscience. It is often hypothesized that brain function relies on population, rather than single neuron coding. A illuminating example comes from the visual system: feature-selective nearby neurons in the visual cortex often display similar coding properties (Hubel and Wiesel, 1963), suggesting the population coding hypothesis. Key for this type of modeling are the assumptions of relatively homogeneous neurons' properties (as e.g. similar feature tuning curves in the visual systems), and of some degree of redundancy in single neurons' coding.

Firing rate models have two main great advantages: thanks to their simplicity, they allow for mathematical analysis; additionally, they are computationally very efficient. For these reasons, they rapidly became a standard tool to investigate both the computational principles underlying brain functions and the collective dynamics of neuronal populations.

Still, traditional firing rate models have two major limitations which limit

their range of applicability in neuroscience. First, firing rate models do not generally represent proper mathematical reductions of the underlying network of spiking neurons but rather are heuristic. As such there is in general no precise relationship between the parameters in the traditional firing rate model and those in the full network of spiking neurons, and there is no clear link between the macroscopic states of the network with the microscopic dynamics of the constituent neurons. Second, these models are not accurate in describing the dynamics of collective states where a significant fraction of the neurons fires spikes in synchrony. Synchronous firing has been suggested to be the mechanism responsible for the generation of large scale neuronal oscillations, the rhythmic patterns ubiquitous in electrical recordings of brain activity (Buzsáki, 2006). Networks of spiking neurons may engage in synchronous firing in several circumstances, either due to exogenous factors (e.g. transient external inputs), or to endogenous characteristics of the circuit, as the presence of significant synaptic delays.

In this dissertation, we will investigate the synchrony-based oscillations that emerge in networks of spiking neurons due to the presence of synaptic delays. We will employ a novel firing rate model recently derived for networks of so called quadratic integrate-and-fire (QIF) neurons (Montbrió et al., 2015). We will illustrate that the novel firing rate model properly describes the dynamical regimes that emerge in networks of synaptically-coupled spiking neurons, including synchrony-based oscillations.

Outline of the thesis

In this thesis, we will extensively analyze a firing rate model recently derived for networks of QIF neurons, that we call QIF firing rate equations (QIF-FRE). The model is exact, meaning that it can be rigorously mathematically derived from the underlying network of spiking neurons. Employing the QIF-FRE thus has the unique advantage of allowing for an extensive comparison of the macroscopic mean-field dynamics with the single neuron properties.
Specifically, we will consider the effect that synaptic delays (in forms of fixed delays and synaptic filters) have on the macroscopic dynamics of the QIF-FRE, and therefore on the dynamics of the underlying network

of spiking neurons. We will focus on the deterministic, noiseless aspects of the dynamics. The results are expected to hold as long as the system is in the so called mean-driven regime, i.e. low noise case. The central questions addressed with this dissertation may be summarized as follows:

- How do synaptic delays shape the dynamics of large networks of spiking neurons? Can synaptic delays produce self-sustained collective oscillations? If so,
  - What is the mechanism generating these oscillations?
  - Are the oscillations robust to neuronal heterogeneity?
- How does the microscopic dynamics of the neurons relate to the collective mean-field dynamics?
- How do the exact QIF-FRE relate to traditional firing rate equations?

Specifically, *Chapter 1* serves as a background for the rest of the Thesis. We first review some relevant concepts on neuronal modelling, and then illustrate several examples of network of spiking neurons where synchronous firing emerges as a consequence of synaptic delays. Comparing these results with an analysis of the corresponding traditional rate equations, we demonstrate that generally traditional rate models fail to capture synchronous states induced by synaptic delays. Finally, we introduce the firing rate model employed throughout the thesis, the QIF-FRE.

In *Chapter 2*, we analyse the effect of first order synaptic kinetics on the QIF-FRE. We show that the QIF-FRE, at variance with traditional rate models, correctly capture the synchrony-induced macroscopic oscillations that arise in networks of inhibitory neurons with first order synaptic kinetics. We analytically determine the parameter region of stable self-sustained oscillations, and show that the QIF-FRE also qualitatively capture the dynamics of networks of biophysically detailed conductance-based model neurons. Lastly, we study the limit of slow synaptic kinetics, and determine a relation between the QIF-FRE and the traditional Wilson-Cowan-like firing rate equations.

Chapter 3 is devoted to the study the role of fixed delays on the QIF-FRE. We extensively analyze the system dynamics, which includes synchronous, partially synchronous and chaotic regimes, for both identical and heterogeneous populations of QIF neurons. We identify a novel three-frequency modulated partially synchronous state, and study its transition into chaos. We then explore the relation among the microscopic and the collective dynamics, particularly in the non-trivial partially synchronous and chaotic regimes. Finally, we compare the dynamics of the QIF-FRE to the corresponding traditional rate model with delays.

Chapter 4 serves as a preliminary study bridging *Chapter 2* and *Chapter 3*. We consider the simultaneous effect of fixed delays and synaptic kinetics on the QIF-FRE, illustrating by analyzing the oscillatory instabilities of the model that it is mainly the fixed time delay that determines the system dynamics. Then, we compare the dynamics of the QIF-FRE with that of the corresponding version of the traditional firing rate equations.

In the final chapter, *Conclusions and discussion*, we summarize the main contributions of this dissertation, and illustrate some possible future directions of investigation.

CHAPTER 1

Synchronization in networks of spiking neurons with synaptic dynamics

This chapter serves as a background and introduction to the following chapters of this thesis. We briefly discuss some concepts of synchronization, and models of neuronal and synaptic dynamics. Then, we show some examples of synchronous dynamics in networks of spiking neurons induced by synaptic delays. We then compare the network dynamics with the corresponding (heuristic) firing rate description. Finally, we introduce the firing rate equations that we will employ in the following chapters of the dissertation.

1.1 Synchrony and neuronal oscillations

Synchronization is a ubiquitous natural phenomenon. In Biology, examples include the synchronous flashing of fireflies, the unison chirping of crickets, the synchronous firing of pacemaker cells in the heart, and of circadian neurons in the suprachiasmatic nucleus of the brain (Strogatz, 2003). Synchronization is a simple illustration of emergent collective behavior, where a congregation of elements concur to produce a collective effect. Importantly, the emergence of this macroscopic order is a self-organization process: fireflies, circadian neurons, or any other oscil-

latory system engaged in a synchronous rhythm, just adjust their intrinsic rhythms one with respect to the others, thanks to their mutual interactions (Pikovsky et al., 2001).
In neuroscience, synchronization has often been related to the oscillations observed in electrical recordings of neural activity (Buzsáki, 2006). Norbert Wiener was among the firsts to propose a relation among brain oscillations and synchronization. Wiener was investigating the alpha rhythm emerging in human EEG recordings, an oscillation that was attracting increasing attention since it was observed for the first time a few decades earlier by Hans Berger (Berger, 1929). Wiener hypothesized that this rhythm might originate from a population of synchronizing neural oscillators (Wiener, 1961). Even though not providing much evidence supporting the hypothesis (apart from a power spectrum that has never been replicated), Wiener studies have certainly the merit of raising much interest in biological oscillators (Strogatz, 1994). Besides alpha waves, electrical recordings of brain activity reveal the presence of oscillations with a wide range of frequencies (Buzsáki and Draguhn, 2004). These rhythms appear at different spatial scales, from LFP recordings of few hundreds of neurons, to EEG and MEG recordings of larger cortical areas (Wang, 2010). Brain oscillations have been implicated in several brain functions, such as perceptual binding (Von der Malsburg and Schneider, 1986; Gray et al., 1989; Engel and Singer, 2001), information processing and transfer (Fries, 2005; Palmigiano et al., 2017; Rohenkohl et al., 2018), attention (Fries et al., 2001), and memory (Fell et al., 2001; Axmacher et al., 2006; Fell and Axmacher, 2011).

1.1.1 Modeling Synchronization

From a mathematical standpoint, the first attempt to understand the emergence of biological rhythms in terms of mutual synchronization of populations of oscillators is due to Wiener's studies of alpha waves (Wiener, 1961). However Wiener's approach, based on Fourier integrals, was not successful, and turned out to be a dead end (Strogatz, 2000). A proper mathematical formulation of the ideas introduced by Wiener was later developed by Arthur Winfree (Winfree, 1967). Winfree assumed that, in the weak coupling regime, an oscillator could be described only by a phase variable, assuming the oscillations' amplitude to remain constant. Additionally, the oscillator's response to perturbations (for

instance induced by the interaction with other oscillators) should depend on its phase, introducing the concept of phase response curve. Kuramoto, with an elegant mathematical formulation, further simplified Winfree's model, obtaining a model where interactions depend only on the phase differences between oscillators (Kuramoto, 1975, 1984). Thanks to its mathematical tractability, the Kuramoto model soon became the standard tool to investigate synchronization transitions in populations of coupled oscillators in several different setups, for a review see (Acebrón et al., 2005). Interestingly, it predicts the qualitative structure of the power spectrum shown by Wiener to support his hypothesis (Strogatz, 1994).
The Kuramoto model has been widely employed to investigate the emergence of neuronal rhythms (Breakspear et al., 2010; Cabral et al., 2011; Ton et al., 2014; Villegas et al., 2014; Petkoski et al., 2016), with recent theoretical advances (Montbrió and Pazó, 2018).
However, despite retaining some of the fundamental features, it has two important limitations when applied to model neuronal dynamics:

- Neurons are excitable units, not self-sustained oscillators. Rhythmic firing is elicited only by sufficiently strong incoming inputs.
- Neurons interact in an all-or-none fashion. Kuramoto-like interactions continuously depend on the phase difference among the oscillators, while neurons interact via pulse-like signals, the action potentials.

These characteristics are considered in the more biophysically-realistic models that we briefly discuss in the next section.

1.2 Modeling collective neuronal dynamics

Building mathematical models of any physical or biological system require a careful compromise between the degree of detail and the complexity of the model. An extremely detailed model might take into account exceptionally well all the details of the physical system under analysis, but also rapidly become so complex to be almost impossible to analyze. Certainly, the degree of detail we wish to include in our model also depends on the scope of our analysis.
Modeling neuronal dynamics also requires a compromise between greater biophysical detail and feasible analysis. If the aim is describing the collective activity of a large neuronal population two strategies might be

employed. The dynamics of each single cells can be described (with a certain degree of detail), resulting in a quite complex and high-dimensional model for the whole network–possibly also containing equations for the synaptic transmission. Alternatively, the network might be described by some average, "macroscopic", quantity (as we shall see in the following, the firing rate) in analogy to what is typically done e.g. in thermodynamics. As to the single neurons dynamics, a plethora of alternative models have been developed, ranging from biophysically detailed models to simplified phenomenological descriptions of integrate-and-fire type (Dayan and Abbott, 2001). Similarly, synaptic processing can be modeled with different degrees of details, as we will see later in this section. In the following we further discuss the different classes of models mentioned above.

1.2.1 Spiking neuron models

The stereotypical neuronal signals are the action potentials, pulse-like events of rapid depolarization and subsequent hyperpolarization of the membrane voltage of the cells. The classical model of action potential generation, the Hodgkin-Huxley model, is a four-dimensional system of differential equations that describe the subthreshold dynamics of the membrane potential, together with sodium and potassium channels kinetics (Hodgkin and Huxley, 1952). Thanks to its biophysical realism, it can faithfully account for experimental data on the electrical properties of excitable cells. Alternatively to biophysical models, phenomenological models of action potential generation were developed, the so called integrate-and-fire models. Here, only the basic electrical properties of the cell membrane are retained. The simplest (and also earliest) example of such models was proposed by Lapique (Lapique, 1907), that introduced what is nowadays known as leaky integrate-and-fire (LIF) neuron . The LIF neuron describes the cell with a linear differential equation for the membrane voltage, constructed in analogy with an RC circuit with a leakage current (Dayan and Abbott, 2001). A simple generalization of the LIF model of the integrate-and-fire class is the quadratic integrate-and-fire neuron (QIF) (Ermentrout and Kopell, 1986; Izhikevich, 2007) that captures the qualitative behavior of the frequency-current curve of a larger family of more realistic models (i.e. of Hodgkin-Huxley-type). The loss of biophysical detail of integrate-and-fire models compared to Hodgkin-Huxley-type models is compensated by the simplified descrip-

tion, facilitating more efficient numerical implementation and mathematical insights.

1.2.2 Synaptic processing

To model a neuronal network, we must additionally properly describe neuronal interactions. This is particularly relevant for synchronous and oscillatory dynamics, since the synaptic time course is known to play a fundamental role in generating oscillations– see e.g. (Wang and Buzsáki, 1996; Brunel and Wang, 2003).
There are two main types of synaptic interactions: chemical synapses, and gap junctions (or electrical synapses). In the following, we discuss the main characteristics of chemical interactions, as this will be the type of interaction considered in this thesis *.
Chemical synapses filter the action potentials, transmitting them from the axon of the presynaptic neuron to the dendrites of the postsynaptic neuron. The transmission takes place at the synaptic cleft with a series of complex biochemical processes. The ionic currents due to the incoming action potential in the presynaptic neuron interact with specific proteins at the presynaptic terminal, releasing neurotransmitters in the extracellular medium. The neurotransmitters bind to the chemical receptors at the postsynaptic terminal, resulting in the opening of the ionic channels producing an influx of ions in the postsynaptic neuron (the postsynaptic current).
Several detailed mathematical models have been developed that faithfully describe this complex sequence of biochemical processes, see e.g. (Destexhe et al., 1998). These models accurately describe the kinetics of the chemical reactions involved, and fit patch-clamp experimental data extremely well. However, they are quite complex, and therefore are often simplified in terms of phenomenological models (Roth and van Rossum, 2009). Typically, the whole synaptic transmission process is reduced to two main stages: the release of neurotransmitter in the synaptic cleft, and the opening and closing of postsynaptic ion channels. The neurotransmitter release is modeled as a brief pulse of neurotransmitter concentration that follows the presynaptic action potential (Destexhe et al., 1998). The pulse typically is delayed, producing a brief latency in the postsynaptic

*The effects of gap junction coupling on the model presented in this thesis are analyzed in (Pietras et al., 2019).

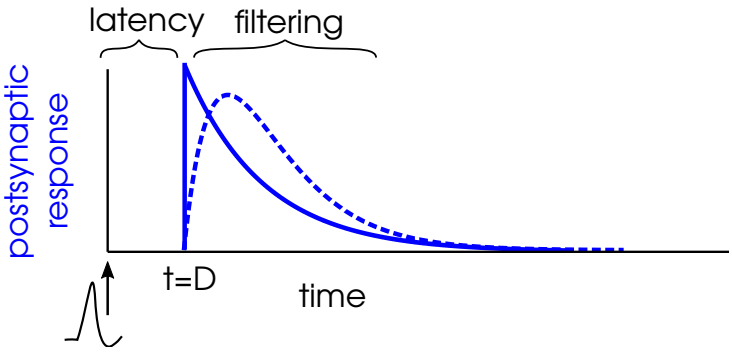

Figure 1.1: Sketch of the time course of the postsynaptic current elicited by a pre-synaptic action potential. Solid blue line: instantaneous rise synapses. Dashed blue line: alpha synapses.

response (Markram et al., 1997; Bartos et al., 2001; Angulo et al., 1999). The kinetics of the ion channels, or the fraction of open channels, have a rising and decaying phase. The time course of the fraction of open channels following a presynaptic spike is commonly taken to be a double exponential, with two time constants characterizing the opening and closing phase of the process. Often, the two time constants are assumed to be equal, resulting in the so called alpha synapses (Roth and van Rossum, 2009). For certain types of synapses, the rising phase is much faster than the decaying phase, so that it is reasonable to assume an instantaneous opening followed by an exponential decay. An illustration of these two types of synaptic time course is shown in Fig. 1.1. The solid blue line corresponds to the approximation of instantaneous opening of the channel (instantaneous rise synapses), while the dashed blue line to alpha synapses. The arrival of a presynaptic action potential (at $t = 0$) elicits a response after a latency (delay) D.

The general shape of the postsynaptic current following a presynaptic action potential is then a delayed double exponential, characterized by three time scales: the latency, the rising time, and the decaying time constants.

To investigate the synchronization properties of neuronal populations then typically we are at face with the study of high-dimensional networks of synaptically-coupled spiking neurons. As discussed so far, the network constituents can be either biophysically-detailed models (e.g. the Hodgkin-Huxley model), or more idealized models (of integrate-and-fire type). Synaptic interactions can be as detailed as describing all bio-

chemical processes occurring at the synaptic cleft, or just one or two phenomenological differential equations. Either way, any study aiming at investigating collective phenomena in large neuronal networks has to deal with an extremely high number of equations (few thousands neurons for each cubic millimeter of brain tissue), rendering the analysis of the system extremely complex.

1.2.3 Firing rate models

Researchers alternatively formulated a different class of models, that rather than focusing on the dynamics of single neurons, focus on the average collective activity of local neuronal population. This class of models describes the activity of a neuronal population (a localized portion of brain tissue, containing a few thousands neurons) via (few) collective variables. In the second half of the XX century, several authors explored the possibility of modeling the dynamics of neuronal circuits via their *population* firing rate, the fraction of active neurons at a given instant in time (Beurle, 1956; Griffith, 1963; Anninos et al., 1970; Amari, 1971, 1972). The turning point in the field came with the work of Wilson and Cowan (Wilson and Cowan, 1972, 1973), that with an elegant mathematical formulation derived two nonlinear coupled differential equations for the mean activity of local excitatory and inhibitory populations. In their beautiful 1972 paper, Wilson and Cowan outline the assumptions that underlie the model equations. The properties of local neuronal pools must be homogeneous, and most of the arguments exploited are the standard arguments of mean-field formulations in statistical physics. A particularly relevant assumption underlying the model is that neuronal spiking is uncorrelated, i.e. absence of spike-to-spike correlations. Neurons are assumed to fire spikes asynchronously, and spike-correlations are neglected. Wilson Cowan-type models usually undergoes the name of firing rate models, as they describe each neuronal population via its (population) average firing rate. Throughout the thesis, we will also refer to this class of models as heuristic firing rate equations (H-FRE).

In its simplest form, the H-FRE for one recurrently coupled population (excitatory or inhibitory) is the following:

$$\tau_m \dot{R} = -R + \Phi(I), \tag{1.1}$$

where R is the firing rate of the population, τ_m the time constant of the

rate dynamics, and I the input current. The time constant τ_m is related to the time coarse-graining procedure that was originally employed to derive Eq. (1.1). It can be interpreted as the neuronal membrane time constant, as long as fast transients in the rate dynamics are discarded (Gerstner, 2000). The function Φ is the transfer function of the neuronal population. In the original formulation of Wilson and Cowan the transfer function Φ determines the fraction of active neurons given an input I at stationarity. It is of sigmoidal shape, with an expansive nonlinearity at low rates and a saturation at high rates (Wilson and Cowan, 1972). Alternatively, the function Φ can be interpreted as the frequency-current (f-I) curve of single cells, i.e. the neurons' stationary firing rate response to applied inputs. In the latter case, unless an explicit refractoriness is imposed in the neuronal model, the f-I curve does not saturate. In subsequent analysis, unless otherwise specified, we adopt the f-I curve*

$$\Phi(I) = \frac{1}{\sqrt{2}\pi\tau_m}\sqrt{I + \sqrt{I^2 + \Delta^2}}. \tag{1.2}$$

Depending on the form of the synaptic current, the model Eq. (1.1) may show a rich dynamical repertoire, including multistability between high and low activity states and oscillations (Kilpatrick, 2015). In Comment 1.2.1 we briefly review the dynamics of model Eq. (1.1) in its simplest setting of one recurrently coupled population with instantaneous synaptic kinetics.

Comment 1.2.1: Analysis of H-FRE with instantaneous synaptic kinetics

A Wilson-Cowan equation for a recurrently coupled population with instantaneous synapses can be written as

$$\tau_m\dot{R} = -R + \Phi(\Theta + J\tau_m R), \tag{1.3}$$

where Θ is the constant mean external input current and J the strength of recurrent coupling. In this simple case, the only stationary solutions of Eq. (1.3) are fixed points. Imposing $\dot{R} = 0$, we find the

*A plot of this function for several values of parameter Δ is shown in Fig. 1.4.

implicit equation for the fixed points:

$$R_* = \Phi(\Theta + J\tau_m R_*). \tag{1.4}$$

Depending on parameters values, the fixed point condition may give one or multiple solutions– see left panel of Fig. 1.2. Linearization around the fixed point gives the characteristic equation:

$$\lambda = -1 + \tau_m J \Phi', \tag{1.5}$$

where Φ' is the derivative of the transfer function with respect to its argument, evaluated at the fixed point. Setting $\lambda = 0$, we find the loci of a stationary (saddle node) bifurcation of the fixed points in parametric form:

$$(\Theta, J)_{\text{SN}} = \left[-\pi^2 r^2 - 3\Delta^2/(2\pi r)^2, 2\pi^2 r + \Delta^2/\left(2\pi^2 r^3\right)\right], \tag{1.6}$$

where $r = \tau_m R$. The boundaries Eq. (1.6), plotted as blue lines in the right panel of Fig.1.2, delimit a region in the (Θ, J) plane of bistability between a low activity and a high activity state (cyan region in the right panel of Fig. 1.2). In the same panel of Fig.1.2 we additionally show with dashed orange lines the stationary bifurcations obtained with a different (saturating) transfer function, $\tilde{\Phi}(I) = \alpha/\left(1 + e^{-\beta I}\right)$.

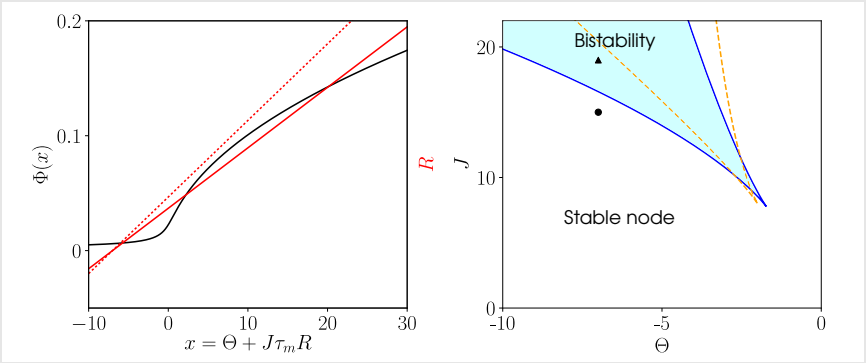

Figure 1.2: Graphical solution of Eq. (1.4) and related phase diagram. Left panel: graphical solution of Eq. (1.4) for $\Theta = -7$ and: $J = 19$ (solid red line), $J = 15$ (dotted red line). The black line is the transfer function Eq. 1.2. As the coupling is increased, two solutions (a saddle and a node) emerge.
Right panel: phase diagram of Eq. (1.3). Blue lines represent the saddle node bifurcation Eq. (1.6). In the cyan region, two stable fixed points coexist. In the white region, the system has only one stable node. The symbols correspond to the parameters chosen for the graphical solutions of the left panel. The dashed orange lines, defined by $(\Theta, J)_{\tilde{\text{SN}}} = \left[\beta^{-1}\left(\alpha/\left(r-\alpha\right)+\log\left(r/\left(\alpha-r\right)\right)\right), \alpha r^{-1}\left(\alpha\beta - r\beta\right)^{-1}\right]$, are the saddle node bifurcations of Eq. (1.3) with f-I curve $\tilde{\Phi}$ (see text). Parameters: Left panel: $\Theta = -7$, $J = 20$, $\Delta = 1$, $\tau_m = 10$ ms. Right panel: $\Delta = 1$, $\beta = 1$, $\alpha = 0.5$.

The usefulness of firing rate models is twofold: on one hand, they have been proven to be a remarkable tool to model several brain functions, as decision making (Wong and Wang, 2006; Rabinovich et al., 2008a,b), learning and memory (Hopfield, 1984; Durstewitz et al., 2000; Mongillo et al., 2008), motor control (Zhang, 1996), perception (Moreno-Bote et al., 2007; Rankin et al., 2014, 2015), and visual processing (Schuster and Wagner, 1990; Ben-Yishai et al., 1995). On the other hand, they are very useful to investigate fundamental principles underlying the dynamics of large populations of spiking neurons. Yet, firing rate models do not provide an exact correspondence with the underlying networks of spiking neurons, but rather are heuristic. There is no clear correspondence among the underlying network parameters, and the parameters of the rate model. Additionally, they are usually derived based on statistical assumptions such that of uncorrelated spiking. They are precisely these limitations that cause traditional, Wilson-Cowan like firing rate models to fail to describe synchronous neuronal activity, as we will outline in the next section.
In the next sections we present numerical simulations of networks of spiking neurons where we consider the impact of synaptic processing. In fact, as previously mentioned, the synaptic time course is crucial in generating synchronous spiking. Comparing the network simulations and an analysis of the corresponding H-FRE we will illustrate that, when some degree of synchronous spiking is present in the network, traditional rate models of Wilson-Cowan type fail to capture the underlying networks dynamics.

1.3 Synaptic time delays favor the emergence of oscillations in populations of spiking neurons

Synaptic processing generates some fixed delay among neuronal interaction. In this section we will show simulations of networks of spiking neurons with fixed synaptic delays, and compare their dynamics with the corresponding traditional firing rate equations. As model neurons, we will employ both a conductance-based Hodgkin-Huxley type neuronal model, the Wang-Buzsáki neuron (WB) (Wang and Buzsáki, 1996), and the quadratic integrate-and-fire (QIF) neuron (Ermentrout and Kopell, 1986; Izhikevich, 2007). Details on the numerical simulations shown in this Chapter are given in Appendix A.

1.3.1 Synchronization in recurrently coupled networks of spiking neurons with synaptic latency

It is well known that generally, time delays induce oscillations in dynamical systems (MacDonald, 1989). An early study on the influence of time delay in coupled oscillators is due to Schuster and Wagner (Schuster and Wagner, 1989), that showed that at variance with the zero delay case, two phase oscillators coupled with time delays may synchronize with a multitude of different frequencies. Interestingly, these frequencies tend to vanish for very large delays, a phenomenon known as frequency suppression (Niebur et al., 1991), which holds also for networks of such oscillators.
Yeung and Strogatz first thoroughly analyzed the effect of delays on the canonical model of synchronization in populations of coupled oscillators, the Kuramoto model. They found bistability between synchrony (again, with multiple possible frequencies) and incoherence, and cluster states (Yeung and Strogatz, 1999) . Multistability of synchronous solutions is also found in ensembles of coupled rotators (Kim et al., 1997). In populations of limit cycle oscillators, time delay can also result in amplitude death (Reddy et al., 1999).
All these results regard network of oscillators continuously coupled, i.e. where the interactions depend continuously in time on the phase difference among the oscillators. These type of models are reasonable

representation of neuronal dynamics only in the weak coupling limit (Izhikevich, 2007).
Synaptic delays profoundly shape the dynamics of networks of pulse-coupled integrate-and-fire oscillators. Generally, they favor the emergence of synchronization. Importantly, this delay-induced synchrony is typically more robust for inhibitory, rather than for excitatory coupling (Ernst et al., 1995, 1998). This holds particularly for short delays, where only inhibition may lead to synchronous firing (Gerstner and van Hemmen, 1992, 1993; Gerstner et al., 1996). Notably, the prominent role of inhibition in synchronizing neural firing holds not only when a fixed delay is explicitly introduced into the equations, but also for any effective delay introduced by the synaptic coupling (Van Vreeswijk et al., 1994).
In the following, we illustrate numerical simulations of populations of heterogeneous WB and QIF neurons showing transitions to synchronized firing due to the delayed coupling. Neurons are recurrently coupled all-to-all via the delayed mean firing rate of the population (the delay is set to 3 ms). Fig. 1.3 shows the result for a population of excitatory (left column) or inhibitory (right column) WB neurons. In the two simulations, the excitatory (inhibitory) coupling strength is suddenly increased at $t = 100$ ms. At the beginning of the simulations, neurons fire asynchronously, with a given average firing rate. When the coupling is sufficiently strong, the asynchronous state becomes unstable, and the system undergoes an Hopf bifurcation giving rise to macroscopic oscillations. These macroscopic rate oscillations are due to spike synchronization, as illustrated by the raster plots shown in panels (c,d) of Fig. 1.3. These synchrony-based macroscopic oscillations are fast, with frequency ~ 100 Hz, as it is generally observed in oscillations induced by short delays (Brunel and Wang, 2003).
The same collective oscillations also appear in a population of heterogeneous QIF neurons. Also here, as shown in Fig. 1.4, when the recurrent coupling is sufficiently strong (either excitatory or inhibitory), the neurons synchronize producing macroscopic rate oscillations. Again, the network dynamics underlying the macroscopic oscillations is synchronous (see the raster plots in panels (c,d) of Fig. 1.4).

Importantly, in all these simulations, the large majority of the neurons of the populations are supra-threshold when there is no coupling, i.e. they fire spikes periodically according to their own natural frequency. The transition to oscillations is therefore the typical synchronization transition

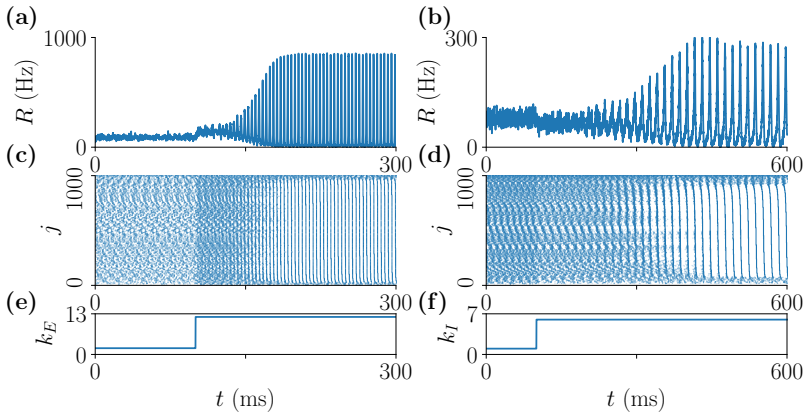

Figure 1.3: Networks of heterogeneous excitatory (left) and inhibitory (right) Wang-Buzsáki neurons with synaptic delay display macroscopic oscillations when recurrent excitation (respectively inhibition) is sufficiently strong. Panels (a,b): time series of the population firing rate. Panels (c,d): raster plots showing spiking events of the population. A sudden increase in coupling strength (shown in panels (e,f) for excitation and inhibition respectively), results in synchronized firing of the population. Parameters: $I_{\text{app}} = 1.34\ \mu\text{A/cm}^2$, $\sigma = 0.05\ \mu\text{A/cm}^2$.

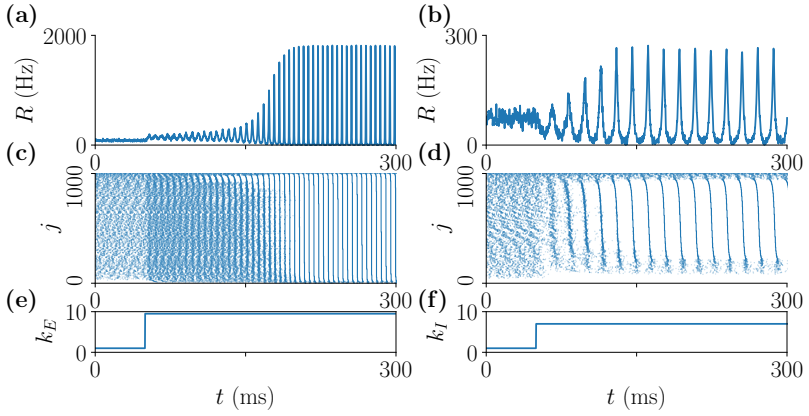

Figure 1.4: Networks of heterogeneous excitatory (left) and inhibitory (right) QIF neurons with synaptic delay display macroscopic oscillations when recurrent excitation (respectively inhibition) is sufficiently strong. Panels (a,b): time series of the population firing rate. Panels (c,d): raster plots showing spiking events of the population. A sudden increase in coupling strength (shown in panels (e,f) for excitation and inhibition respectively), results in synchronized firing of the population. Parameters: $\Theta = 2.5$, $\Delta = 1$.

in a system of coupled oscillators, as the one of the Kuramoto model with time delays (Yeung and Strogatz, 1999).

However, neurons are excitable cells, often silent for long time windows,

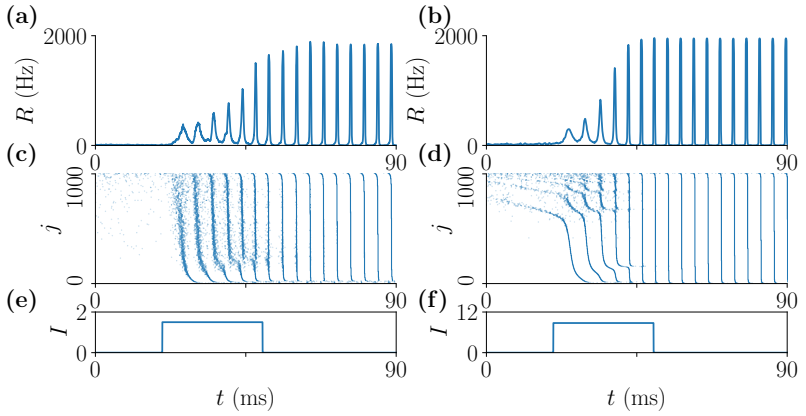

Figure 1.5: Networks of heterogeneous WB (left) and QIF (right) neurons in the excitable regime synchronize due to sufficiently strong recurrent excitation. Panels (a,b): time series of the population firing rate for WB (a) and QIF (b) neurons. Panels (c,d): raster plots showing spiking events of the populations. A transient step current (shown in panels (e,f)) produces synchronous spiking, which is then sustained by the strong recurrent excitation. WB parameters: $k_E = 18$ mV, $\sigma = 0.05\ \mu\text{A/cm}^2$ mV, $\bar{I} = -0.1601\mu\text{A/cm}^2$. QIF parameters: $J = 15$, $\Delta = 0.8$, $\Theta = -2.5$.

and spikes are triggered by external inputs. The dynamics of populations where most of the neurons are excitable, clearly cannot be described by models of self-sustained oscillators where rhythmic firing is implicitly assumed. The QIF and the WB neuron can readily switch from the excitable to the periodic regime by changing the input current to the neuron. With no inputs, we expect the network activity of a population with most of the neurons in the excitable regime to be low. However, what happens when a common current is injected into the network producing a burst of spikes, transiently synchronizing the neurons? Simulations in Fig. 1.5 show that, after removal of the transient input to the population, neurons keep firing in a synchronized manner, thanks to the strong recurrent excitatory coupling. Therefore, these networks are typically bistable: according to initial conditions, the population will settle in a (low activity) asynchronous state, or in an (oscillatory) high activity state. Again, this phenomenon is general, and related to the coupling properties

of the network rather than to the particular microscopic model considered. Similar results can be indeed obtained with simulations of other types of integrate-and-fire models, or other biophysically-detailed models.
The oscillations described in this section manifest themselves at the population level, and we would expect a description of collective neural dynamics to capture them. In the next section we discuss how the dynamics of traditional firing rate models is affected by time delays.

1.3.2 Dynamics of traditional rate models with synaptic delays

The Wilson-Cowan equation for a population of recurrently coupled neurons with fixed delays is:

$$\tau_m \dot{R} = -R + \Phi\left(J\tau_m R(t-D) + \Theta\right), \tag{1.7}$$

where D is the time delay and times are rescaled by the rate time constant. Equation (1.7) has been widely employed to investigate the emergence of delay-driven oscillations in networks of spiking neurons (Roxin et al., 2005; Hutt and Atay, 2006; Battaglia et al., 2007; Brunel and Hakim, 2008; Roxin and Montbrió, 2011).
The fixed points of Eq. (1.7), as well as their stationary bifurcations, are the same as the ones of the model without delays Eq. (1.3) (see comment 1.2.1). However the presence of delays introduces oscillatory instabilities in the form of Hopf bifurcations. To look for instabilities of the fixed point $R = R_*$, we study the linear evolution of a small perturbation around the fixed point. Namely, we substitute in Eq. (1.7) the ansatz $R(t) = R_* + \delta R e^{\lambda t}$, where $\delta R \ll 1$, obtaining the characteristic equation:

$$\lambda = -1/\tau_m + J\Phi' e^{-\lambda D}, \tag{1.8}$$

where Φ' is the derivative of the transfer function evaluated at the fixed point.
The stationary bifurcations shown in Comment 1.2.1 are obtained setting $\lambda = 0$ in Eq. (1.8). To look for the oscillatory instabilities, we set $\lambda = i\omega$ (purely imaginary eigenvalue). In this case, Eq. (1.8) is equivalent to the system of equations (Roxin et al., 2005; Roxin and Montbrió, 2011):

$$\tau_m \omega = -\tan(\omega D), \tag{1.9a}$$
$$J_H = \left[\cos\left(\omega D\right)\Phi'\right]^{-1}. \tag{1.9b}$$

Eqs. (1.9a) has an infinite number of solutions, of which however only the first is the relevant instability (the others are instabilities of unstable solutions). The first oscillatory instability given by Eqs. (1.9) is the black line shown in the phase diagram illustrated in the left panel of Fig. 1.6. For low coupling strength, the fixed point is stable (grey region). When recurrent inhibition is sufficiently strong, the system undergoes an Hopf bifurcation and a self-sustained oscillation is stable–see also the numerical simulations of the right panel of Fig. 1.6. Importantly,

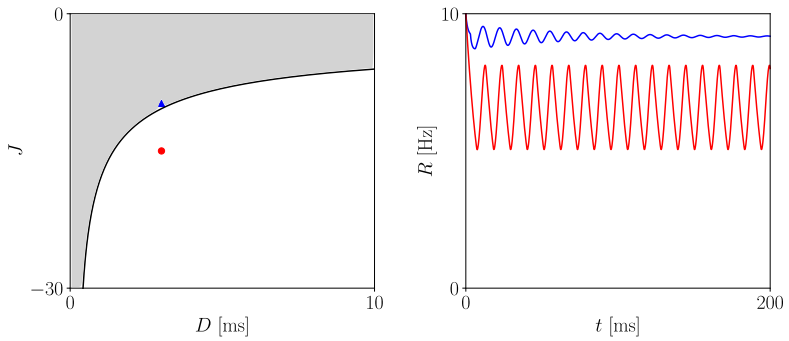

Figure 1.6: Hopf instability of the Wilson-Cowan model Eq.(1.7). Left panel:phase diagram of the system. The black line is the Hopf bifurcation obtained from Eqs.(1.9). In the grey region, the fixed point is stable. In the white region self-sustained oscillations are stable. The symbols correspond to the numerical simulations shown in the right panel. Right panel: numerical simulations of Eq.(1.7) for $J = -10$ (blue line) and $J = -15$ (red line). In both simulations, $D = 3$ ms.
In both panels, we use the transfer function defined by Eq.(1.2). Other parameters: $\tau_m = 10$ ms, $\Theta = 1$, $\Delta = 0.01$.

oscillations emerge only for inhibitory coupling*. This is in contrast with the numerical results presented in the previous section on networks of spiking neurons, where oscillations emerged not only for inhibitory, but also for excitatory coupling. A closer analysis, presented in *Chapter*

*It can be proved using the transfer function Φ defined by Eq.(1.2). Eq. (1.9a) has solutions in two ranges: $\pi/2 \leq \omega D \leq \pi$ and $3\pi/2 \leq \omega D \leq 2\pi$. The first range always results in a negative value of the critical coupling J_H, since the f-I curve is an increasing function. Solutions in the second range, that might produce a critical positive coupling, always correspond to negative values of the firing rate, and are therefore unphysical. Note that oscillations in Eq.(1.7) have been reported in the Literature exclusively for inhibitory coupling (Roxin et al., 2005; Brunel and Hakim, 2008; Roxin and Montbrió, 2011)

3, also reveals how the traditional rate model Eq. (1.1) has oscillatory instabilities only for $\Theta > 0$, at variance with networks of spiking neurons, where even when the majority of neurons are excitable, oscillations due to strong recurrent excitatory connections are possible.
Still, for inhibitory populations, the rate model Eq. (1.1) provides useful insights: first, it predicts the emergence of oscillations for large enough inhibitory coupling strength (Roxin et al., 2005). Secondly, it is also able to predict the range of frequencies of the emerging oscillations: $1/4D < f < 1/2D$ (Brunel and Wang, 2003; Roxin et al., 2005). It also gives a simple mechanistic interpretation of the nature of these oscillations: the delay provides windows of low inhibition where the activity can be high, producing in turn windows of strong shunting inhibition that suppresses the network activity. Traditionally, these oscillations have been related to the sparsely synchronized states arising in networks of spiking neurons with inhibition and strong noise. These states are characterized by low irregular microscopic firing and coherent collective rhythms (Brunel and Hakim, 1999, 2008) with a period again determined the synaptic delay D, in the range between $2D$ and $4D$. This "stochastic" form of synchronization is substantially different from the states we described in the previous sections, where the firing frequency of the neurons in the synchronized cluster is the same as the frequency of the mean field oscillation. However, also for those highly synchronous oscillations, it can be shown that, especially for large heterogeneity, the frequency for inhibitory coupling is in the same range.
Still, the WC equation Eq. (1.1) with time delays does not account for any of the rhythms sustained by excitatory coupling shown in the previous section. This discrepancy is related to one of the main hypothesis underlying the WC model, the absence of spike correlations. Neglecting such correlations prevents the possibility of accounting for those highly synchronous states.
In the next section, we show how similar discrepancies occur also when an extra variable describing synaptic dynamics is explicitly taken into account.

1.4 Networks of recurrently coupled inhibitory neurons with synaptic kinetics generate fast oscillations

A large body of experimental and computational work indicate that networks of spiking neurons with recurrent inhibitory interactions and synaptic dynamics readily generate oscillations (Whittington et al., 1995; Traub et al., 1996; Wang and Rinzel, 1992, 1993; Van Vreeswijk et al., 1994; Nischwitz and Glünder, 1995; Wang and Buzsáki, 1996; Brunel and Wang, 2003; Olmi et al., 2014). Such inhibition-generated rhythms usually are referred to as Interneuronal-Gamma (ING) oscillations, as their frequency is typically in the gamma (30-100 Hz) range (Bartos et al., 2007; Buzsáki and Wang, 2012). Two possible network states (or microstates) underlie such oscillations in inhibitory populations: a highly synchronous regime, with a large fraction of neurons firing at the population frequency (Whittington et al., 1995; Nischwitz and Glünder, 1995; Wang and Buzsáki, 1996), or a stochastic regime, where neurons fire irregularly at low rates due to strong noise, the sparsely synchronized state previously mentioned (Brunel and Wang, 2003). Here we focus on the highly synchronous regime, and we leave for the *Conclusions and discussion* further considerations on the relation among the two states.
The interplay between inhibition and synaptic integration determines the frequency of the population rhythm, with a prominent role for the decay times of the post-synaptic potentials (Whittington et al., 1995; Traub et al., 1996). Figure 1.7 shows an illustration of such oscillations in a network of globally coupled WB neurons (Wang and Buzsáki, 1996). Panels (a,c) show the results of a numerical simulation of the network for fast synapses (time constant $\tau_d = 5$ ms), compared to the membrane time constant of the neuron model ($\tau_m = 10$ ms). Although the neurons have different intrinsic frequencies due to a distribution in external input currents, the raster plot reveals that fast inhibitory coupling produces the frequency entrainment of a large fraction of the neurons in the ensemble. This collective synchronization is reflected at the macroscopic scale as an oscillation with the frequency of the synchronous cluster of neurons (Winfree, 1967; Kuramoto, 1984). Indeed, panel (a) shows the time series of both the mean synaptic activation variable S, and the mean firing rate R, which display ING oscillations. Panels (b,d) of Fig. 1.7 show the

disappearance of the synchronous state when the synaptic kinetics is slow ($\tau_d = 50$ ms).
The same behavior holds also for networks of QIF neurons, see Fig. 1.8. Again, when synaptic kinetics is fast, the network shows sustained oscillations in the gamma range due to partially synchronous spiking. Increasing the time constant of the synaptic dynamics suppresses the oscillations, and desynchronizes the network (panels b,d).
In the next section, we compare the dynamics of the traditional firing rate model Eq. (1.1) to the network simulations shown here.

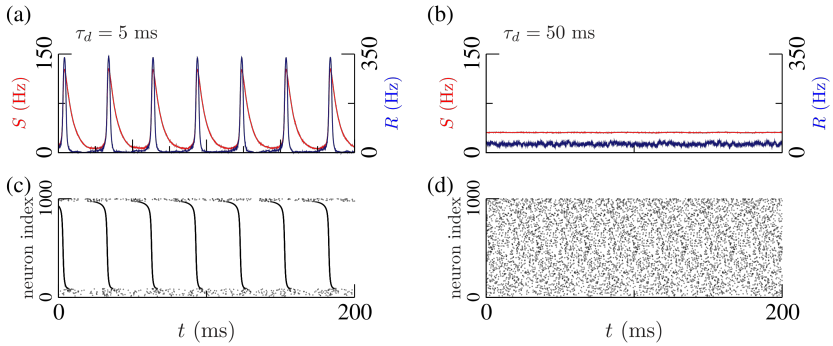

Figure 1.7: Networks of heterogeneous inhibitory neurons with fast synaptic kinetics ($\tau_d = 5$ ms) display macroscopic oscillations in the gamma range (ING oscillations) due to collective synchronization. Panels (a) and (c) show the time series of the synaptic variable S (red) and mean firing rate R (blue), and the raster plot of a population of $N = 1000$ inhibitory Wang-Buzsáki neurons (Wang and Buzsáki, 1996) with first order fast synaptic kinetics. The oscillations are suppressed considering slow inhibitory synapses ($\tau_d = 50$ ms), as shown in Panels (b) and (d). Parameters: $\bar{I} = 0.5$ μA/cm^2, $\sigma = 0.01$ μA/cm^2 and $k_I = 6$ mV See Appendix A for details on the numerical simulations.

1.4.1 A heuristic firing rate equation with synaptic kinetics

A heuristic firing rate description of the spiking network simulated in Figs. 1.7 and 1.8 takes the form (Wilson and Cowan, 1972; Cowan, 2014)

$$\tau_m \dot{R} = -R + \Phi(-J\tau_m S + \Theta), \tag{1.10a}$$
$$\tau_d \dot{S} = -S + R. \tag{1.10b}$$

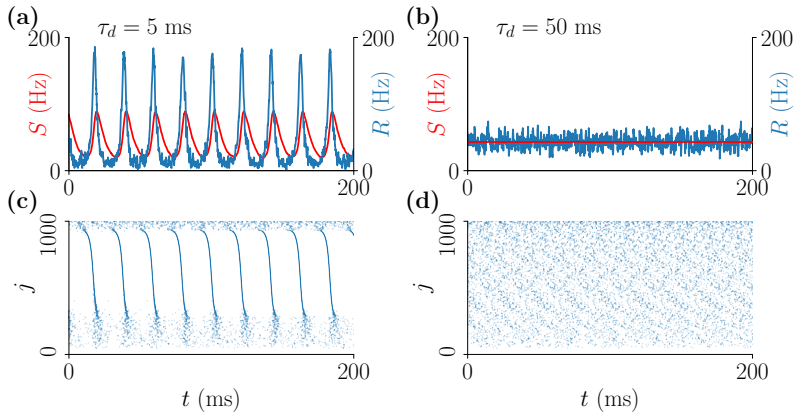

Figure 1.8: Networks of heterogeneous inhibitory QIF neurons with fast synaptic kinetics ($\tau_d = 5$ ms) display macroscopic oscillations in the gamma range (ING oscillations) due to collective synchronization. Panels (a) and (c) show the time series of the synaptic variable S (red) and mean firing rate R (blue), and the raster plot of a population of $N = 1000$ inhibitory QIF neurons with first order fast synaptic kinetics. The oscillations are suppressed considering slow inhibitory synapses ($\tau_d = 50$ ms), as shown in Panels (b) and (d). Other parameters: $\Theta = 4$, $\Delta = 0.3$, $J = -5$. See Appendix A for details on the numerical simulations.

where R represents the mean firing rate in the population, S is the synaptic activation, and the time constants τ_m and τ_d are the neuronal and synaptic time constants respectively (Ledoux and Brunel, 2011; Keeley et al., 2017). In contrast with the network model, the H-FRE Eqs. (1.10) cannot generate sustained oscillations. In fact, a linear stability analysis of steady state solutions in Eqs. (1.10) shows that the resulting eigenvalues are

$$\lambda = -\alpha(1 \pm \sqrt{1-\beta}), \tag{1.11}$$

where the parameter $\alpha = (\tau_m + \tau_d)/(2\tau_m\tau_d)$ is always positive. Additionally, the parameter $\beta = [4\tau_m\tau_d(1 + J\tau_m\Phi')]/(\tau_m + \tau_d)^2$ is also positive, since the f-I curve $\Phi(x)$ is an increasing function, and its derivative evaluated at the steady state is then $\Phi' > 0$. Therefore the real part of the eigenvalue λ is always negative and hence steady states are always stable, although damped oscillations are possible, e.g. for strong enough coupling J. Hence, traditional firing rate equations of Wilson-Cowan type do not show the oscillations that emerge in networks of inhibitory neurons with first order kinetics.

In summary, all the examples shown so far in this chapter show that traditional firing rate models are not an appropriate description of networks that show some degree of spike synchronization. This suggests that there is an additional mechanism in the network dynamics, key for driving oscillatory behavior, that is missing in the H-FRE.
In the next section we will discuss a recently derived firing rate model that, exactly obtained from networks of QIF neurons, can capture synchronous states, and therefore describe the synchrony-based oscillations shown in the previous sections.

1.5 An exact firing rate model for networks of QIF neurons

Following the work of Wilson and Cowan, several approaches have been developed to infer low dimensional descriptions of the collective activity of neuronal populations. They can be broadly cast into two main classes of models. The first, which followed in spirit the approach of Wilson and Cowan, typically use differential (or integro-differential) equations to describe the evolution of some macroscopic variable related to the neuronal populations, as the firing rate (Wilson and Cowan, 1972; Gerstner, 1995, 2000; Schwalger et al., 2017), or the mean synaptic activity (Robinson et al., 1997). Models belonging to this first class are also referred to as neural mass (Freeman, 1975), or neural field models (Coombes, 2005). The second class of models are derived using the so called population density method, as they derive evolution equations for the probability density of the membrane potentials (Knight et al., 1996; Nykamp and Tranchina, 2000; Brunel and Hakim, 1999; Knight et al., 2000; Mattia and Del Giudice, 2002; Dumont et al., 2014). Typically, models belonging to the first class are simpler and more amenable to mathematical analysis; however, often they fail to describe states with rapid variations of the activity, due to the time coarse-graining applied to derive the model equations (Gerstner, 2000; Schaffer et al., 2013). Population density models are able in contrast to capture fast transient and synchronous states (Nykamp and Tranchina, 2000). However, both the mathematical and the computational analysis of such models is convoluted.
In the following, we introduce a recently derived firing rate model for QIF neurons. We review the main steps of the derivation of the model

equations, closely following (Montbrió et al., 2015). Remarkably, the model nicely connects the two classes mentioned before, as we will see in the following.
The quadratic integrate-and-fire model is the canonical representative for Class-I neurons, neurons that fire at arbitrarily low frequencies close to the spiking threshold. It describe the evolution of the voltage of the cell with a first order differential equation:

$$\tau_m \dot{V} = V^2 + I, \tag{1.12}$$

where I is an input current. Eq. (1.12) needs the resetting condition:

$$\text{If} \quad V \geq V_{\text{th}} \quad \text{then} \quad V_{\text{reset}} \leftarrow V, \tag{1.13}$$

where crossing V_{th} the neuron emits a spike. In the theoretical analysis, it is useful to impose that $V_{\text{th}} = -V_{\text{reset}} \to \infty$.
We analyze population of all-to-all coupled QIF neurons, which is then described by

$$\tau_m \dot{V}_j = V_j^2 + \eta_j + J\tau_m s(t) + I(t) \tag{1.14}$$

where $j = 1, \ldots, N$, s is the synaptic activity, and J the coupling or synaptic strength. The terms η_j represent the quenched heterogeneity of the networks, and determine each neuron natural firing frequency. In absence of synaptic coupling and time varying inputs, η_j determines whether neuron j is in the excitable ($\eta_j < 0$, the membrane potential converges to a stable fixed point) or oscillatory ($\eta_j > 0$) regime. In the latter case, the interspike interval of the neuron is given by ISI $= \pi\tau_m/\sqrt{\eta_j}$.
The total synaptic activity can be written in general form as:

$$s(t) = \frac{1}{N} \sum_{j=1}^{N} \sum_{k \backslash t_j^k < t} \int_{-\infty}^{t} dt' a_{\tau_d}(t - t') \delta(t' - t_j^k) \tag{1.15}$$

where t_j^k is the time of the k_{th} spike emitted by neuron j, δ the Dirac delta function, and a_{τ_d} the synaptic kernel function. The derivation reviewed in the following holds for general forms of the synaptic activation $s(t)$. In the next chapters of this thesis, we will focus on three specific cases:

Chapter 2 $\tau_d \dot{s} = -s + r(t),$ (1.16a)

Chapter 3 $s = r(t - D),$ (1.16b)

Chapter 4 $\tau_d \dot{s} = -s + r(t - D).$ (1.16c)

where $r(t)$ is the population instantaneous firing rate,

$$r(t) = \lim_{\tau_s \to 0} \frac{1}{N\tau_s} \sum_{j=1}^{N} \sum_{k \backslash t_j^k < t} \int_{t-\tau_s}^{t} dt' \delta(t' - t_j^k), \tag{1.17}$$

and D the time delay. Eq. (1.16b) represents instantaneous-delayed synapses, Eq. (1.16a) exponentially decaying synapses, and Eq. (1.16c) delayed exponential synapses.

1.5.1 Population density description

We consider a large population of neurons $N \gg 1$. In this limit, η's are random variables distributed according to a density $g(\eta)$. We drop the indices j from Eq. (1.14), which now describe the velocity field of the population.
The population of neurons can be described by the conditional density function $\rho(V|\eta, t)$, where $\rho(V|\eta, t)dVd\eta$ will be the fraction of neurons with $V \in [V, V + dV]$ and $\eta \in [\eta, \eta + d\eta]$. The total (marginal) voltage density at time t will then be

$$\bar{\rho}(V, t) = \int_{-\infty}^{\infty} \rho(V|\eta, t) g(\eta) d\eta. \tag{1.18}$$

Imposing the conservation of the total number of neurons on $\bar{\rho}$ implies that the following continuity equation must hold for each value of η:

$$\tau_m \partial_t \rho + \partial_V \left[\left(V^2 + \eta + J\tau_m s(t) + I(t) \right) \rho \right] = 0. \tag{1.19}$$

A periodic boundary condition for the flux, consistent with the resetting condition Eq. (1.13), is also imposed (Dumont et al., 2014):

$$\lim_{V \to -\infty} \left[\dot{V}(V|\eta, t) \rho(V|\eta, t) \right] = \lim_{V \to +\infty} \left[\dot{V}(V|\eta, t) \rho(V|\eta, t) \right]. \tag{1.20}$$

In the stationary state, the distribution of voltages is inversely proportional to the velocity, $\rho^*(V|\eta) \propto (V^2 + \eta + J\tau_m s)$ for each value of η. A natural ansatz for Eq. (1.19) is to assume that, independently from initial conditions, the time dependent solutions of Eq. (1.19) are Lorenztian distributions for each value of η. We therefore assume the following form for the distribution ρ:

$$\rho(V|\eta, t) = \frac{1}{\pi} \frac{x(\eta, t)}{[V - y(\eta, t)]^2 + x(\eta, t)^2} \tag{1.21}$$

where $x(\eta, t)$ and $y(\eta, t)$ are respectively the time dependent width and median of the Lorentzian distribution of voltages for every value of η. Note that, imposing the ansatz Eq.(1.21), the boundary condition Eq. (1.20) is automatically satisfied:

$$\lim_{V\to-\infty}\left(\dot{V}\rho\right) = \lim_{V\to+\infty}\left(\dot{V}\rho\right) = x(\eta,t)/\pi. \tag{1.22}$$

Eq. (1.22) also identifies the firing rate for each value of η as $\pi r(\eta, t) = x(\eta, t)$, therefore relating the width of the distribution of voltages with the firing rate for a given value of η. Then, we can obtain the total firing rate marginalizing over η*:

$$r(t) = \pi^{-1}\int_{-\infty}^{\infty} x(\eta,t)g(\eta)d\eta. \tag{1.23}$$

Additionally, from $y(\eta, t)$, we can simply derive the median membrane potential of the population †:

$$v(t) = \int_{-\infty}^{\infty} y(\eta,t)g(\eta)d\eta. \tag{1.24}$$

We can now substitute the ansatz Eq. (1.21) into the continuity equation Eq. (1.19). With some algebra, we find that x and y must obey two coupled differential equations, that can be written in compact form as:

$$\tau_m\partial_t w(\eta,t) = i\left[\eta + Js(t) - w(\eta,t)^2 + I(t)\right], \tag{1.25}$$

where $w(\eta, t) \equiv x(\eta, t) + iy(\eta, t)$. The system described by Eq. (1.25) is still infinite dimensional, since there is one equation for each value of η. However, choosing a particular form for the distribution $g(\eta)$, sharply reduces the dimensionality of the system. Indeed, distributing η according to a Lorentzian distribution of median Θ and width Δ,

$$g(\eta) = \frac{1}{\pi}\frac{\Delta}{(\eta-\Theta)^2+\Delta^2}, \tag{1.26}$$

and extending the integrals Eqs. (1.23) and (1.24) to the complex η plane, we find that only one value of η is relevant. More specifically, assuming

*Please note that in this section we denote firing rate and the mean membrane potential with lower case r and v.

†In the text, we will refer to this quantity as the *mean* membrane potential, as it can be also written as $v(t) = \int_{-\infty}^{\infty} d\eta g(\eta)\left[\lim_{R\to\infty}\int_{-R}^{R}\rho\left(V|\eta,t\right)VdV\right]$.

$\eta = \eta_r + i\eta_i$, we can perform the integrals Eqs. (1.23) and (1.24) by closing the integration path with a half circle in the lower half plane $\eta_r < 0$, since this guarantees that the width $x(\eta, t)$ remains positive zero if initially so. Applying residue theorem, we find that the mean firing rate and the mean voltage only depend on $w(\eta, t)$ evaluated at one of the poles of $g(\eta)$,

$$\pi r(t) + iv(t) = w(\Theta - i\Delta, t). \tag{1.27}$$

Additionally, given this form of $g(\eta)$, also the integral Eq. (1.18) can be performed*, resulting in a voltage distribution $\bar{\rho}(V, t)$ with Lorentzian shape of half width πr and center v

$$\bar{\rho}(V, t) = \frac{r(t)}{[V - v(t)]^2 + \pi^2 r(t)^2}. \tag{1.28}$$

Evaluating now Eq. (1.25) at $\eta = \Theta - i\Delta$, we obtain two nonlinear ordinary differential equations for the evolution of the mean firing rate and the mean membrane potential of the populations of neurons:

$$\tau_m \dot{r} = \frac{\Delta}{\pi\tau_m} + 2rv, \tag{1.29a}$$

$$\tau_m \dot{v} = v^2 + \bar{\eta} - (\pi\tau_m r)^2 + J\tau_m s(t). \tag{1.29b}$$

Initial conditions of the membrane voltages of the populations inside the Lorentzian manifold, clearly will follow the evolution given by Eqs.(1.29). However, it can be proven that the Lorentzian manifold is always attracting, as far as $\Delta > 0$ (Montbrió et al., 2015; Pietras and Daffertshofer, 2016). Namely, any initial condition will always converge toward the manifold defined by Eq.(1.28), with r and v evolving according to Eqs.(1.29). The reason for that is that the LA ansatz Eq.(1.21) is equivalent to the Ott-Antonsen (OA) ansatz for populations of phase oscillators (Ott and Antonsen, 2008, 2009). Specifically, the original work by Ott & Antonsen applies to the Kuramoto model, and it shows that the model admits an exact, low-dimensional description in terms of the Kuramoto order parameter (Ott and Antonsen, 2008). The same theory holds for large populations of globally pulse-coupled oscillators (Pazó and Montbrió, 2014), and in particular for ensembles

*Note that, to solve this integral and integrals Eqs. (1.23) and (1.24), Δ must be strictly positive, so that the poles of $g(\eta)$ do not fall on the real axis. Also, to integrate Eq. (1.18), we need to impose $x(\eta, 0) > 0$, to avoid additional singularities of $\rho(V|\eta, t)$.

of theta-neurons (Luke et al., 2013; So et al., 2014; Laing, 2014, 2015; Coombes and Byrne, 2019; Roulet and Mindlin, 2016). The theta-neuron phase-model can be transformed to a voltage-based description, the QIF model (Ermentrout and Kopell, 1986). Similarly, the macroscopic description for networks of theta-neurons (in terms of the Kuramoto order parameter) transforms into a more natural description for ensembles of QIF neurons in terms of two mean-field quantities of particular relevance in neuroscience: the mean firing rate, and the mean membrane potential (Montbrió et al., 2015).
The two equations Eqs. (1.29), or QIF-Firing rate equations (QIF-FRE) together with the relations specifying the synaptic coupling $s(t)$ (see Eqs.(1.16)) fully describe the dynamics of the network of QIF neurons Eqs. (1.14).

1.5.2 Analysis of the QIF-FRE with instantaneous synapses

In this section, we briefly overview the asymptotic dynamics of the QIF-FRE Eqs. (1.29) with instantaneous synaptic kinetics. We refer the reader to (Montbrió et al., 2015) for a more detailed analysis of the system.
In their simplest variant of infinitely fast synapses $s(t) = r(t)$, the QIF-FRE Eqs. (1.29) take the form:

$$\tau_m \dot{r} = \frac{\Delta}{\pi\tau_m} + 2rv, \tag{1.30a}$$

$$\tau_m \dot{v} = v^2 + \Theta - (\pi\tau_m r)^2 + J\tau_m r(t). \tag{1.30b}$$

The only attractors of Eqs. (1.30) are fixed points. Specifically, three regions with different attractors in parameters space can be distinguished (see Fig.1.9): a region where the only stable solution is a node (white area), a region with one stable focus (grey shading), and a region of bistability of the stable focus and the stable node (cyan region). The blue line, delimiting the bistability region, depicts a saddle node bifurcation, which can be obtained in parametric form: $(\Theta, J)_{\text{SN}} = [-\pi^2 r^2 - 3\Delta^2/(2\pi r)^2, 2\pi^2 r + \Delta^2/(2\pi^2 r^3)]$. The red dotted line, defined by $\Theta_f = -[J/(2\pi)]^2 - (\pi\Delta/J)^2$, separates the region of stable focus from the one of stable node.
Compare the phase diagram of Fig. 1.9 with the corresponding phase

diagram of the Wilson-Cowan equation (see Fig. 1.2 of comment 1.2.1). The stationary (saddle node) bifurcations of the two models are the same. However, while in the Wilson-Cowan equation the fixed points are always of node-type, in the QIF-FRE a stable solution is of focus type. This simple but fundamental difference have important implications when synaptic delays are additionally considered, as we will see in the following chapters.

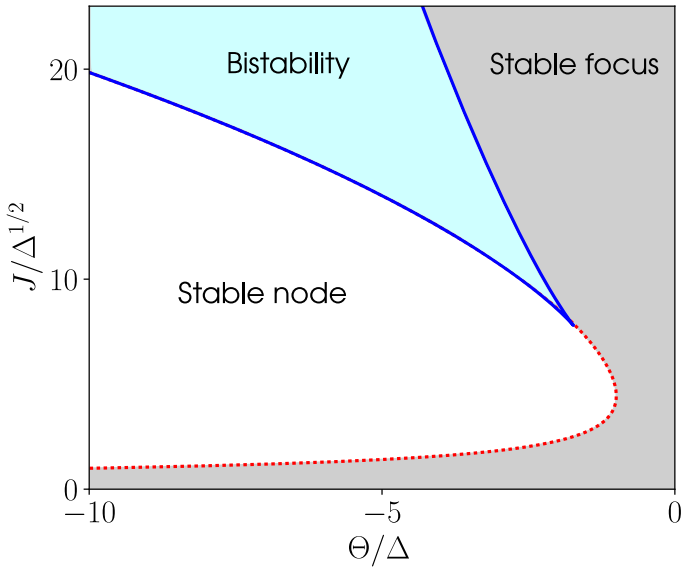

Figure 1.9: Phase diagram of the QIF-FRE Eqs. (1.30). White region: stable node. Gray region: stable focus. Cyan region: bistability among a stable node and a stable focus. The blue line is a saddle node bifurcation, while the red dotted line separates the region of stable node from stable focus.

The QIF-FRE Eqs. 1.29 have been recently analyzed in several different setups (Ratas and Pyragas, 2016, 2017; Dumont et al., 2017; Schmidt et al., 2018; Esnaola-Acebes et al., 2017; Laing, 2018; di Volo and Torcini, 2018). In the following chapters, we analyze and discuss the effect of fixed synaptic delays and synaptic kinetics on the firing rate equations Eqs. (1.29), and compare them with the traditional rate equations presented in the previous sections of this chapter. We will show that, at variance with the H-FRE, the QIF-FRE fully capture the dynamics of networks of spiking neurons, including the synchronous states showed

in this chapter, and more complex forms of synchrony-driven oscillatory dynamics.

CHAPTER 2

Firing rate equations require a spike synchronization mechanism to correctly describe fast oscillations in inhibitory networks

In this chapter, we investigate the dynamics of the QIF-FRE with first order synaptic kinetics. These results are published in:
Devalle F, Roxin A, Montbrió E (2017) *Firing rate equations require a spike synchrony mechanism to correctly describe fast oscillations in inhibitory networks.* PLoS Comput Biol 13(12): e1005881.

2.1 An exact firing rate equation which captures spike synchrony

Here we show that the mechanism responsible for the generation of the oscillations shown in Fig. 1.3 is the interplay between the mean firing rate and membrane potential, the dynamics of which reflect the degree of spike synchrony in the network. To do this, we use a set of exact macroscopic equations which have been recently derived from a population of heterogeneous quadratic integrate-and-fire (QIF) neurons (Montbrió et al., 2015). We refer to these equations as the QIF-FRE. The

QIF-FRE with exponential synapses have the form

$$\tau_m \dot{R} = \frac{\Delta}{\pi\tau_m} + 2RV, \tag{2.1a}$$

$$\tau_m \dot{V} = V^2 - (\pi\tau_m R)^2 - J\tau_m S + \Theta, \tag{2.1b}$$

$$\tau_d \dot{S} = -S + R. \tag{2.1c}$$

where Δ is a parameter measuring the degree of heterogeneity in the network and the other parameters are as in the H-FRE Eqs. (1.10). Eqs. (2.1) are an exact macroscopic description of the dynamics in a large network of heterogeneous QIF neurons with inhibitory coupling. In contrast with the traditional firing rate equations Eqs. (1.10), they contain an explicit dependence on the subthreshold state of the network, and hence capture not only macroscopic variations in firing rate, but also in spike synchrony. Specifically, a transient depolarizing input which drives the voltage to positive values (the voltage has been normalized such that positive values are suprathreshold, see Materials and Methods) will lead to a sharp growth in the firing rate through the bilinear term in Eq. (2.1a). Simulations in the corresponding network model reveal that this increase is due to the synchronous spiking of a subset of neurons (Montbrió et al., 2015). This increase in firing rate leads to a hyperpolarization of the mean voltage through the quadratic term in R in Eq. (2.1b). This term describes the effect of the neuronal reset. This decrease in voltage in turn drives down the mean firing rate, and the process can repeat. Therefore the interplay between mean firing rate and mean voltage in Eqs. (2.1) can generate oscillatory behavior; this behavior corresponds to transient bouts of spike synchrony in the spiking network model.

It is precisely the latency inherent in this interplay which provides the effective delay, which when coupled with synaptic kinetics, generates self-sustained fast oscillations. In fact, in the limit of instantaneous synapses ($\tau_d \to 0$), Eqs. (2.1) robustly display damped oscillations due to the spike generation and reset mechanism described in the preceding paragraph (Montbrió et al., 2015). Contrast this with the dynamics in Eqs.(1.10) in the same limit: the resulting H-FRE is one dimensional and hence cannot oscillate.

On the face of things the Eqs. (2.1) appear to have an utterly distinct functional form from the traditional Wilson-Cowan Eqs.(1.10). In particular, the f-I curve in H-FRE traditionally exhibits an expansive nonlinearity at low rates and a linearization or saturation at high rates, e.g.

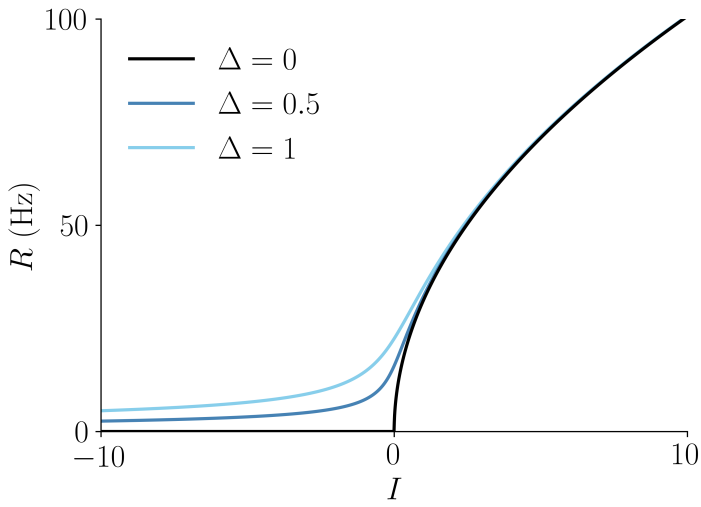

Figure 2.1: The f-I curve $\Phi(I)$, Eq. (2.3), for several values of the heterogeneity parameter Δ. The membrane time constant is $\tau_m = 10$ms.

a sigmoid. There is no such function visible in the QIF-FRE which have only quadratic nonlinearities. However, this seeming inconsistency is simply due to the explicit dependence of the steady-state f-I curve on the subthreshold voltage in Eqs. (2.1). In fact, the steady-state f-I curve in the QIF-FRE is "typical" in the qualitative sense described above. Specifically, solving for the steady state value of the firing rate in Eqs. (2.1) yields

$$R_* = \Phi(-J\tau_m R_* + \Theta), \tag{2.2}$$

where

$$\Phi(I) = \frac{1}{\sqrt{2}\pi\tau_m}\sqrt{I + \sqrt{I^2 + \Delta^2}}. \tag{2.3}$$

The f-I curve Eq. (2.3) is shown in Fig. 2.1 for several values of the parameter Δ, which measures the degree of heterogeneity in the network. Therefore, the steady-state firing rate in Eqs. (2.1), which corresponds exactly to that in a network of heterogeneous QIF neurons, could easily be captured in a heuristic model such as Eqs. (1.10) by taking the function Φ to have the form as in Eq. (2.3). On the other hand, the non-steady behavior in Eqs. (2.1), and hence in spiking networks as well, can be quite different from that in the heuristic Eqs. (1.10).

2.1.1 Fast oscillations in the QIF-FRE

We have seen that decreasing the time constant of synaptic decay τ_d in a network of inhibitory spiking neurons lead to sustained fast oscillations, while such a transition to oscillations is not found in the heuristic rate equations, in which the synaptic dynamics are taken into account Eqs. (1.10). The exact QIF-FRE, on the other hand, do generate oscillations in this regime. Figure 2.2 shows a comparison of the firing rate R and synaptic variable S from simulations of the QIF-FRE Eqs.(2.1), with that of the H-FRE Eqs. (1.10), for two different values of the synaptic time constants. Additionally, we also performed simulations of a network of $N = 5 \times 10^4$ QIF neurons. The mean firing rate of the network is shown in red, and perfectly agrees with the firing rate of the low dimensional QIF-FRE (solid black lines). The function Φ in Eqs. (1.10) is chosen to be that from Eq. (2.3), which is why the firing rate from both models converges to the same steady state value when oscillations are not present (panels (b,d) for $\tau_d = 50$ ms). We will study the transition to fast oscillations in Eqs.(2.1) in greater details in the following sections.

2.2 Linear stability analysis of the QIF-FRE

We can investigate the emergence of sustained oscillations in Eqs. (2.1) by considering small amplitude perturbations of the steady-state solution. If we take $R = R_* + \delta R e^{\lambda t}$, $V = V_* + \delta V e^{\lambda t}$ and $S = S_* + \delta S e^{\lambda t}$, where δR, δV, $\delta S \ll 1$, then the sign of the real part of the eigenvalue λ determines whether the perturbation grows or not. Plugging this ansatz into Eqs. (2.1) yields three coupled linear equations which are solvable if the following characteristic equation also has a solution

$$-2J\tau_m R_* = (1+\tau_d\lambda)\left[(2\pi\tau_m R_*)^2 + \left(\tau_m\lambda + \frac{\Delta}{\pi\tau_m R_*}\right)^2\right]. \quad (2.4)$$

The left hand side of Eq. (2.4) is always negative and, for $\tau_d = 0$, this implies that the solutions λ are necessarily complex. Hence, for instantaneous synapses, the fixed point of the QIF-FRE is always of focus type, reflecting transient episodes of spike synchrony in the neuronal ensemble (Montbrió et al., 2015). In contrast, setting $\tau_d = 0$ in the H-FRE, the system becomes first order and oscillations are not possible. This is the

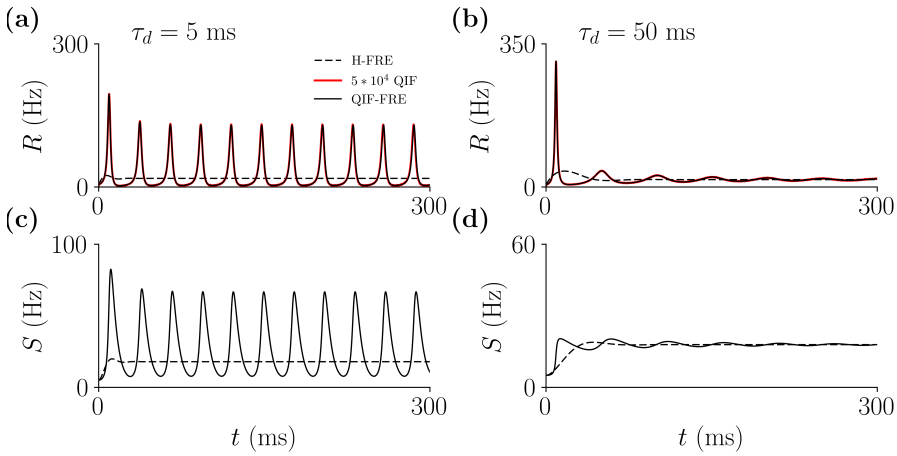

Figure 2.2: Heuristic FRE Eqs. (1.10) do not display inhibition-based fast oscillations. In contrast, networks of QIF neurons (red) and their corresponding QIF-FRE Eqs. (2.1) (solid black) do show ING oscillations for fast synaptic kinetics ($\tau_d = 5$ ms). These oscillations are suppressed for slow synaptic kinetics ($\tau_d = 50$ ms), as in the Wang-Buzsáki model shown in Fig. 1.3. Panels (a,b) show the times series of the Firing Rate variable R of the FRE models, as well as the mean firing rate of a population of $N = 5 \times 10^4$ QIF neurons (red). Panels (c,d) show the time series of the synaptic S variables for the H-FRE (dashed line) and QIF-FRE (solid line). Parameters: $\tau_m = 10$ ms, $J = 21$, $\Theta = 4$, $\Delta = 0.3$. Initial values: $R(0) = S(0) = 5$ Hz, $V(0) = 0$.

critical difference between the two firing rate models. In fact, and in contrast with the eigenvalues Eq. (1.11) corresponding to the growth rate of small perturbations in the H-FRE, here oscillatory instabilities may occur for nonvanishing values of τ_d. Figure 2.3 shows the Hopf boundaries obtained from Eq. (2.4), as a function of the normalized synaptic strength $j = J/\sqrt{\Theta}$ and the ratio of the synaptic and neuronal time constants $\tau = \sqrt{\Theta}\tau_d/\tau_m$, and for different values of the ratio $\delta = \Delta/\Theta$ —see Materials and Methods, Eqs.(2.16-2.18). The shaded regions correspond to parameter values where the QIF-FRE display oscillatory solutions.

2.2.1 Identical neurons

In the simplest case of identical neurons we find the boundaries of oscillatory instabilities explicitly. Indeed, substituting $\lambda = \nu + i\omega$ in Eq. (2.4)

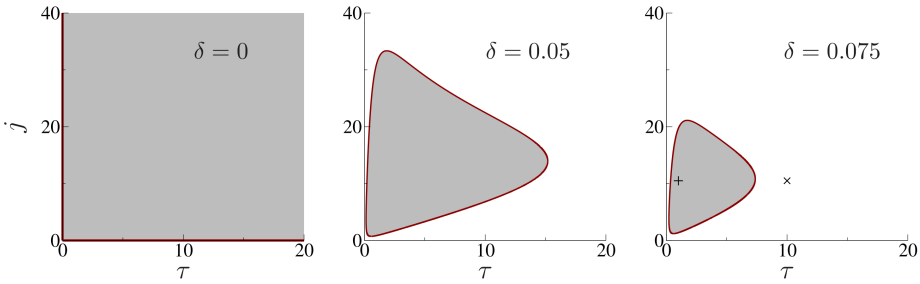

Figure 2.3: The ratio of the width to the center of the distribution of currents Eq. (1.26), $\delta = \Delta/\Theta$, determines the presence of fast oscillations in the QIF-FRE. Oscillations disappear above the critical value given by Eq. (2.6). The panels show the Hopf boundaries of QIF-FRE with first-order synapses, for different values of δ, obtained solving the characteristic Eq. (2.4) with $\mathrm{Re}(\lambda) = 0$, see Materials and Methods. Shaded regions are regions of oscillations. Symbols in the right panel correspond to the parameters used in Fig 2.2.

we find that, near criticality ($|\nu| \ll 1$), the real part of the eigenvalue is

$$\nu \approx J\tau \frac{R_*}{1 + (2\pi\tau_d R_*)^2}. \tag{2.5}$$

Thus, the fixed point (2.2) is unstable for $J\tau > 0$, and changes its stability for either $J = 0$, or $\tau = 0$. In particular, given a non-zero synaptic time constant there is an oscillatory instability as the sign of the synaptic coupling J changes from positive to negative. Therefore oscillations occur only for inhibitory coupling (Van Vreeswijk et al., 1994; Ermentrout, 1994; Hansel et al., 1995). The frequency along this Hopf bifurcation line is determined entirely by the intrinsic firing rate of individual cells $\omega_c = 2\pi R_*$.

On the other hand, in the limit of fast synaptic kinetics, i.e. $\tau_d = 0$ in Eq. (2.4), we find another Hopf bifurcation with $\omega_c = \frac{1}{\tau_m}\sqrt{2\tau_m R_*(J + 2\pi^2\tau_m R_*)}$. This reflects the fact that oscillations cannot be induced if the synaptic interactions are instantaneous. The left panel of Figure 2.3 shows the phase diagram with the Hopf boundaries depicted in Red, reflecting that oscillations are found for all values of inhibitory coupling and for non-instantaneous synaptic kinetics.

2.2.2 Heterogeneous neurons

Once heterogeneity is added to the network the region of sustained oscillatory behavior shrinks, see Fig.2.3, center and right. The red closed curves correspond to the Hopf bifurcations, which have been obtained in parametric form from the characteristic equation (2.4), see Materials and Methods. Note that for small levels of δ, oscillations are present in a closed region of the phase diagram, and disappear for large enough values of τ (the synaptic time constant relative to the neuronal time constant). Further increases in δ gradually reduce the region of oscillations until it fully disappears at the critical value

$$\delta_c = \left(\frac{\Delta}{\Theta}\right)_c = \frac{1}{5}\sqrt{5-2\sqrt{5}} = 0.1453\ldots, \tag{2.6}$$

which has been obtained analytically from the characteristic Eq. (2.4), see Materials and Methods. This result is consistent with numerical studies investigating oscillations in heterogeneous inhibitory networks which indicate that gamma oscillations are fragile against the presence of quenched heterogeneity (Wang and Buzsáki, 1996; White et al., 1998; Tiesinga and José, 2000).

In the following, we compare the phase diagrams of Fig. 2.3 with numerical results using heterogeneous ensembles of Wang-Buzsáki neurons with first order synapses. Instead of using the population mean firing rate or mean synaptic activation, in Fig. 2.4 we computed the amplitude of the population mean membrane potential. This variable is less affected by finite-size fluctuations and hence the regions of oscillations are more easily distinguishable. The results are summarized in Fig. 2.4 for different values of δ and have been obtained by systematically increasing the coupling strength k for fixed values of τ_d. The resulting phase diagrams qualitatively agree with those shown in Fig. 2.3 . As predicted by the QIF-FRE, oscillations are found in a closed region in the (τ_d, k) parameter space, and disappear for large enough values of δ. Here, the critical value of $\delta = \sigma/\bar{I}$ is about 6%, smaller than the critical value given by Eq. (2.6). This is due to the steep f-I curve of the WB model, which implies a larger dispersion in the firing rates of the neurons even for small heterogeneities in the input currents.

Additionally, for small τ_d (fast synaptic kinetics) and strong coupling k, we observed small regions where the oscillations coexist with the asynchronous state —not shown. Numerical simulations indicate that

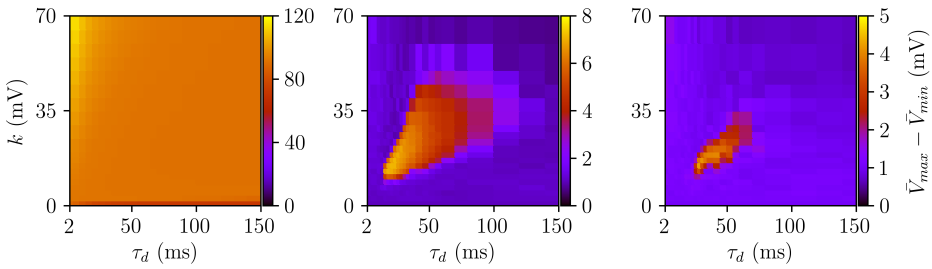

Figure 2.4: Amplitude of the oscillations of the mean membrane potential for a population of $N = 1000$ WB neurons. From left to right: $\delta = \sigma/\bar{I} = 0, 0.05$ and 0.06. Central and Right panels have $\sigma = 0.01$ μA/cm^2. See Materials and Methods for details.

this bistability is not present in the QIF-FRE. For strong coupling, and co-existing with the asynchronous state, we also observed various clustering states, already reported in the original paper of Wang & Buzsáki (Wang and Buzsáki, 1996). Clustering in inhibitory networks has also been observed in populations of conductance-based neurons with spike adaptation (Kilpatrick and Ermentrout, 2011) or time delays (Ernst et al., 1998). The fact that such states do not emerge in the model Eqs. (2.10) may be due to the purely sinusoidal shape of the phase resetting curve of the QIF model (Okuda, 1993; Hansel et al., 1993; Kori and Kuramoto, 2001; Kori, 2003; Politi and Rosenblum, 2015; Clusella et al., 2016).

2.3 Firing Rate Equations in the limit of slow synapses

We have seen that the oscillations which emerge in inhibitory networks for sufficiently fast synaptic kinetics are correctly described by the firing rate equations Eqs. (2.1), but not by the heuristic Eqs. (1.10). The reason for this is that the oscillations crucially depend on the interaction between the population firing rate and the subthreshold membrane potential during spike initiation and reset; this interaction manifests itself at the network level through spike synchrony. Therefore, if one could suppress the spike synchrony mechanism, and hence the dependence on the subthreshold membrane potential, in Eqs. (2.1), the resulting equations ought to bear resemblance to Eqs. (1.10). In fact, as we saw in Fig. 2.2, the two firing

rate models become more similar when the synaptic kinetics become slower.

Next we show that the two models become identical, formally, in the limit of slow synaptic kinetics. To show this, we assume the synaptic time constant is slow, namely $\tau_d = \bar{\tau}_d/\epsilon$ where $0 < \epsilon \ll 1$, and rescale time as $\bar{t} = \epsilon t$. In this limit we are tracking the slow synaptic dynamics in while the neuronal dynamics are stationary to leading order, i.e.

$$R_* = \Phi(-J\tau_m S + \Theta). \tag{2.7}$$

Therefore, the dynamics reduce to the first order equation

$$\tau_d \dot{S} = -S + \Phi(-J\tau_m S + \Theta). \tag{2.8}$$

Notably, this shows that the QIF-FRE Eqs. (2.1), and the H-FRE (1.10), do actually have the same dynamics in the limit of slow synapses. In other words, Eq. (2.8) is formally equivalent to the Wilson-Cowan equations for a single inhibitory population, and this establishes a mathematical link between the QIF-FRE and Heuristic firing rate descriptions. Additionally, considering slow second order synaptic kinetics (not shown), allows one to reduce the QIF-FRE with either alpha or double exponential synapses to a second-order system that formally corresponds to the so-called neural mass models largely used for modeling EEG data, see e.g. (Freeman, 1975; Jansen and Rit, 1995; Robinson et al., 1997; Coombes et al., 2014; Ashwin et al., 2016).

2.3.1 External inputs and breakdown of the slow-synaptic limit Eq. (2.8)

It is important to note that, in the derivation of Eq. (2.8) we considered external inputs Θ to be constant. Then, if synapses are slow, the neuronal variables (R in the case of Eqs. (1.10) and R and V in the case of Eqs. (2.1)) decay rapidly to their fixed point values. However even in the limit of slow synapses, such reduction can break down if external inputs are time-varying $\Theta = \Theta(t)$, with a time-scale which itself is not sufficiently slow.

To demonstrate this, in Fig. 2.5, we compared the dynamics of the QIF-FRE and H-FRE with the approximation Eq. (2.8), for periodic stimuli of various periods —panels (g-i)—, and always considering slow synapses, $\tau_d = 100$ ms. As expected, the models show good agreement

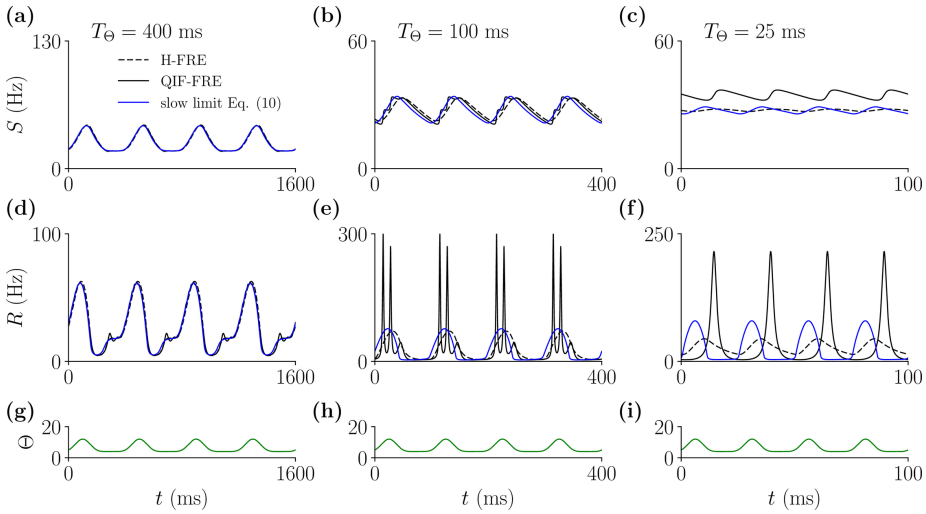

Figure 2.5: The reduction of the QIF-FRE to Eq.(2.8) breaks down when neurons receive time-varying inputs. Panels (a-c): S-variable time series for QIF-FRE (solid Black), H-FRE (dashed Black) and Eq. (2.8) (Blue), for decreasing values of the period T_Θ of the external periodic forcing $\Theta(t) = 4 + [1 + \sin(2\pi t/T_\theta)]^3$ —shown in panels (g-i). In all cases, the synaptic time constant is slow $\tau_d = 100$ ms, compared to the membrane time constant $\tau_m = 10$ ms. Panels (d-f): R-variable time series. In the case of model Eq. (2.8), the firing rate has been evaluated using Eq.(2.7). Other parameters are $J = 21$, $\Delta = 0.3$.

for very slow external inputs —see panels (a,d)—, but this discrepancy is strongly magnified for fast external inputs Specifically, for fast inputs —see panels (c,f)—, the dynamics of the S and R variables of the QIF-FRE are clearly different form those of the other models. This illustrates that even in the limit of slow synapses, the response of spiking networks to arbitrary time-varying inputs will always generate some degree of spike synchrony.

2.4 Discussion

Firing rate models, describing the average activity of large neuronal ensembles are broadly used in computational neuroscience. However, these models fail to describe inhibition-based rhythms, typically observed in networks of inhibitory neurons with synaptic kinetics (Wang and Buzsáki, 1996; Whittington et al., 1995; White et al., 1998; Whittington et al.,

2000; Tiesinga and José, 2000; Brunel and Hansel, 2006; Brunel and Hakim, 2008; Bartos et al., 2007; Wang, 2010). To overcome this limitation, some authors heuristically included explicit delays in traditional FRE, and found qualitative agreement with the oscillatory dynamics observed in simulations of spiking neurons with both synaptic kinetics and fixed time delays (Roxin et al., 2005; Roxin and Montbrió, 2011; Brunel and Hakim, 2008; Keeley et al., 2017). Nonetheless it remains unclear why traditional H-FRE with first order synaptic kinetics do not generate inhibition-based oscillations.

Here we have investigated a novel class of FRE which can be rigorously derived from populations of spiking (QIF) neurons (Montbrió et al., 2015). Networks of globally coupled QIF neurons with fast inhibitory synapses readily generate fast self-sustained oscillations. The corresponding exact FRE, which we call the QIF-FRE, therefore also generates oscillations. The benefit of having a simple macroscopic description for the network dynamics is its amenability to analysis. In particular, the nonlinearities in Eqs.(2.1), which arise due to the spike initiation and reset mechanism in the QIF model, conspire to generate damped oscillations which reflect transient spike synchrony in the network. This oscillatory mode can be driven by sufficiently fast recurrent inhibitory synaptic activation, leading to sustained oscillations. This suggests that any mean-field description of network activity which neglects subthreshold integration will not properly capture spike-synchrony-dependent dynamical behaviors, including fast inhibitory oscillations.

The QIF-FRE have also allowed us to generate a phase diagram for oscillatory behavior in a network of QIF neurons with ease via a standard linear stability analysis, see Fig.2.3. This phase diagram agrees qualitatively with that of an equivalent network of Wang-Buzsáki neurons, suggesting that the QIF-FRE not only provide an exact description of QIF networks, but also a qualitatively accurate description of macroscopic behaviors in networks of Class I neurons in general. In particular, the QIF-FRE capture the fragility of oscillations to quenched variability in the network, a feature that seems to be particularly pronounced for Class 1 neuronal models compared to neural models with so-called Class 2 excitability (Tikidji-Hamburyan et al., 2015).

Finally we have shown that the QIF-FRE and the heuristic H-FRE are formally equivalent in the limit of slow synapses. In this limit the neuronal dynamics is slaved to the synaptic activation and well-described by Eq. (2.8), as long as external inputs are stationary. In fact, in the

absence of quenched heterogeneity ($\Delta = 0$), the approximation for slow synapses Eq. (2.8) is also fully equivalent to the reduction for slow synapses in networks of Class 1 neurons derived by Ermentrout in (Ermentrout, 1994). This further indicates that the QIF-FRE are likely valid for networks of Class 1 neurons in general. However, we also show that in the more biologically plausible scenario of time-varying external drive some degree of neuronal synchronization is generically observed, as in Fig. (2.5), and the slow-synapse reduction Eq. (2.8) is not valid.

The results presented here are obtained under two important assumptions that need to be taken into account when comparing our work to the existing literature on fast oscillations in inhibitory networks. (*i*) A derivation of an exact firing rate model for a spiking neuron network is only possible for ensembles of QIF neurons, which are the canonical model for Class 1 excitability (Ermentrout, 1994; Izhikevich, 2007). Although many relevant computational studies on fast inhibitory oscillations also consider Class 1 neurons (Wang and Buzsáki, 1996; White et al., 1998; Brunel and Hakim, 1999; Brunel and Wang, 2003; Tiesinga and José, 2000; Hansel and Mato, 2003; Keeley et al., 2017), experimental evidence indicates that fast spiking interneurons are highly heterogeneous in their minimal firing rates in response to steady currents, and that a significant fraction of them are Class 2 (Golomb et al., 2007; Tateno et al., 2004; Tateno and Robinson, 2007; Mancilla et al., 2007) —but see also (La Camera et al., 2006). (*ii*) Our derivation of the QIF-FRE is valid for networks of globally coupled QIF neurons, with Lorentzian-distributed currents. In this system inhibition-based oscillations are only possible when the majority of the neurons are self-sustained oscillators, i.e. for $\Theta > 0$ in Eq. (1.26), and are due to the frequency locking of a fraction of the oscillators in the population (Winfree, 1967; Kuramoto, 1984) —as it can be seen in the raster plot of Fig. 1.3(c). In this state, the frequency of the cluster of synchronized oscillators coincides with the frequency of the mean field. The value of the frequency itself is determined through an interplay between single-cell resonance and network effects. Specifically, the synchronized neurons have intrinsic spiking frequencies near that of the mean-field oscillation and hence are driven resonantly. This collective synchronization differs from the so-called sparse synchronization observed in inhibitory networks of identical Class 1 neurons under the influence of noise (Brunel and Hakim, 1999; Brunel and Wang, 2003; Tiesinga and José, 2000; Brunel and Hakim, 2008). In the sparsely synchronized state neurons fire stochastically at very low rates, while the

population firing rate displays the fast oscillations as the ones reported here.

Oscillatory phenomena arising from single-cell resonances, and which reflect spike synchrony at the population level, are ubiquitous in networks of spiking neurons. Mean-field theory for noise-driven networks leading to a Fokker-Planck formalism, allows for a linear analysis of the response of the network to weak stimuli when the network is in an asynchronous state (Ostojic and Brunel, 2011; Ledoux and Brunel, 2011). Resonances can appear in the linear response when firing rates are sufficiently high or noise strength sufficiently low. Recent work has sought to extend H-FRE in this regime by extracting the complex eigenvalue corresponding to the resonance and using it to construct the linear operator of a complex-valued differential equation, the real part of which is the firing rate (Schaffer et al., 2013). Other work has developed an expression for the response of spiking networks to external drive, which often generates resonance-related damped oscillations, through an eigenfunction expansion of the Fokker-Planck equation (de Monte and d'Ovidio, 2002). Our approach is similar in spirit to such studies in that we also work with a low dimensional description of the network response. In contrast to previous work our equations are an exact description of the macroscopic behavior, although they are only valid for networks of heterogeneous QIF neurons. Nonetheless, the QIF-FRE are simple enough to allow for an intuitive understanding of the origin of fast oscillations in inhibitory networks, and in particular, of why these oscillations are not properly captured by H-FRE.

2.5 Materials and Methods

2.5.1 Populations of inhibitory Quadratic Integrate and Fire neurons

We model fast-spiking interneurons, the dynamics of which are well-described by the Hodgkin-Huxley equations with only standard spiking currents. Many models of inhibitory neurons are Class 1 excitable (Rinzel and Ermentrout, 1989), including for example the Wang-Buszáki (WB) (Wang and Buzsáki, 1996), and the Morris-Lecar models (Morris and Lecar, 1981). Class 1 models are characterized by the presence of a saddle-node bifurcation on an invariant circle at the transition from quies-

cence to spiking. One consequence of this bifurcation structure is the fact the spiking frequency can be arbitrarily low near threshold. Additionally, near threshold the spiking dynamics are dominated by the time spent in the vicinity of the saddle-node itself, allowing for a formal reduction in dimensionality from the full neuron model to a reduced normal form equation for a saddle-node bifurcation (Ermentrout, 1994; Izhikevich, 2007; Ermentrout and Terman, 2010). This normal form, which is valid for any Class 1 model near threshold, is known as the quadratic integrate-and-fire model (QIF). Using a change of variables, the QIF model can be transformed to a phase model, called Theta-Neuron model (Ermentrout and Kopell, 1986), which has an strictly positive Phase Resetting Curve (PRC). Neuron models with strictly positive PRC are called Type 1 neurons, indicating that perturbations always produce an advance (and not a delay) of their phase. In general, Class 1 neurons have a Type 1 PRC (Ermentrout, 1994), but see (Achuthan et al., 2011; Ermentrout et al., 2012).

In a network of QIF neurons, the neuronal membrane potentials are $\{\tilde{V}_i\}_{i=1,\ldots,N}$, which obey the following ordinary differential equations (Ermentrout and Kopell, 1986; Latham et al., 2000; Hansel and Mato, 2003):

$$C\frac{d\tilde{V}_i}{dt} = g_L\frac{(\tilde{V}_i - V_t)(\tilde{V}_i - V_r)}{(V_t - V_r)} + I_{0,i} \tag{2.9}$$

where C is the cell capacitance, g_L is the leak conductance and $I_{0,i}$ are external currents. Additionally, V_r and V_t represent the resting potential and threshold of the neuron, respectively. Using the change of variables $\tilde{V}_i' = \tilde{V}_i - (V_t + V_r)/2$, and then rescaling the shifted voltages as $V_i = \tilde{V}_i'/(V_t - V_r)$, the QIF model (2.9) reduces to

$$\tau_m\dot{V}_i = V_i^2 + I_i \tag{2.10}$$

where $\tau_m = C/g_L$ is the membrane time constant, $I_i = I_{0,i}/(g_L(V_t - V_r)) - 1/4$ and the overdot represents derivation with respect to time t. Note that in the model (2.10) the voltage variables V_i and the inputs I_i do not have dimensions. Thereafter we work with QIF model its simplest form Eq. (2.10). We assume that the inputs are

$$I_i = \eta_i - J\tau_m S, \tag{2.11}$$

where J is the inhibitory synaptic strength, and S is the synaptic gating variable. Finally, the currents η_i are constants taken from some prescribed

distribution that here we consider it is a Lorentzian of half-width Δ, centered at Θ

$$g(\eta) = \frac{1}{\pi}\frac{\Delta}{(\eta-\Theta)^2+\Delta^2}. \tag{2.12}$$

In numerical simulations the currents were selected deterministically to represent the Lorentzian distribution as: $\eta_i = \Theta + \Delta\tan(\pi/2(2i - N-1)/(N+1))$, for $i = 1,\ldots,N$. In the absence of synaptic input, the QIF model Eqs.(2.10,2.11) exhibits two possible dynamical regimes, depending on the sign of η_i. If $\eta_i < 0$, the neuron is excitable, and an initial condition $V_i(0) < \sqrt{-\eta_i}$, asymptotically approaches the resting potential $-\sqrt{-\eta_i}$. For initial conditions above the excitability threshold, $V_i(0) > \sqrt{-\eta_i}$, the membrane potential grows without bound. In this case, once the neuron reaches a certain threshold value $V_\theta \gg 1$, it is reset to a new value $-V_\theta$ after a refractory period $2\tau_m/V_\theta$ (in numerical simulations, we choose $V_\theta = 100$). On the other hand, if $\eta_j > 0$, the neuron behaves as an oscillator and, if $V_\theta \to \infty$, it fires regularly with a period $T = \pi\tau_m/\sqrt{\eta_i}$. The instantaneous population mean firing rate is

$$R = \lim_{\tau_s\to 0}\frac{1}{N}\frac{1}{\tau_s}\sum_{j=1}^{N}\sum_{k}\int_{t-\tau_s}^{t} dt'\delta(t'-t_j^k), \tag{2.13}$$

where t_j^k is the time of the kth spike of jth neuron, and $\delta(t)$ is the Dirac delta function. Finally, the dynamics of the synaptic variable obeys the first order ordinary differential equation

$$\tau_d\dot{S} = -S + R. \tag{2.14}$$

For the numerical implementation of Eqs. (2.13,2.14), we set $\tau_s = 10^{-2}\tau_m$. To obtain a smoother time series, the firing rate plotted in Fig. 2.2 was computed according to Eq. (2.13) with $\tau_s = 3\cdot 10^{-2}\tau_m$.

Fixed points of the QIF-FRE Eqs. 2.1

The fixed points of the QIF-FRE (2.1) are obtained imposing $\dot{R} = \dot{V} = \dot{S} = 0$. Substituting this into Eqs. (2.1), we obtain the fixed point equation $V^* = -\Delta/(2\pi\tau_m R^*)$, the firing rate given by Eq. (2.2) and $S_* = R_*$. Note that for homogeneous populations, $\Delta = 0$, the f-I curve Eq. (2.3) reduces to

$$\Phi(I) = \frac{1}{\pi}\sqrt{|I|_+},$$

which displays a clear threshold at $I = 0$ (Here, $|I|_+ = I$ if $I \geq 0$, and vanishes for $I < 0$.) This function coincides with the *squashing function* found by Ermentrout for homogeneous networks of Class 1 neurons (Ermentrout, 1994). As expected, for heterogeneous networks, the well-defined threshold of $\Phi(I)$ for $\Delta = 0$ is lost and the transfer function becomes increasingly smoother.

2.5.2 Nondimensionalized QIF-FRE

The QIF-FRE (2.1) have five parameters. It is possible to non-dimensionalize the equations so that the system can be written solely in terms of 3 parameters. Generally, we adopt the following notation: we use capital letters to refer to the original variables and parameters of the QIF-FRE, and lower case letters for non-dimensional quantities. A possible non-dimensionalization, valid for $\Theta > 0$, is

$$\dot{r} = \delta/\pi + 2rv, \tag{2.15a}$$
$$\dot{v} = v^2 - \pi^2 r^2 - js + 1, \tag{2.15b}$$
$$\tau \dot{s} = -s + r, \tag{2.15c}$$

where the overdot here means differentiation with respect to the non-dimensional time

$$\tilde{t} = \frac{\sqrt{\Theta}}{\tau_m} t.$$

The other variables are defined as

$$r = \frac{\tau_m}{\sqrt{\Theta}} R, \quad v = \frac{V}{\sqrt{\Theta}}, \quad s = \frac{\tau_m}{\sqrt{\Theta}} S.$$

On the other hand, the new coupling parameter is defined as

$$j = \frac{J}{\sqrt{\Theta}}. \tag{2.16}$$

and the parameter

$$\delta = \frac{\Delta}{\Theta}, \tag{2.17}$$

describes the effect of the Lorentzian heterogeneity (1.26) into the collective dynamics of the FRE (1.29). Though the Lorentzian distribution does not have finite moments, for the sake of comparison of our results with

those of studies investigating the dynamics of heterogeneous networks of inhibitory neurons, e.g.(Wang and Buzsáki, 1996; White et al., 1998), the quantity δ can be compared to the coefficient of variation, which measures the ratio of the standard deviation to the mean of a probability density function. Finally, the non-dimensional time

$$\tau = \frac{\sqrt{\Theta}}{\tau_m}\tau_d, \tag{2.18}$$

measures the ratio of the synaptic time constant to the most-likely period of the neurons (times π),

$$\bar{T} = \pi\frac{\tau_m}{\sqrt{\Theta}}.$$

In numerical simulations we will use the original QIF-FRE (2.1), with $\Theta = 4$, and $\tau_m = 10$ms. Thus $\bar{T} = 10\pi/3 \approx 15.71$ms, so that the most likely value of the neurons' intrinsic frequency is $\bar{f} \approx 63.66$ Hz. However, our results are expressed in a more compact form in terms of the quantities j, δ, τ, and we will use them in some of our calculations and figures.

2.5.3 Parametric formula for the Hopf boundaries

To investigate the existence of oscillatory instabilities we use Eq. (2.4) written in terms of the non-dimensional variables and parameters defined previously, which is

$$-2jr_* = (1+\tilde{\lambda}\tau)\left[(2\pi r_*)^2 + \left(\tilde{\lambda} + \frac{\delta}{\pi r_*}\right)^2\right]. \tag{2.19}$$

Imposing the condition of marginal stability $\tilde{\lambda} = i\tilde{\omega}$ in Eq. (2.19) gives the system of equations

$$0 = 2jr_* + 4\pi^2 r_*^2 + 4v_*^2 - (1-4v_*\tau)\tilde{\omega}^2 \tag{2.20a}$$
$$0 = \tilde{\omega}(4v_* - 4\pi^2 r_*^2\tau - 4v_*^2\tau + \tau\tilde{\omega}^2) \tag{2.20b}$$

where the fixed points are obtained from Eq. (2.2) solving

$$0 = v_*^2 - \pi^2 r_*^2 - jr_* + 1, \tag{2.21}$$

with

$$v_* = -\frac{\delta}{2\pi r_*}$$

Eq. (2.20b) gives the critical frequency

$$\tilde{\omega} = \frac{2}{\tau}\sqrt{(\pi\tau r_*)^2 + \tau v_*(\tau v_* - 1)}.$$

The Hopf boundaries can be plotted in parametric form solving Eq. (2.21) for j, and substituting j and $\tilde{\omega}$ into Eq. (2.20a). Then solving Eq. (2.20a) for τ gives the Hopf bifurcation boundaries

$$\tau^{\pm}(r_*) = \frac{\pi^2 r_*^2 - 1 + 7v_*^2 \pm \sqrt{(\pi^2 r_*^2 - 1)^2 - (14 + 50\pi^2 r_*^2)v_*^2 - 15v_*^4}}{16 v_*(\pi^2 r_*^2 + v_*^2)}. \tag{2.22}$$

Using the parametric formula

$$\left(j(r_*), \tau^{\pm}(r_*)\right)^{\pm} = \left(v_*^2/r_* + 1/r_* - \pi^2 r_*, \tau^{\pm}(r_*)\right).$$

we can be plot the Hopf boundaries for particular values of the parameter δ, as r_* is changed. Figure 2.3 shows these curves in red, for $\delta = 0.035$ and $\delta = 0.075$. They define a closed region in parameter space (shaded region) where oscillations are observed.

2.5.3.1 Calculation of the critical value δ_c, Eq. (2.6)

The functions $\tau^{\pm}$ meet at two points, when the argument of the square root in Eq. (2.22) is zero. This gives four different roots for δ, and only one of them is positive and real

$$\delta^*(r_*) = \frac{2\pi r_*}{\sqrt{15}}\sqrt{8\sqrt{1 + 5\pi^2 r_*^2 + 10\pi^4 r_*^4} - 7 - 25\pi^2 r_*^2}.$$

This function has two positive zeros, one at $r_{*min} = 0$, and one at $r_{*max} = 1/\pi$, corresponding, respectively, to the minimal ($j \to \infty$) and maximal ($j = 0$) values of the firing rate for identical neurons ($\delta = 0$). Between these two points the function attains a maximum, where $r_{*min} = r_{*max} = r_{*c}$, with

$$r_{*c} = \frac{1}{\sqrt{2\sqrt{5}\pi}} = 0.1505\ldots$$

The function $\delta^*(r_*)$ evaluated at its local maximum $r_* = r_{*c}$ gives Eq. (2.6).

2.5.4 Populations of Wang-Buzsáki neurons

We perform numerical simulations using the the Wang-Buzsáki (WB) neuron (Wang and Buzsáki, 1996), and compare them with our results using networks of QIF neurons. The onset of oscillatory behavior in the WB model is via a saddle node on the invariant circle (SNIC) bifurcation. Therefore, the populations of WB neurons near this bifurcation are expected to be well described by the theta-neuron/QIF model, the canonical model for Class 1 neural excitability (Ermentrout and Kopell, 1986; Ermentrout, 1994).

We numerically simulated a network of N all-to-all coupled WB neurons. The evolution equations of the WB neuron are given in Appendix A.

In Fig. 2.4, we systematically varied the coupling strength and the synaptic time decay constant to determine the range of parameters displaying oscillatory behavior. For each fixed value of τ_d we varied the coupling strength k; we performed two series of simulations, for increasing and decreasing coupling strength. In Fig. 2.4 we only show results for increasing k.

All quantities were measured after a transient of 1000 ms. To obtain the amplitude of the oscillations of the mean membrane potential, we computed the maximal amplitude $\bar{V}_{\text{max}} - \bar{V}_{\text{min}}$ over time windows of 200 ms for 1000 ms, and then averaged over the five windows.

CHAPTER 3

Dynamics of a large systems of spiking neurons with synaptic delays

In this chapter, we analyse the QIF-FRE with fixed delays. The results are published in:
Devalle, F., Montbrió, E., Pazó, D. (2018). *Dynamics of a large system of spiking neurons with synaptic delay.* Physical Review E, 98(4), 042214.

3.1 Model Description

We consider a network of $N \gg 1$ all-to-all coupled QIF neurons. The membrane potential of the neurons is governed by the following quadratic differential equation (Izhikevich, 2007)

$$\tau \dot{V}_j = V_j^2 + I_j \qquad j = 1, \ldots, N \tag{3.1}$$

where τ is a time constant. Every time the membrane potential of a neuron reaches an upper threshold $V_{\text{th}} \gg 1$ it is said to fire. Obviously, in addition to (3.1), one must define a spike-resetting condition

$$\text{If} \quad V_j > V_{\text{th}} \quad \text{then} \quad V_{\text{reset}} \leftarrow V_j. \tag{3.2}$$

In our theoretical analysis we consider the limits $V_{\text{th}} = -V_{\text{reset}} \to \infty$, which is faithfully reproduced in numerical simulations in the following

way: first, we consider $V_{\text{th}} = -V_{\text{reset}} = 500$. Then, after the firing, we set the neuron at V_{reset} after an inactive period of $2\tau/V_{\text{th}}$. This is the approximate time that a neuron needs to reach $+\infty$ from V_{th} and return from $-\infty$ to V_{reset} *.

The input in Eq. (3.1) is determined by two distinct contributions:

$$I_j = \eta_j + Js\left(t\right). \tag{3.3}$$

The first term represents the quenched heterogeneity, which for neurons in the oscillatory regime ($\eta_j > 0$), determines the intrinsic interspike interval (ISI)

$$T_j = \pi\tau/\sqrt{\eta_j}. \tag{3.4}$$

The second term corresponds to the mean field coupling, where J is the coupling strength and $s\left(t\right)$ is the mean synaptic activation. We consider networks of spiking neurons with delayed, mean-field coupling

$$s(t) = \frac{\tau}{N\tau_s}\sum_{j=1}^{N}\sum_{k}\int_{t-D-\tau_s}^{t-D}\delta\left(t' - t_j^k\right)dt'. \tag{3.5}$$

where t_j^k is the time of the kth spike of neuron j, and τ_s the synaptic time constant. After adopting the thermodynamic limit, $N \to \infty$, we take the limit $\tau_s \to 0$, so that s becomes proportional to the instantaneous population-averaged firing rate at time $t - D$:

$$\lim_{\tau_s\to 0}\lim_{N\to\infty} s(t) = \tau\, r(t-D) \equiv \tau\, r_D.$$

Finally, we assume a Lorentzian (Cauchy) distribution of the quenched heterogeneity

$$g\left(\eta\right) = \frac{\Delta/\pi}{\left(\eta - \bar{\eta}\right)^2 + \Delta^2}. \tag{3.6}$$

3.2 Low-dimensional description: Firing rate equations

In the thermodynamic limit, the network of QIF neurons can be reduced to a finite set of FRE (Montbrió et al., 2015; Pietras and Daffertshofer,

*For the numerical simulations of the population of QIF neurons we use the Euler method with time step $\delta t = 10^{-5}$. For the integration of the FREs Eqs. (3.9) we use a third-order Adams-Bashforth-Moulton predictor-corrector scheme with a timestep $\delta t = 10^{-4}$ (Press et al., 1992). In all simulations shown, initial transients were discarded.

2016). This is possible assuming that the conditional neuron densities $\rho(V|\eta,t)$ are Lorentzian for all η values (Montbrió et al., 2015), which is mathematically equivalent as to invoke the so-called Ott-Antonsen (OA) theory (Ott and Antonsen, 2008).

Considering the QIF model in Sec. 3.1, the FRE consist of a system of two delay differential equations for the firing rate r and for the mean membrane potential

$$v = \int_{-\infty}^{\infty} d\eta\, g(\eta) \left[\lim_{R\to\infty} \int_{-R}^{R} dV\, \rho(V|\eta,t) V \right],$$

which read (Montbrió et al., 2015; Pazó and Montbrió, 2016)

$$\tau \dot{r} = \frac{\Delta}{\pi\tau} + 2rv, \tag{3.7a}$$

$$\tau \dot{v} = v^2 + \bar{\eta} - (\pi\tau r)^2 + J\tau r_D. \tag{3.7b}$$

These FRE describe the evolution of the population of infinitely many spiking neurons in terms of the firing rate r and the mean-membrane potential v of the population of QIF neurons Eq. (3.1). Eqs. (3.7) have 5 parameters, which can be reduced to 3 by nondimensionalization. In Ref. (Pazó and Montbrió, 2016) the FRE Eqs. (3.7) were analyzed under the restriction $\bar{\eta} > 0$, and they were rescaled accordingly. Such rescaling allows to systematically vary the time delay parameter D (including the case $D = 0$), and facilitates the comparison with the classical and well-studied Kuramoto model with delay (Yeung and Strogatz, 1999; Choi et al., 2000; Earl and Strogatz, 2003; Montbrió et al., 2006; Lee et al., 2009).

Alternatively, here we consider a new nondimensionalization which allows us to investigate the dynamics of the FRE Eqs. (3.7) in the entire range of $\bar{\eta}$, so that the majority of the neurons can be either self-oscillatory ($\bar{\eta} > 0$) or quiescent/excitable ($\bar{\eta} < 0$). Specifically, we rescale time and v by D and τ as

$$\tilde{t} = D^{-1} t\,, \quad \tilde{v} = D\tau^{-1} v, \tag{3.8}$$

so that the new, non-dimensional rate is $\tilde{r} = Dr$. Then the dynamics of the FRE can be completely explored, without loss of generality, considering the rescaled parameters

$$\tilde{J} = D\tau^{-1} J\,, \quad \tilde{\bar{\eta}} = D^2\tau^{-2}\bar{\eta}\,, \quad \tilde{\Delta} = D^2\tau^{-2}\Delta,$$

and setting $\tau = D = 1$ in Eqs. (3.7). Specifically, we investigate the nondimensional system of equations

$$\frac{d\tilde{r}}{d\tilde{t}} = \frac{\tilde{\Delta}}{\pi} + 2\tilde{r}\tilde{v}, \tag{3.9a}$$

$$\frac{d\tilde{v}}{d\tilde{t}} = \tilde{v}^2 + \tilde{\bar{\eta}} - (\pi\tilde{r})^2 + \tilde{J}\tilde{r}_{D=1}. \tag{3.9b}$$

To lighten the notation we drop the tildes hereafter (also in the figure labels).

3.3 Populations of Identical Neurons

As we discussed previously, the case of identical oscillatory neurons has been investigated in (Pazó and Montbrió, 2016) using a certain rescaling that required $\bar{\eta} > 0$. Here we adopt the rescaling in Eq. (3.8), which allows us for an exhaustive investigation of the dynamics of the system by systematically varying the parameter $\bar{\eta}$.

Before starting the analysis, we emphasize that the Lorentzian ansatz (or the equivalent OA ansatz) is not strictly valid for identical oscillators. In this case the system is partially integrable and its phase space is foliated by a continuum of invariant manifolds, being the Lorentzian ansatz a particular one. Actually, for the case of identical neurons ($\Delta = 0$), the correct approach is to resort to the so-called Watanabe-Strogatz theory (Watanabe and Strogatz, 1994), instead of the OA ansatz (Pikovsky and Rosenblum, 2011; Laing, 2018). Nevertheless, from a physical perspective the OA/Lorentzian ansatz is very significant since any small amount of noise and/or heterogeneity destroys the degeneracy and, at least for the systems analyzed so far, the density converges to a vicinity of the OA manifold (Tyulkina et al., 2018).

Hence, in the following we analyze the identical case taking into account that its full significance holds once a small amount of noise or heterogeneity is added to the system. However, to avoid the inclusion of noise/heterogeneity in the integration algorithm, we use initial conditions in the Lorentzian manifold in all the numerical simulations of ensembles of identical QIF neurons Eqs. (3.1).

3.3.1 Analytical results: The incoherent and the fully synchronized states

3.3.1.1 The incoherent state

Equation (3.9) has at most four fixed points. In some parameter values one of these points is located in the negative rate region ($r < 0$), and we refer to it as "unphysical". Moreover, for $\Delta = 0$, the axis $r = 0$ is invariant so that solutions initiated with $r(0) > 0$ remain positive for all times. The equilibria of Eqs. (3.9) can be grouped into two sets of fixed points:

- The first pair of fixed points is located in the (r, v) plane at

$$\mathbf{a}_\pm = \left(\frac{J \pm \sqrt{J^2 + 4\pi^2\bar{\eta}}}{2\pi^2}, 0 \right).$$

  For $J > 0$, these fixed points are born at a saddle-node bifurcation located at

$$J_{\mathrm{sn}} = 2\pi\sqrt{-\bar{\eta}}.$$

  This line is partly depicted as a solid green straight line in the phase diagram Fig. 3.1, and is located in the region $\bar{\eta} < 0$. Note that the fixed point $\mathbf{a}_-$ becomes unphysical for $\bar{\eta} > 0$, while $\mathbf{a}_+$ exists for $J < 0$ only if $\bar{\eta} > 0$. As shown below, the fixed point $\mathbf{a}_+$ is stable in a wide range of parameter values. We will refer to $\mathbf{a}_+$ as the incoherent, or the asynchronous state. For finite networks $\mathbf{a}_+$ becomes a so-called splay state, with all neurons firing with the same ISI, and one neuron firing every ISI$/N$ time units.

- The second pair of fixed points,

$$\mathbf{q}_\pm = \left(0, \pm\sqrt{-\bar{\eta}}\right),$$

  only exists for $\bar{\eta} < 0$. They correspond to quiescent states, and coincide with the fixed points of an individual QIF neuron. Hence, $\mathbf{q}_-$ (resp. $\mathbf{q}_+$) is trivially stable (unstable). The bifurcation at $\bar{\eta} = 0$ (green dashed line in Fig. 3.1) is somewhat peculiar because it is not a simple saddle-node bifurcation of $\mathbf{q}_+$ and $\mathbf{q}_-$ as expected. For $J > 0$, it involves the simultaneous collision with $\mathbf{a}_-$, while for $J < 0$ it coincides with the appearance of $\mathbf{a}_+$ for $\bar{\eta} > 0$.

		ASYNC	FULL SYNC	QPS	M-QPS	COLLECTIVE CHAOS
IDENTICAL	**Single neuron:**	Periodic	Periodic	2F-Quasip.	3F-Quasip.	Chaotic-like ($\lambda = 0$)
	Mean field:	Constant	Periodic	Periodic	2F-Quasip.	Chaotic
		ASYNC	**PS-I**	**PS-II**	**M-PS**	**COLLECTIVE CHAOS**
HETEROGENEOUS	**Single neuron:**	Periodic	Periodic, 2F-Quasip.	Periodic, 2F-Quasip.	2F-Quasip., 3F-Quasip.	Chaotic-like ($\lambda < 0$)
	Mean field:	Constant	Periodic	Periodic	2F-Quasip.	Chaotic

Table 3.1: Classification of the different dynamical states observed for populations of both identical, and heterogeneous QIF neurons. The names of the states are the following: ASYNC: Asynchronous or incoherent state. FULL SYNC: fully synchronized state. QPS: Quasiperiodic partial synchronization. M -QPS: modulated quasiperiodic partial synchronization. PS-I and PS-II stands for type I and type II partially synchronous states. M-PS: modulated partially synchronous state. The prefix 2F- and 3F- indicate the number of frequencies of the corresponding quasiperiodic dynamics. For each state we specify the dynamics at the macroscopic level (mean field) and at the microscopic level (single neuron). For the states of collective chaos, λ is the Lyapunov exponent of a single neuron forced by the mean field.

Next we study the linear stability of the fixed points. The incoherent state $\mathbf{a}_-$ is always unstable, while the linear stability analysis of the high activity, asynchronous state $\mathbf{a}_+$ reveals interesting features. Imposing the condition of marginal stability $\lambda = i\Omega$ in the linearization of Eq. (3.9), we find a family of oscillatory instabilities at

$$J_H^{(n)} = \pi\left(\Omega_n^2 - 4\bar{\eta}\right) \times \begin{cases} \left(6\Omega_n^2 + 12\bar{\eta}\right)^{-1/2}, \text{ odd } n \\ \left(2\Omega_n^2 - 4\bar{\eta}\right)^{-1/2}, \text{ even } n \end{cases} \tag{3.10}$$

where $\Omega_n = n\pi$. We point out that these instabilities (represented as blue and red lines in the phase diagram Fig. 3.1) are actually Hopf-like, rather than Hopf, because of two facts: (i) The amplitude equations, computed in the Supplemental Material of (Pazó and Montbrió, 2016), are degenerated. (ii) In the supercritical case, we find that the emerging limit cycle has a period $2\pi/\Omega_n$, which remains constant as one moves away from threshold. This is apparently related to the reversible character of Eqs. (3.9) for $\tilde{\Delta} = 0$ (note the invariance $t \to -t$, $v \to -v$) that, as argued in (Pazó and Montbrió, 2016), stabilizes symmetric orbits with fixed periods when D is nonzero.

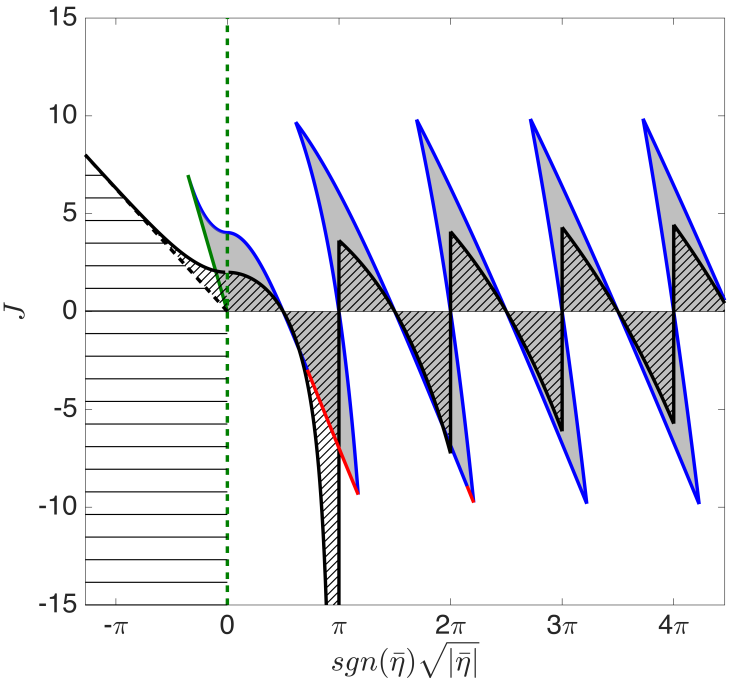

Figure 3.1: Phase diagram for identical neurons, $\Delta = 0$. Shaded region: The asynchronous state ($\mathbf{a}_+$) is stable. Slantwise hatched region: full synchrony is unstable. Horizontally hatched region: The fully synchronized state does not exist and the only attractor is the global rest state $\mathbf{q}_-$. The orbit of fully synchronized self-sustained oscillations is created at the dashed black line (at $\bar{\eta} < 0$), Eq. (3.14). Blue and red lines are the loci of the sub- and super-critical Hopf-like instabilities of incoherence Eqs. (3.10). Solid green line: saddle-node bifurcation. The vertical dashed green line separates the oscillatory from the excitable regime of the QIF neuron.

3.3.1.2 The fully synchronized state

Besides the stability boundary of the asynchronous state, we can also analytically determine the boundaries of full synchrony, $V_j = V(t),\ \forall j$. The FRE Eq. (3.9) are not suitable for this analysis, since the fully synchronized state corresponds to a degenerate infinite trajectory along the v-axis. Full synchrony is hence investigated using the original Eqs. (3.1).

As shown in (Pazó and Montbrió, 2016), for oscillatory dynamics ($\bar{\eta} > 0$) the stability region of full synchrony is bounded by the family of

curves

$$J_s^{(n')} = 2\sqrt{\bar{\eta}}\cot\left(\frac{\sqrt{\bar{\eta}}}{n'}\right) \quad \text{with} \quad n' = 1, 3, .., \tag{3.11}$$

and by the evenly spaced lines $\sqrt{\bar{\eta}} = m\pi$ with $m = 1, 2, 3, ...$

On the other hand, in the case $\bar{\eta} < 0$, we emphasize that the term 'full synchronization' cannot be strictly used since the neurons are excitable and not self-sustained oscillators. However, to simplify the notation, in the following we refer to collective oscillatory states with $\bar{\eta} < 0$ as fully synchronized states. Indeed, due to the presence of time delay, collective self-sustained oscillations could be in principle maintained for strong enough excitatory coupling. To study the existence and stability of these states, we rewrite the QIF model Eq. (3.1) as

$$\dot{V}_j = V_j^2 - |\bar{\eta}| + Jr_D. \tag{3.12}$$

Then, to investigate the existence of a fully synchronized state, we can drop the index j in Eq. (3.12). Note that, in the absence of coupling, Eq. (3.12) has one stable (s) and one unstable (u) fixed points

$$V_u^* = -V_s^* = \sqrt{|\eta|}.$$

Between consecutive spikes, the evolution of the membrane potential of all neurons is given by

$$\dot{V} = V^2 - |\bar{\eta}|. \tag{3.13}$$

Considering that the neurons' membrane potentials reach infinity at $t = 0$, we find that their membrane potentials at the time immediately before receiving the spike, $t = D^- = 1^-$, must satisfy the following equation,

$$\int_{-\infty}^{V\left(1^-\right)} \frac{dV}{V^2 - |\bar{\eta}|} = 1,$$

which gives

$$V\left(1^-\right) \equiv V^- = -\sqrt{|\bar{\eta}|}\coth\sqrt{|\bar{\eta}|}.$$

A necessary condition for the existence of self-sustained collective oscillations is that an excitatory spike causes a jump in V beyond the unstable fixed point, which enables the repetition of the cycle. More precisely, immediately after receiving the first spike, $t = 1^+$, the membrane potential V^+ must satisfy $V^+ > V_u^*$. Then, for $\bar{\eta} < 0$, we find that fully

synchronized solutions exist above the critical coupling

$$J_c = V_u^* - V^- = 2\sqrt{|\bar{\eta}|}\frac{e^{2\sqrt{|\bar{\eta}|}}}{e^{2\sqrt{|\bar{\eta}|}} - 1}. \tag{3.14}$$

To analyze the stability of full synchrony, we study the evolution of an infinitesimal perturbation δV of a single neuron membrane potential away from the cluster formed by the rest of the population. The perturbed neuron and the cluster before the incoming spike evolve according to the flow given by Eq. (3.13). The multiplier of the linearized flow ($\dot{\delta V} = 2V\delta V$) is antisymmetric causing convergence for negative V, and divergence for positive V. Hence, to have a stable fully synchronous solution, the neurons need to spend more time in the convergent region of the flow than in the divergent one. This holds if the instantaneous jump of the membrane potential due to the incoming spike is large enough. Then the critical coupling corresponds to $V^+ = |V^-|$, i.e. $J_s = 2|V^-|$, or

$$J_s = 2\sqrt{|\bar{\eta}|}\coth\sqrt{|\bar{\eta}|}. \tag{3.15}$$

This function is precisely the boundary in Eq. (3.11) with $n' = 1$, which extends to the negative $\bar{\eta}$ region, since $\cot(ix) = -i\coth(x)$. Note also that J_s approaches J_c as $\bar{\eta} \to -\infty$.

3.3.2 Phase diagram

The phase diagram shown in Fig. 3.1 summarizes our analytical results for populations of identical neurons. On the y axis we represent the coupling strength J, which can be either excitatory or inhibitory. On the x axis we represent a quantity that, if positive, is proportional to the natural frequency of the neurons, see Eq. (3.4). Regions with qualitatively different dynamics are highlighted with different combinations of colors and patterns. In the gray shaded regions, the asynchronous state $\mathbf{a}_+$ is stable, while slantwise hatching indicates instability of the fully synchronized state. On the other hand, in the horizontally-hatched area, the global quiescent state $\mathbf{q}_-$ is the only attractor of the system. In the unhatched white region, full synchrony is a stable attractor (and typically the only one–see below), but several of such states may coexist in certain regions for $\bar{\eta} > 0$.

More specifically, in the excitable region ($\bar{\eta} < 0$) of the diagram the global quiescent state $\mathbf{q}_-$ is always stable. In addition, the stability

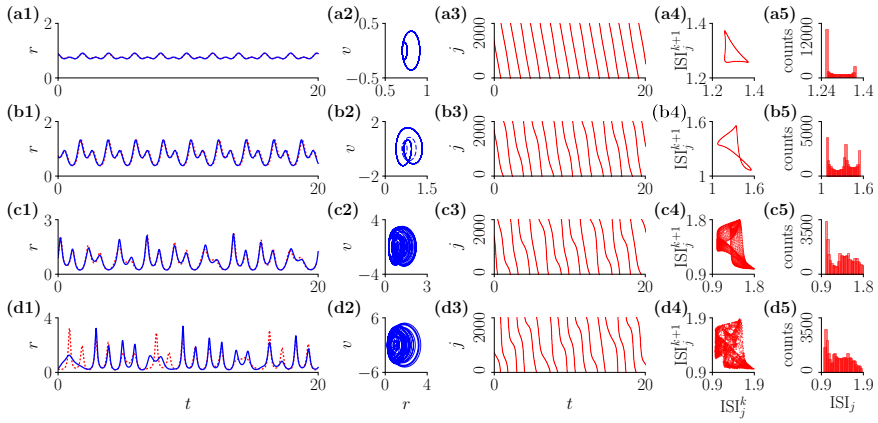

Figure 3.2: Macroscopic (columns 1-2) and microscopic (columns 3-5) dynamics of QPS (rows a,b), M-QPS (row c) and collective chaos (row d), see Table 3.1. Column 1: time series of the mean firing rate. Blue lines correspond to numerical simulations of the FRE Eqs. (3.9), while red dotted lines are obtained computing the mean firing rate of a population of $N = 2000$ QIF neurons. Column 2: (r, v) phase portraits, numerically obtained using Eqs. (3.9). In panel (b2) two coexisting periodic attractors are shown: QPS-asym(I) (solid) and QPS-asym(II) (dashed) —see also inset of Fig. 3.3. Panels (b1,b3-5) correspond to QPS-asym(I). Columns (3-5) show the dynamics of a population of $N = 2000$ QIF neurons. Column 3: raster plots. Neurons are ordered according to their firing time at the beginning of the simulation (due to the first order nature of the QIF model, this ordering is preserved in time). Columns 4 and 5 show return ISI plots and ISI distributions of an arbitrary neuron j. The return plots of panels (a4,b4) are closed curves, indicating quasiperiodic microscopic dynamics in the QPS-sym and QPS-asym. The corresponding ISI histograms (a5,b5) show two (QPS-sym) or three (QPS-asym) peaks. In the M-QPS, neurons are quasiperiodic with three characteristic frequencies — the return plots of panel (c4) is a closed surface in 3D, and therefore its projection in 2D fills a defined region of the space. Parameters: (row a) $J = -9.2$, (row b) $J = -9.5$, (row c) $J = -10.3$, (row d) $J = -10.6$. We use $\sqrt{\bar{\eta}} = 3.6$ in all simulations.

region of the asynchronous state $\mathbf{a}_+$ (grey shading) is bounded by the saddle-node bifurcation J_{sn} (green line), and the Hopf-like bifurcation line $J_H^{(1)}$, Eq. (3.10) (blue line). The two lines meet at a Zero-Hopf codimension-two point. In the unhatched grey region $\mathbf{a}_+$ coexists not only with $\mathbf{q}_-$, but also with the fully synchronized state. This oscillatory state becomes stable at the solid black line Eq. (3.15).

On the other hand, the positive $\bar{\eta}$ region of the diagram is characterized by a sequence of subcritical (blue lines) and supercritical (red lines) Hopf-like bifurcations, defined by Eq. (3.10), that switch the stability of the incoherent state $\mathbf{a}_+$. Remarkably, in this region (where neurons are self-sustained oscillators), the phase diagram bears strong resemblance with that of the Kuramoto model with time delays (Yeung and Strogatz, 1999; Choi et al., 2000; Earl and Strogatz, 2003; Montbrió et al., 2006; Lee et al., 2009). The two systems display tent-shaped regions with an even spacing given by the equality between the delay ($D = 1$) and the intrinsic ISI Eq. (3.4), as well as bistability regions between full sync and incoherence (unhatched gray regions). However, while in the Kuramoto model the Hopf bifurcations are always subcritical, here we find supercritical Hopf bifurcations for some $\bar{\eta}$ values in the inhibitory ($J < 0$) part of the diagram. Near the supercritical Hopf bifurcations, in the unshaded hatched region, both the incoherent and the fully synchronous states are unstable, and partial synchrony (QPS, M-QPS, and collective chaos) is found. In the next section we classify these states in terms of their macroscopic and microscopic dynamics, and investigate their bifurcations.

Finally, we discuss an interesting feature of the phase diagram in Fig. 3.1 —see also the phase diagram in (Pazó and Montbrió, 2016). Note that, at variance with the vertically oriented, tent-shaped regions of the Kuramoto model (Yeung and Strogatz, 1999; Choi et al., 2000; Earl and Strogatz, 2003; Montbrió et al., 2006; Lee et al., 2009), here the regions of stability are tilted. This discrepancy between populations of QIF neurons and the Kuramoto model can be understood as follows: in the QIF model the neurons always advance their phase in response to excitatory inputs, and always delay their phase in response to inhibitory inputs —i.e. they have a so-called Type 1 phase resetting curve. This produces the progressive 'advancement' of the boundaries in the excitatory part of the phase diagram as the strength of the excitatory coupling J is increased —given that neurons increase their firing frequency and thus their effective

value of $\bar{\eta}$. Similarly, in the inhibitory region, the neurons slow down their firing frequency in response to inhibitory inputs, and this progressively 'delays' the boundaries for $J < 0$. In contrast, in the classical Kuramoto model, the terms producing advances and delays in response to excitation and inhibition are not included (Montbrió and Pazó, 2018), and hence the boundaries are not tilted.

3.3.3 Numerical analysis of partially synchronous states

Next we perform a numerical exploration of the partially synchronized states arising both in the white slantwise-hatched region of Fig. 3.1, as well as in some neighboring regions. In Table 3.1 these partially synchronized states are classified according to their dynamics, both for identical and for heterogeneous (in Sec. V) populations of QIF neurons. The macroscopic dynamics of the states is investigated performing numerical simulations of the FRE Eq. (3.9), and illustrated in the columns 1 and 2 of Fig. 3.2. To investigate the single neuron dynamics associated to the macroscopic states we also performed numerical simulations of the original system of QIF neurons Eqs. (3.1), and depicted the raster plots (column 3), and the ISI return maps (column 4) and histograms (column 5). Finally, in column 1, we also show the time series of the population-mean firing rate of the network simulations (dashed red lines), which show a perfect agreement with the time series of the FRE (blue lines) —except in panel (d1), where the collective dynamics is chaotic.

Note that stable partially synchronized states are not only found in the slantwise-hatched region of Fig. 3.1, but also in a neighborhood of this region with $\sqrt{\bar{\eta}} > \pi$. This is because the region where the Hopf-like bifurcation $J_H^{(1)}$ is supercritical (around the red line at $\sqrt{\bar{\eta}} \approx \pi$ in Fig. 3.1) extends to $\sqrt{\bar{\eta}} > \pi$, and hence one expects a low-amplitude periodic solution bifurcating from incoherence, $\mathbf{a}_+$, coexisting with a fully in-phase synchronized state. In Figs. 3.2(a1) and 3.2(a2) we respectively show the time series and the phase portraits corresponding to the numerical integration of Eqs. (3.9) for $\sqrt{\bar{\eta}} = 3.6$. These simulations confirm the presence of a small amplitude symmetric limit cycle, which grows in size as parameters are moved away from the instability.

As analyzed in (Pazó and Montbrió, 2016), in Fig. 3.2(a1) the oscillation period of the mean field is exactly $T = 2$ (or, in dimensional form, $T = 2D$). The periodic dynamics of the global quantities leads to quasiperiodic dynamics of the individual neurons, i.e. Quasiperiodic

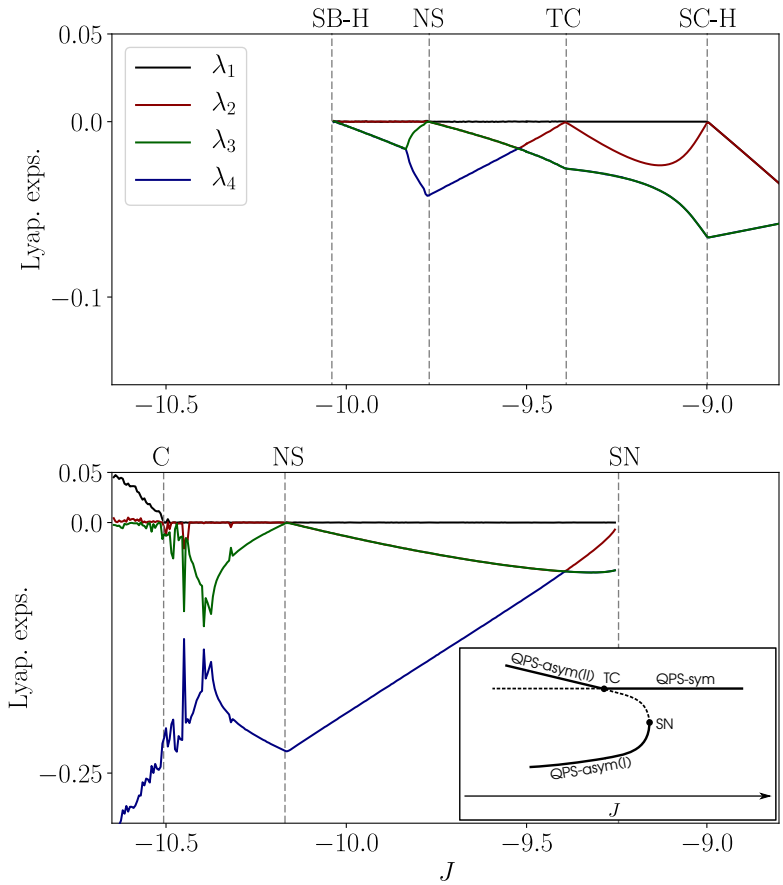

Figure 3.3: Four largest Lyapunov exponents for two alternative bifurcation sequences in a range of negative J values and fixed $\sqrt{\overline{\eta}} = 3.6$. For each solution, the continuation was carried out either increasing or decreasing parameter J adiabatically. In the top panel the vertical dashed lines indicate, from right to left: a supercritical Hopf bifurcation (SC-H), a transcritical bifurcation (TC), a Neimark-Sacker bifurcation (NS), and a subcritical Hopf bifurcation (SB-H). In the bottom panel the vertical dashed lines indicate, from right to left: a saddle-node bifurcation (SN), a Neimark-Sacker bifurcation (NS), and the onset of chaos (C). The inset shows a sketch of the bifurcation diagram connecting the two bifurcation sequences.

partial synchrony (QPS). This may be appreciated plotting the ISIs of a single neuron versus their consecutive ISIs. The resulting return plot, shown in Fig. 3.2(a4), forms a closed curve indicating quasiperiodic

dynamics. Interestingly, the ISIs of the neurons are always shorter than the period of the firing rate oscillations, as shown by the ISI histogram in Fig. 3.2(a5). The bimodal structure of the distribution is related to double-loop shape of the macroscopic periodic attractor.

The limit cycle that emerges via the Hopf-like instability displays a robust $v \to -v$ symmetry that only breaks down after another bifurcation. In (Pazó and Montbrió, 2016), for $\sqrt{\bar{\eta}} = 3$, it was shown that symmetry broke down after a period-doubling bifurcation. Here, taking a slightly larger value of $\sqrt{\bar{\eta}}$ and increasing inhibition, we observe an imperfect symmetry breaking transition, with two coexisting attractors, see Fig. 3.2(b1,b2) and Fig. 3.3. These asymmetric periodic orbits —which we call QPS-asym(I) and QPS-asym(II)— are not related by symmetry. In fact, each attractor is born via a different bifurcation, see details below. In these asymmetric states the period differs from $2D$, but still neurons are quasiperiodic, see Fig. 3.2(b4,b5).

Increasing inhibition further, the macroscopic dynamics becomes more irregular, with no evident periodicity, see Fig. 3.2(c1,c2). Below, we show the analysis of the Lyapunov exponents indicating quasiperiodic mean field dynamics with two incommensurable frequencies. As a consequence of this quasiperiodic forcing, the neurons exhibit three-frequency quasiperiodic motion, see Fig. 3.2(c4). We call this new state modulated QPS, or simply M-QPS, due to the additional modulating frequency. To the best of our knowledge this state has been only reported in a very different setup (Nakagawa and Kuramoto, 1995; Clusella and Politi, 2018). Lowering J further, the M-QPS eventually turns into a chaotic state, see Fig. 3.2(d1,d2).

To determine the bifurcations linking different partially synchronous states (QPS, M-QPS, or collective chaos), we computed the four largest Lyapunov exponents of the FRE on the line along the J direction with $\bar{\eta}$ value of Fig. 3.2. Employing the usual method (Farmer, 1982), parameter J was quasi-adiabatically decreased and increased, to detect eventual bistabilities. Two parallel sequences of bifurcations were eventually detected, as shown in top and bottom panels of Fig. 3.3. In the top panel, moving leftwards, the fixed point attractor ($\mathbf{a}_+$), first undergoes a supercritical Hopf-like bifurcation, after which the stable attractor of the system is a symmetric QPS attractor. The symmetry breaking takes place at a transcritical bifurcation (TC), after which the limit cycle is asymmetric (QPS-asym(II)). At a lower J value, the asymmetric periodic orbit undergoes Neimark-Sacker bifurcation giving rise to M-QPS —

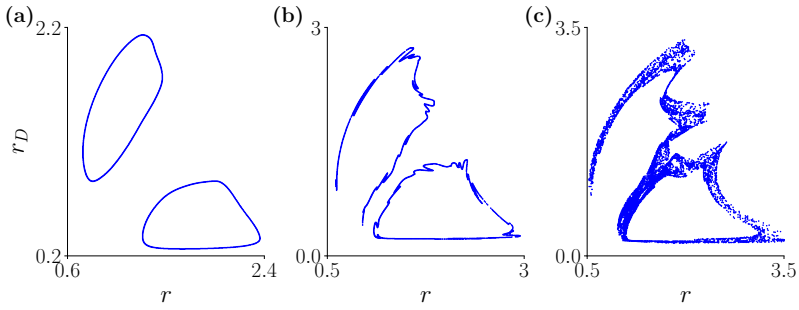

Figure 3.4: Poincaré sections of the FRE (3.9) for $\sqrt{\overline{\eta}} = 3.6$, and for three different values of the inhibitory coupling strength: (a) $J = -10.3$; (b) $J = -10.48$; (c) $J = -10.6$. The Poincaré surface is $v = 0,\ \dot{v} < 0$.

given that we find two vanishing Lyapunov exponents. Further decreasing inhibition, the M-QPS disappears in a subcritical Hopf bifurcation (SB-H).

In the other sequence of bifurcations —bottom panel of Fig. 3.3— another asymmetric orbit (QPS-asym(I)) is born at a saddle-node (SN) bifurcation. As QPS-asym(II), it also undergoes a Neimark-Sacker bifurcation as J is decreased giving rise to M-QPS. In Figs. 3.2 and 3.4 we show the M-QPS state corresponding to this particular sequence of bifurcations. However, note that M-QPS states resulting from either route in Fig. 3.3 have the same dynamical features (two vanishing largest Lyapunov exponents and three-frequency microscopic motion). Lockings occur at certain windows of J, where the second largest Lyapunov exponent is not zero. To further prove the macroscopic quasiperiodic nature of the M-QPS, we also show Poincaré sections for three different values of J in Fig. 3.4. As J is lowered the torus corrugates as typically observed in the transition to chaos via fractalization of the torus (Curry and Yorke, 1978), see Fig. 3.4(b). The torus breaks down around $J = -10.5$, and the attractor turns fractal. Notably, the chaotic attractor achieves rapidly an information dimension larger than three according to the Kaplan-Yorke formula (Kaplan and Yorke, 1979) since $\lambda_1 > |\lambda_3|$, see bottom panel of Fig. 3.3; in contrast with the dimension slightly above two found in (Pazó and Montbrió, 2016) for the chaotic attractor born from the period doubling cascade. It is important to stress that, in spite of the positive Lyapunov exponent (of the collective dynamics), the microscopic dynamics remains nonchaotic, because the individual oscillators have only one degree of freedom. In fact the structure of the model imposes the

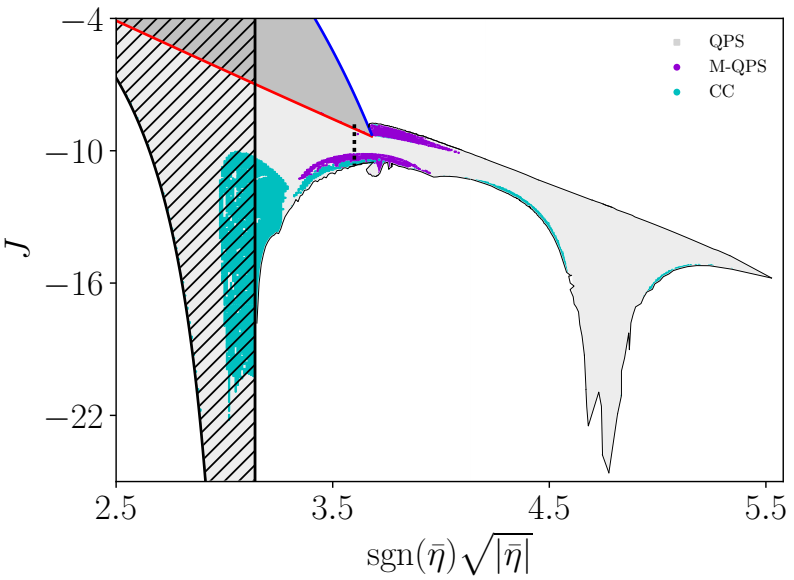

Figure 3.5: Numerical exploration of the partially synchronized states (QPS,M-QPS, collective chaos) near the supercritical Hopf bifurcation in phase diagram Fig. 3.1. In the light gray region the largest Lyapunov exponent is zero, and QPS is stable. The purple dots correspond to two vanishing Lyapunov exponents, indicating quasiperiodic dynamics. In the cyan region the dynamics is chaotic. The vertical dashed black line at $\sqrt{\bar{\eta}} = 3.6$ corresponds to the range of parameters explored in Fig. 3.3.

neurons to fire sequentially, see Fig. 3.2(d3). Finally, the inset in Fig. 3.3 is our conjecture of how the two bifurcation sequences in the main panels are connected: the unstable branch the SN bifurcation collides with the symmetric QPS state at the TC bifurcation.
In the preceding figures we have shown the transitions along a specific $\bar{\eta}$ value. Seeking a more global picture we decided to sweep parameters J and $\bar{\eta}$ monitoring the largest Lyapunov exponents. This permits to identify the attractor types efficiently. Figure 3.5 shows the region spanned by partially synchronized dynamics [*]. The light gray and purple regions indicate QPS and M-QPS states, respectively, while cyan dots correspond to chaotic dynamics. It surprised us the extension of the parameter region where QPS coexists with full synchrony (light shaded

[*]Actually, we have not explored the region close to the supercritical bifurcation just above $\sqrt{\bar{\eta}} = 2\pi$.

unhatched area). There is a "tongue" extending to very negative J values around $\sqrt{\overline{\eta}} = 4.7$ that looks like an "echo" at $3\pi/2 = 4.712\ldots$ of the infinite tongue just below $\sqrt{\overline{\eta}} = \pi$. We have not an intuitive explanation for this. Quasiperiodic dynamics (M-QPS) is found always not far from the degenerate point were the instability boundaries for $n = 1$ and $n = 2$, see Eq. (3.10), meet. This is probably not casual (further analysis is nonetheless beyond our scope*). Regarding the chaotic state, it shows up in two distinct regions: the leftmost one is related to the period-doubling scenario observed in (Pazó and Montbrió, 2016), while the rightmost one is correspond to the quasiperiodic route uncovered here.

3.4 Populations of Heterogeneous neurons

In this section we consider that the neurons in the network are non-identical, and investigate how this alters the phase diagram in Fig. 3.1, and the partially synchronous states depicted in Fig. 3.2. Hence, in the following we assume that the half-width Δ of the Lorentzian distribution Eq. (3.6) is not zero. Under the presence of Lorentzian heterogeneity fully and partially synchronous states discussed previously are unattainable. In the following the generic term 'partial synchronization' refers to any state of the network which is not an incoherent state.

States reminiscent of QPS and collective chaos persist for finite values of Δ, with individual neurons displaying different motions depending on their native T_j values. We denote these states as partial synchronization-I (PS-I) and PS-II for the states reminiscent of full synchrony and QPS, respectively. In PS-I most neurons are 1:1 entrained to the global frequency, and the remaining neurons are either entrained with a different ratio or display quasiperiodic dynamics. In the case of PS-II only a minority of the neurons entrains 1:1 with the macroscopic oscillation. We use the distinction between PS-I and PS-II for convenience, but we emphasize that there is not a clearcut distinction between both states and one can transit from one to the other continuously. As for the other states, the asynchronous state continues to exist after introducing the heterogeneity, although not in the form of a splay state. Finally, M-QPS is replaced by a modulated PS states, or M-PS, while collective chaos continues to exist,

*The degenerate point is a codimension-three point because the instability for $n = 1$ is degenerate exactly at that point (see the Supplemental Material of (Pazó and Montbrió, 2016)).

see Table I.

Next we analyze how the stability regions of incoherence, which can still be analytically computed from the FRE Eqs. (3.9), change due to the presence of heterogeneity. Unfortunately, in the heterogeneous case, a stability analysis similar to that of Sec. IVA for the case of synchronous states is not possible. Later in this section we examine how the partially synchronized states found in the region $\bar{\eta} > 0$ for identical inhibitory neurons are altered by quenched disorder.

3.4.1 Stability boundaries of incoherence and phase diagram for $\Delta = 0.1$

It is important to note that the presence of heterogeneity removes all degeneracies of the FRE Eqs. (3.9). The fixed points can be still obtained in parametric form, as well as the boundaries corresponding to saddle-node bifurcations of the asynchronous/incoherent states, [green lines in Fig. 3.6]. However, these expressions are lengthy and here we omit them for the sake of clarity, see (Montbrió et al., 2015). Linearizing and imposing the condition for marginal stability, also the loci of the Hopf bifurcations can be obtained in parametric form [black lines in Fig. 3.6]. We finally used numerical simulations of Eqs. (3.9) to detect the regions where partially synchronous states become unstable, or cease to exist [dark gray region in Fig. 3.6].

The phase diagram in Figure 3.6 summarizes these results for $\Delta = 0.1$, and displays the regions where distinct dynamics occur —compare with the phase diagram Fig. 3.1. As expected, close to the $J = 0$ axis incoherence is the only attractor of the system (dark shaded). Like in the case of identical neurons, bistability regions between incoherence and another state(s) exist (light shaded). Interestingly, for inhibitory coupling, the Hopf bifurcations of the asynchronous state largely overlap with the numerical boundaries of 'pure' incoherence (dark shading). This indicates that, for inhibitory networks, the intervals where the Hopf bifurcations are supercritical are dramatically enlarged as heterogeneity is increased.

3.4.1.1 Phase diagram in the region $\bar{\eta} < 0$

Figure 3.7 displays an enlarged view of the phase diagram Fig. 3.6, around the brown region located at $\bar{\eta} < 0$. The scenario of bifurcations

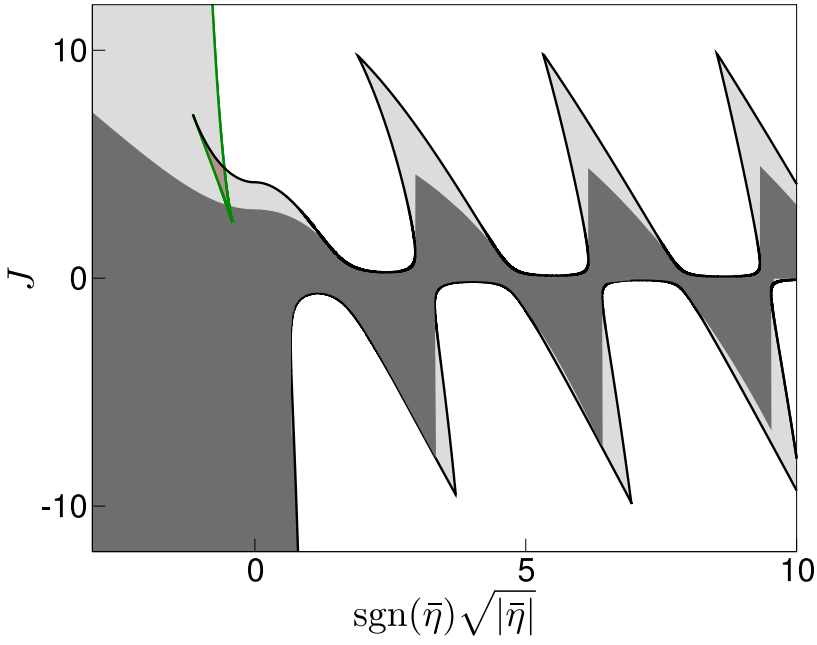

[h!]

Figure 3.6: Phase diagram for populations of heterogeneous neurons, $\Delta = 0.1$. Dark shaded region: Incoherence (fixed point) is the only stable state. Light shaded region: Incoherence (fixed point) coexist with a partially synchronous state (limit cycle). Brown region: Two forms of asynchrony (high and a low activity fixed points) coexist with a partially synchronous state. Green lines are saddle-node bifurcations, and black lines correspond to Hopf boundaries. Note that here, in contrast with Fig. 3.1, the Hopf boundaries are not represented in Blue/Red (we do not explicitly specify whether these boundaries are subcritical or supercritical). The boundary between light and dark shaded regions was obtained numerically.

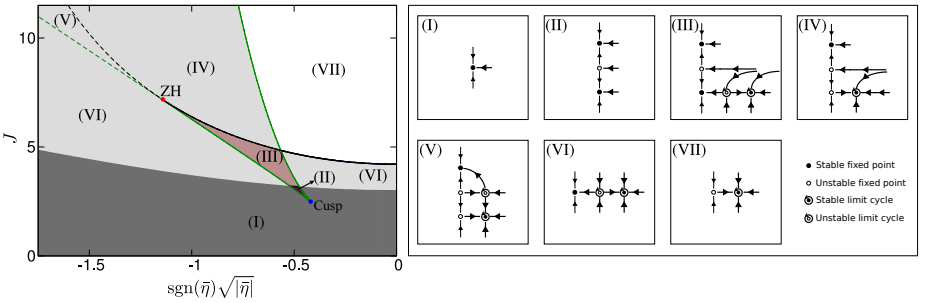

Figure 3.7: Enlarged view of the region of multistability located at $\bar{\eta} < 0$ in Fig. 3.6. Black line: Hopf bifurcation (subcritical). Green lines: saddle-node bifurcations. In the dark shaded region, only the quiescent, low activity state is stable. In the light shaded region, incoherence coexists with a collective oscillatory state —self-sustained due to recurrent excitation. In the brown region the low activity fixed point coexists with a high activity fixed point and with the oscillatory state. In the small dark purple region only the two high and low activity fixed points are attracting. Right panels: Sketches of the Poincaré section in different regions (assuming that it coincides with the one-dimensional manifold that connects different fixed points). The thick lines indicate two-dimensional manifolds, and periodic orbits are indicated by a point surrounded by a small circle.

is quite intricate in this region, and here we describe it in detail. The brown shaded region is interesting since a high-rate and a low-rate fixed points —reminiscent of the fixed points $\mathbf{a}_+$ and $\mathbf{q}_-$— coexist with a periodic orbit. In Fig. 3.7 we have included two dashed lines corresponding to bifurcations involving saddles and/or repellors to fully clarify the transitions between different stable states. We also highlight two codimension-two points: the cusp point where the two saddle-node bifurcations meet, and the zero-Hopf (ZH) point —associated to a zero and a pair of pure imaginary eigenvalues. The different shadings in the figure indicate regions with qualitatively different attractors: in the dark region (I) only one fixed point is stable. In the small dark purple region (II) this fixed point coexists with another stable fixed point. In the light shaded areas (IV,V,VI) a stable fixed point coexists with a stable limit cycle. This limit cycle is the only stable attractor in the white region (VII). Finally, in the brown region (III), there are three coexisting stable attractors: two fixed points, and a limit cycle.

The transitions between any two regions in the diagram can be un-

derstood considering a three-dimensional space. In the right panels of Fig. 3.7 we present sketches of the phase portraits of the different stability regions, by means of Poincaré sections. Thick lines represent two-dimensional manifolds. Comparing the phase diagram in Fig. 3.7 with the results previously obtained for instantaneous interactions (Montbrió et al., 2015), we see that the delay promotes the appearance of a Hopf bifurcation of the asynchronous state. Note that the scenario shown in Fig. 3.7 resembles that of a population of heterogeneous QIF neurons with fast synaptic kinetics (Ratas and Pyragas, 2016), but here we find a codimension-two ZH point, instead of a double-zero eigenvalue point.

3.4.2 Numerical analysis of partially synchronized states in the presence of heterogeneity

Here we explore numerically how the presence of heterogeneity transforms the partially synchronized states described in Sec. IV. In order to circumvent sample-to-sample fluctuations, η_j values are selected deterministically from the Lorentzian distribution setting $\eta_j = \bar{\eta} + \Delta \tan[\pi(2j - N - 1)/(2N + 2)]$, where $j = 1, 2, \ldots, N$. States reminiscent of previous partially synchronous states persist for $\Delta \neq 0$; in columns (1,2) of Fig. 3.8 we show the macroscopic time series of PS-II, M-PS and collective chaos, where blue lines represent numerical integration of the FRE (3.9) and red lines simulation of a population of QIF neurons. All the three states are clearly reminiscent of the QPS, M-QPS and collective chaos states for identical neurons. In the columns (3-5) of Fig. 3.8 we also show the raster plots of the spiking activity of the population of QIF neurons together with the return plots and ISI histograms of a single neuron of the population. Due to the presence of heterogeneity, in the PS-II state neurons can be either periodic or two-frequency quasiperiodic, while in the M-PS they can be two- or three-frequency quasiperiodic, see Table 3.1. The illustrative neuron chosen to plot the return maps and ISI histograms of Fig. 3.8 are, respectively, two-frequency and three-frequency quasiperiodic for panels (a4,a5) and (b4,b5). Note how, as in the QPS-asym in Fig. 3.2(f), the histogram of ISIs for a quasiperiodic neuron in the PS-II state has three peaks, due to the asymmetric shape of the limit cycle.

To further characterize the microscopic dynamics of PS-II, M-PS and collective chaos, in Fig. 3.9 we calculate the time-averaged coupling-

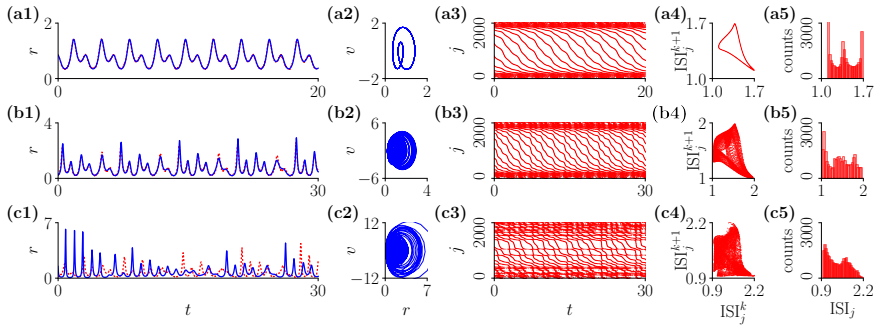

Figure 3.8: Macroscopic (columns 1-2) and microscopic (columns 3-5) dynamics of (row a) PS-II states, (row b) M-PS states, and (row c) collective chaos for heterogeneous neurons, —see Fig. 3.2 and Table 3.1. Column 1: Time series of the firing rate for the FRE Eqs. (3.9) (blue) and for a population of $N = 2000$ QIF neurons Eqs .(3.1) (red dotted). Column 2 shows the corresponding attractors, obtained using the FRE. In rows (a) and (b), the dynamics is periodic but, in contrast with the identical case, here the limit cycle is asymmetric due to the presence heterogeneity. Column 3 shows the raster plots corresponding to numerical simulations of a population of $N = 2000$ QIF neurons Eqs. (3.1), and columns 4 and 5 show the corresponding return plots and ISI histograms, respectively. In the raster plots, each neuron index j corresponds to a specific η_j value (see text). For the computation of return plots and ISI histograms we used neuron $j = 500$. In panels (a4) and (b4) one can see that the neuron behaves quasiperiodically, with two and three incommensurable frequencies, respectively. Note also the three peaks in panel (a5) due to the asymmetry of the limit cycle. In all panels we use $\Delta = 0.1$, $\sqrt{\bar{\eta}} = 3.5$, and (row a) $J = -9.60$; (row b) $J = -10.70$; (row c) $J = -11.30$.

modified ISIs of the neurons, and plot them against each neuron natural ISI T_j. In the PS-II state shown in panel (a), the frequencies of the upper and lower plateaus correspond, respectively, to the average period between two consecutive peaks of the mean field, and to the period of the mean field oscillation in Fig. 3.8. Here it is convenient to recall Table 3.1, where the relations between macroscopic and microscopic dynamics are indicated.

Finally, we investigate the bifurcations that connect these partially synchronous states, again relying on the computation of the Lyapunov spectrum of Eqs. (3.9). As we did in Section IV for identical neurons, we evaluate the four largest Lyapunov exponents along the J direction in the phase diagrams, near the Hopf bifurcation. Figure 3.10 reveals a

scenario qualitatively similar to the identical case (except that, at least for the specific $\bar{\eta}$ value adopted, no bistability was detected). Starting from a fixed point, the Hopf bifurcation produces a periodic solution (PS-II) with a vanishing largest LE, which then undergoes a Neimark-Sacker bifurcation leading to a quasiperiodic solution (M-PS). Eventually, this quasiperiodic solution breaks down giving rise to a chaotic state. Finally, increasing inhibition above a critical level makes the Lyapunov exponents to change abruptly, and chaos is suddenly replaced by a periodic orbit (PS-I). This is in consistency with an exterior crisis undergone by the chaotic attractor.

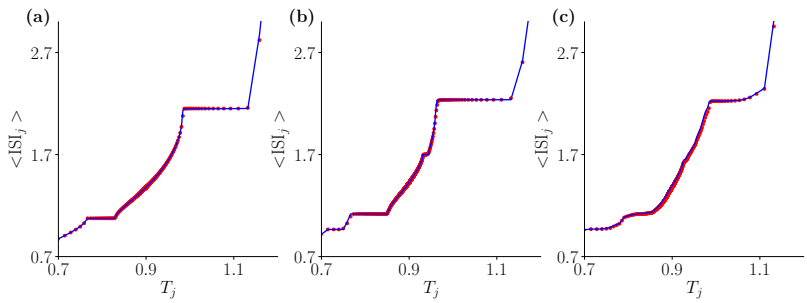

Figure 3.9: Time-averaged coupling-modified ISIs as a function of the intrinsic ISI for a population of 2000 QIF neurons in three different states: (a) PS-II, (b) M-PS, and (c) collective chaos. The red dots are obtained with direct simulations of the population of QIF neurons, while the blue line is obtained forcing each neuron with the FRE. Note the multiple plateaus in the middle panel. Parameters are as in Fig. 3.8: $\sqrt{\bar{\eta}} = 3.5$ and (a) $J = -9.60$; (b) $J = -10.70$; (c) $J = -11.30$.

3.4.3 Boundaries of incoherence for large heterogeneity

At this point, we discussed a fixed value of the heterogeneity $\Delta = 0.1$. We now study the effect of increasing values of Δ on the stability boundaries of incoherence. As previously discussed, the Hopf bifurcations become increasingly supercritical as the level of heterogeneity grows, and this is particularly pronounced for inhibitory coupling. Hence the Hopf boundaries are a good proxy to bound the regions with oscillations of either type (PS-I, PS-II, M-PS, collective chaos).

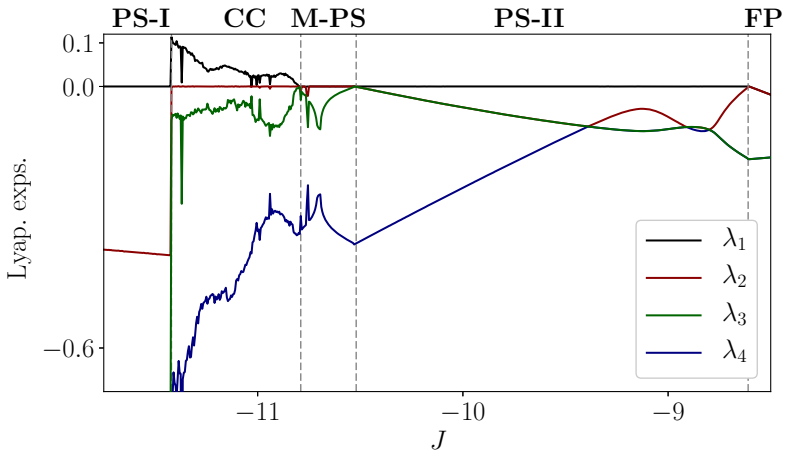

Figure 3.10: The four largest Lyapunov exponents for $\Delta = 0.1$ and $\sqrt{\bar{\eta}} = 3.5$. The stability regions of the different attractors are indicated by vertical gray dashed lines.

Figure 3.11 shows the Hopf boundaries increasing values of Δ. Note that the region of oscillations for inhibitory coupling progressively shrinks, and eventually disappears from the diagram. Accordingly, given a value of $\bar{\eta}$, there is a value of Δ for which, no matter how strong inhibition is, the neurons will not synchronize. The fragility of the oscillations against heterogeneity is consistent with previous computational studies of networks of inhibitory, conductance-based spiking neurons (Wang and Buzsáki, 1996; White et al., 1998; Tiesinga and José, 2000). However, note that synchronization can always be achieved for strong enough excitatory coupling. This highlights a fundamental asymmetry between the excitatory and the inhibitory oscillatory regions in networks of QIF neurons. We emphasize that this asymmetric behavior is not found in the heterogeneous Kuramoto model with delay (Earl and Strogatz, 2003; Montbrió et al., 2006; Lee et al., 2009). A possible explanation for such asymmetry is that, at variance with other self-sustained oscillators, QIF neurons cease to oscillate for strong enough inhibition. On the contrary, excitation just speeds up QIF neurons, which remain oscillatory.

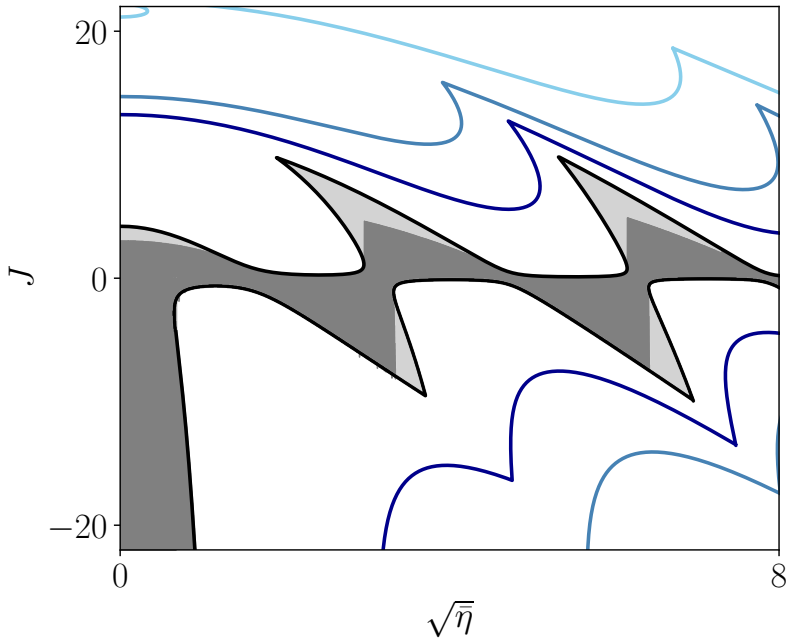

Figure 3.11: Increasing the level of heterogeneity Δ reveals different synchronization scenarios for excitation and inhibition (see text). Black, dark blue, blue and light blue lines correspond, respectively, to the Hopf boundaries of Eqs. (3.9) with $\Delta = 0.1,\ 5,\ 10,\ 20$. These boundaries determine the regions of stability of the incoherent/asynchronous states. In the shaded regions incoherence is stable for $\Delta = 0.1$. In the dark shaded region the only attractor is incoherence.

3.5 Conclusions and Discussion

We analyzed the dynamics of a large population of QIF neurons with synaptic delays. To a large extent the analysis was carried out using the FRE Eqs. (3.9), which is mathematically tractable and allows for an efficient computational analysis. For identical neurons, we have extended the analytical results in (Pazó and Montbrió, 2016) to the excitable regime ($\bar{\eta} < 0$). Our analytical predictions pointed out parameter regimes where non-trivial dynamics should necessarily occur. In these regions of parameters we performed an extensive numerical exploration supported by the computation of the Lyapunov spectrum, which revealed the existence of partially synchronous states. One of these states, which we called M-QPS, appears after a Neimark-Sacker bifurcation of QPS that super-

imposes a second (modulating) frequency. Partially synchronous states —especially QPS— coexist with full synchronization in a large region of the parameter space. The existence in the phase diagram Fig. 3.5 of what looks like a second tongue for QPS is an intriguing finding of this work. Can its origin be understood, at least heuristically? We finally showed that the partially synchronized states observed in the absence of disorder also have their counterpart in the presence of heterogeneity. However, disorder induces diversity in the microscopic behaviors of the single neurons.

To conclude, we demonstrate that most of the dynamics of the FRE Eqs. (3.9) investigated here cannot be reproduced using traditional firing rate models (Wilson and Cowan, 1972; Dayan and Abbott, 2001; Gerstner and Kistler, 2002; Ermentrout and Terman, 2010). To show this we note that the fixed points of Eqs. (3.9) have precisely the structure of traditional firing rate models, while the dynamics is generically different (Devalle et al., 2017). Solving the fixed point equation corresponding to Eq.(3.9a) for v, and substituting it into the fixed point equation corresponding to Eq. (3.9b), one obtains an equation for the steady firing rate

$$r_* = \Phi(Jr_* + \bar{\eta}). \tag{3.16}$$

The function

$$\Phi(x) = \frac{1}{\sqrt{2}\pi}\sqrt{x + \sqrt{x^2 + \Delta^2}},$$

is the so-called 'transfer function' of a population of QIF neurons with Lorentzian distribution of currents (Devalle et al., 2017; Laing, 2014) —steady state equations for arbitrary distributions of currents can be obtained self-consistently, see Eq. (C1) in (Montbrió et al., 2015). Clearly, the traditional first-order firing rate model with time delays

$$\dot{r} = -r + \Phi(Jr_{D=1} + \bar{\eta}), \tag{3.17}$$

largely investigated in the literature has exactly the same fixed points as Eqs. (3.9), but different dynamics —see e.g. (Roxin et al., 2005; Battaglia et al., 2007; Brunel and Hakim, 2008; Roxin and Montbrió, 2011; Ledoux and Brunel, 2011; Keeley et al., 2017; Kim et al., 2018) for studies of Eqs. (3.17) using different transfer functions. Indeed, the linear stabililty analysis of the fixed points of Eq.(3.17) gives the characteristic equation

$$\lambda = -1 + \Phi' J e^{-\lambda},$$

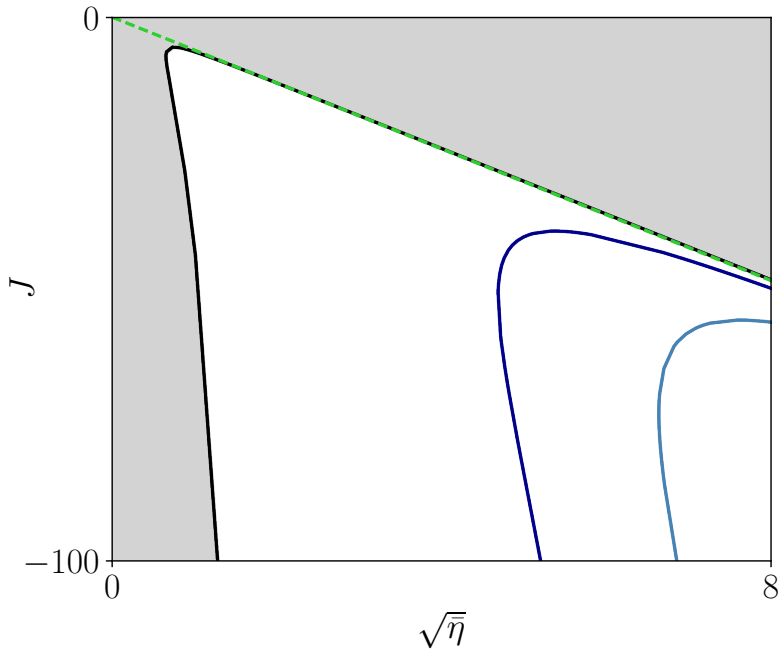

Figure 3.12: Oscillations emerge only for inhibitory coupling in the traditional firing rate model Eq. (3.17). In the gray region, limited by the black line ($\Delta = 0.1$), the fixed point determined by Eq. (3.16) is stable and looses stability via a Hopf bifurcation —compare with Fig. 3.11. The dark blue, and blue curves respectively correspond to $\Delta = 5,$ and 10. The green dashed boundary corresponds to the case $\Delta = 0$ and is a straight line.

where λ is an eigenvalue, and Φ' is the derivative of the transfer function evaluated at the fixed point r_*, determined by Eq. (3.16). The nonstationary instabilities (obtained using the condition of marginal stability $\lambda = i\Omega$) are depicted in Fig. 3.12 for different values of the heterogeneity Δ, and clearly differ from the Hopf boundaries of the FRE (3.9) shown in Fig 3.11. Specifically, the traditional firing rate model Eq. (3.17) only displays oscillations for inhibitory coupling and $\bar{\eta} > 0$, while the FRE Eqs. (3.9) show oscillations for both excitation and inhibition, even for $\bar{\eta} < 0$ —see Figs. 3.1, 3.6, and 3.11. Moreover, the tent-shaped structure of the Hopf boundaries of Eqs. (3.17) is lost in the traditional firing rate model Eq. (3.17).

Nonetheless note that as the heterogeneity Δ is increased, the behavior of the Hopf boundaries of Eq. (3.17) qualitatively agrees with that of

the FRE Eqs. (3.9): The region of oscillations in both models shifts to large $\bar{\eta}$ values, in consonance with the well known result that quenched heterogeneity cannot be counterbalanced by inhibitory coupling to produce synchronization (Wang and Buzsáki, 1996; White et al., 1998; Tiesinga and José, 2000; Devalle et al., 2017). Moreover, we have shown that for large heterogeneity the Hopf boundaries of Eqs. (3.9) become supercritical, and this coincides with what is generically found in traditional firing rate models with small delays (Roxin and Montbrió, 2011). In fact, though Eq.(3.17) is heuristic, it has proven to be remarkably effective at describing the oscillatory dynamics of networks of spiking neurons with strong noise (Roxin et al., 2005; Battaglia et al., 2007; Brunel and Hakim, 2008; Roxin and Montbrió, 2011; Ledoux and Brunel, 2011; Keeley et al., 2017; Kim et al., 2018; Senk et al., 2018), and is a paradigmatic mean-field model to investigate the effect of various types of delays in neuronal networks, see e.g. (Hutt and Atay, 2006; Bressloff and Kilpatrick, 2008; Venkov et al., 2007; Coombes and Laing, 2009; Faye and Faugeras, 2010; Touboul, 2012; Wilson et al., 2012; Veltz, 2013; Veltz and Faugeras, 2013; Faye and Touboul, 2014; Dijkstra et al., 2015).

Finally, we want to note the resemblance of the partially synchronized states investigated here with the so-called sparsely synchronized states (Brunel and Hakim, 2008), in which strong inhibition and noise produce irregular spiking but a coherent macroscopic oscillation. Remarkably, in both states the period of the macroscopic oscillation is determined by the time delay but differs from the ISIs of the single cells. However, microscopically, the neurons have a qualitatively different behavior: in the QPS, their dynamics is purely deterministic and quasiperiodic, while in the sparse synchrony it is stochastic and irregular.

CHAPTER 4

Firing rate equations with synaptic kinetics and fixed delays

In the previous chapters, we separately analyzed the effect of time delays and synaptic kinetics on the dynamics of large networks of spiking neurons. However, the postsynaptic response to a presynaptic action potential is typically characterized by both ingredients, a brief latency (of the order of a few milliseconds, see e.g. (Markram et al., 1997)), followed by a (fast) increase and subsequent decrease of the postsynaptic ionic current.
In this chapter we analyze the QIF-FRE including both a fixed delay and a differential equation for the synaptic kinetics. The model equations we consider are:

$$\tau_m \dot{R} = \frac{\Delta}{\pi\tau_m} + 2RV, \tag{4.1a}$$

$$\tau_m \dot{V} = V^2 - (\pi\tau_m R)^2 + J\tau_m S + \Theta, \tag{4.1b}$$

$$\tau_d \dot{S} = -S + R_D. \tag{4.1c}$$

Note that the fixed point solutions of Eqs. (4.1) are the same as those of the QIF-FRE discussed in chapters 2 and 3. They can be expressed in compact form as $V_* = -\Delta/(2\pi\tau_m R_*)$, $S_* = R_*$, where R_* is the solution of the implicit equation $R_* = \Phi(R_*)$ and Φ is the transfer function for QIF neurons Eq. 2.3.

In this chapter, we will restrict the analysis to $\Theta > 0$, i.e. regimes where the majority of neurons in the population are rhythmically firing.
The number of free parameters in the model equations (4.1) can be reduced with a suitable rescaling. Adopting the same rescaling used in the previous chapter*, we obtain the following (non-dimensional) firing rate equations:

$$\dot{r} = \frac{\delta}{\pi} + 2rv, \tag{4.2a}$$
$$\dot{v} = v^2 - (\pi r)^2 + js + 1, \tag{4.2b}$$
$$\tau \dot{s} = -s + r_d. \tag{4.2c}$$

In the next section we analyze the stability of the fixed point of Eqs. (4.2).

4.1 Oscillatory instabilities

To analyze the stability of the stationary solution of Eqs. (4.2), we linearize around the fixed point setting $r(t) = r_* + \delta r e^{\lambda t}$, $s(t) = s_* + \delta s e^{\lambda t}$ and $v(t) = v_* + \delta v e^{\lambda t}$. We then obtain the following characteristic equation:

$$2jr_* e^{-\lambda d} = (1 + \lambda\tau)\left[(2\pi r_*)^2 + \left(\lambda + \frac{\delta}{\pi r_*}\right)^2\right]. \tag{4.3}$$

Clearly, Eq. (4.3) reduces to the characteristic equation Eq. (2.4) of the system with vanishing delays when $d \to 0$. Imposing the condition of marginal stability $\lambda = i\omega$, we obtain the two following conditions:

$$\omega^2\left(1 + \frac{2\delta\tau}{\pi r_*}\right) - 4\pi^2 r_*^2 - \left(\frac{\delta}{\pi r_*}\right)^2 = -2jr_* \cos\omega d, \tag{4.4a}$$
$$\omega\left[\tau\omega^2 - \frac{\left(2\pi\delta r_* + 4\tau\left(\pi r_*\right)^4 + \tau\delta^2\right)}{\left(\pi r_*\right)^2}\right] = 2jr_* \sin\omega d. \tag{4.4b}$$

*The only extra parameter to be rescaled comparing to *Chapter* 3 is D. The dimensionless variables are then $\tilde{t} = \frac{\sqrt{\Theta}}{\tau_m}t$, $r = \frac{\tau_m}{\sqrt{\Theta}}R$, $v = \frac{V}{\sqrt{\Theta}}$. The new parameters are: $j = \frac{J}{\sqrt{\Theta}}$, $\delta = \frac{\Delta}{\Theta}$, $\tau = \frac{\sqrt{\Theta}}{\tau_m}\tau_d$, $d = \frac{\sqrt{\Theta}}{\tau_m}D$. The overdot in Eqs. (4.2) represents derivative w.r.t. the dimensionless time $\tilde{t}$.

Explicit solutions of Eqs. (4.4) cannot be found; however, parametric formulas for the Hopf bifurcations can be obtained. We first illustrate the simpler case of an identical population of neurons, $\delta = 0$.

4.1.1 Identical neurons $\delta = 0$

Setting $\delta = 0$ in Eqs. (4.4), it is possible to find explicit solutions for d and j, as a function of the Hopf frequency ω. As in the QIF-FRE with instantaneous synaptic kinetics and fixed delays (*Chapter* 3), the system dynamics is characterized by a sequence of Hopf bifurcations. The Hopf boundaries are given by

$$j_H^{(n)} = \pi \alpha_n^{1/2} \left(\omega_n^2 - 4\right) \times \begin{cases} \left(4\alpha_n^{-1} + 8 + 4\omega_n^2 \alpha_n + 2\omega_n^2\right)^{-1/2}, & \text{odd } n \\ \left(4\alpha_n^{-1} - 8 + 4\omega_n^2 \alpha_n - 2\omega_n^2\right)^{-1/2}, & \text{even } n \end{cases} \tag{4.5}$$

$$d_H^{(n)} = \frac{n\pi - \arctan\left(\tau\omega_n\right)}{\omega_n}, \tag{4.6}$$

where $\alpha_n = \sqrt{1 + \tau^2 \omega_n^2}$ and $n \in \mathbb{Z}$. When $\tau \to 0$, we have $\alpha_n = 1$ and $\omega_n = n\pi/d$, then recovering the equations of chapter 3 and (Pazó and Montbrió, 2016) [*]. Remarkably, the formula for the Hopf frequency given by Eq. (4.6) coincides with the formula obtained by Brunel and Wang for the oscillations the emerge in networks of inhibitory spiking neurons with strong noise, the sparsely synchronized state (Brunel and Wang, 2003).

The boundaries Eqs.(4.5,4.6) can be plotted in the plane (d, j) for different values of parameter τ. The resulting phase diagrams are shown in Fig. 4.1. The black lines represent the Hopf bifurcations; in the dark shaded region the fixed point is stable. The tent-shaped structure of both panels is clearly reminiscent of the phase diagrams obtained in the previous chapter for the QIF-FRE with fixed delays. The slower the synaptic kinetics, the more the shape of the tents is modified (right panel of Fig. 4.1). Regions of stable incoherence grow, as the intersections between consecutive Hopf lines shift to larger coupling strengths.

The range of values that parameters can assume is limited by physiological constraints. We then also plot the Hopf lines Eq. (4.5) with

[*]For this reason we indicate ω as ω_n in Eqs. (4.5), even if in this formulation ω has no explicit dependence on n.

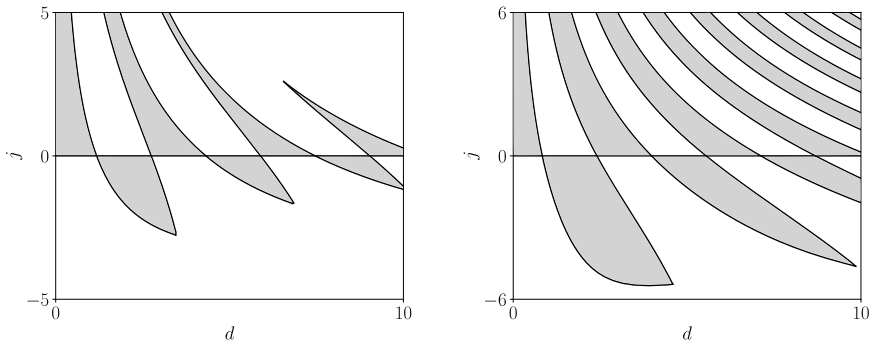

Figure 4.1: Phase diagram of the model Eqs. (4.2) for $\tau = 0.5$ (left) and $\tau = 5$ (right). The black lines are the Hopf bifurcations Eqs.(4.5). Gray shading indicates stability of the fixed point.

dimensional parameters. Synaptic latencies typically are of the order of a few milliseconds (Markram et al., 1997). On the other hand, synaptic decay time constants may vary from a few milliseconds (fast inhibitory GABA-mediated synapses), to tens of milliseconds (slow excitatory NMDA neurotransmitters) (Roth and van Rossum, 2009). In Fig.4.2, we show the phase diagram for Eqs. (4.1) for two values of the intrinsic period of the neurons (left panel: 5 Hz, right panel: 60 Hz) and two values of the synaptic time constant (solid lines: $\tau_d = 5$ ms, dashed lines: $\tau_d = 100$ ms).

In this range of delays, between 0 and 10 ms, only the first three Hopf lines affect the dynamics of the system. When neurons have a low intrinsic firing rate (left panel), oscillations exist mainly in the inhibitory region of the diagram. However, with strong enough coupling and sufficiently large delay, the system undergoes an Hopf bifurcation also for excitatory coupling. With higher intrinsic firing of the neurons (right panel), the crossing of the first Hopf line with the axis $J = 0$ is at $D \simeq 5$ ms, so that the regions of oscillations for excitatory coupling enlarges. As a counter effect, here larger delays prevent oscillations for inhibitory coupling. In both panels, the effect of increasing the synaptic time constant τ_d is modest and mainly quantitative, as it slightly shifts the Hopf lines toward shorter delay (see dashed lines in Fig. 4.2).

These findings indicate that the dynamics of the system strongly depends on the presence of a fixed synaptic delay. Indeed, the effect of varying the synaptic time constant produce no qualitative changes of the phase

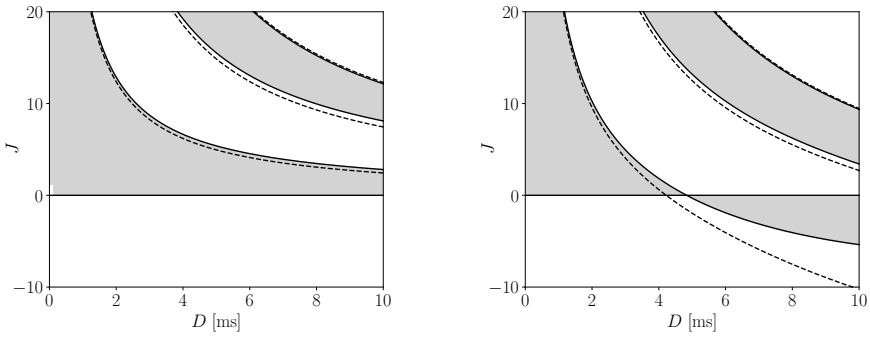

Figure 4.2: Phase diagram of the model Eqs. (4.1) for slow (left) and fast (right) intrinsic frequency of the neurons. The black lines are the Hopf bifurcations Eqs. (4.5). The synaptic time constant τ_d is equal to 10 ms for the solid lines (fast synapses), and to 100 ms for the dashed lines (slow synapses). Grey regions indicate stability of incoherence. Left panel: $\eta = 3.58$. Right panel: $\eta = 0.024$. In both panels, $\tau_m = 10$ ms.

diagram of the model. The characteristic tent-shaped structure of the Hopf bifurcations of the equations with fixed delays persist when the decay time of the synapses is finite. On the other hand, even short delays of the order of few milliseconds (in range with experimental observations of synaptic latencies, see e.g. (Markram et al., 1997)) induce oscillatory dynamics for excitatory coupling, in contrast to the case of first (or second–not shown) order synaptic kinetics, where oscillations appear only for inhibitory interactions.

4.1.2 Heterogeneous neurons $\delta \neq 0$

We now consider an heterogeneous population of neurons, taking $\delta \neq 0$ in Eqs. (4.2). In this case, explicit parametric formulas for j and d cannot be found from Eqs. (4.4), as the fixed point solution of Eqs. (4.2) can be found only numerically.
To plot the Hopf boundaries, we apply the following procedure. Given a value of r_*, from the fixed point condition we find $j_{\text{fp}} = j(r_*)$. Then, we can solve Eq. (4.4b) for $d = d(j_{\text{fp}}, \omega)$. Substituting the solution in Eq.(4.4a), we obtain a numerical solution for ω. We can then plot the boundaries in the plane (d, j), varying parametrically r_*, for different values of δ. The resulting phase diagrams, for $\tau = 0.5$ and $\tau = 5$, are shown in Fig. 4.3. Comparing to the case $\delta = 0$, here incoherence is

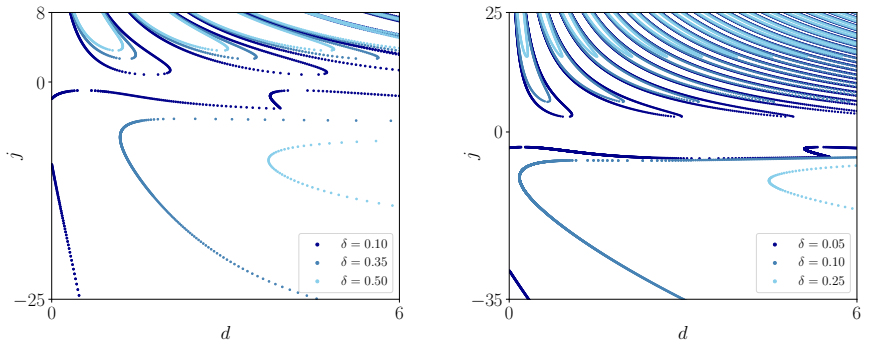

Figure 4.3: Phase diagram of the model Eqs. (4.2) for different values of the heterogeneity δ and the synaptic time constant τ. Left panel: $\tau = 0.5$. Right panel: $\tau = 5$. The scatter points represent the Hopf boundaries obtained from Eqs. (4.4). Different colors stand for different values of the heterogeneity. Oscillations are present inside the islands defined by the Hopf lines.

always stable for small coupling strengths. For small heterogeneity and vanishing delay, for both values of τ, incoherence is unstable in a range of negative j values. This range corresponds to the islands of stable oscillations of the model without delays described in the *Chapter* 2 (see Fig. 2.3). Increasing heterogeneity, while the boundaries in the positive j region persist for large enough coupling, for inhibitory coupling they progressively shift to larger delay values. This is particularly pronounced for large τ values, where already for small values of δ oscillations appear only for large values of the delay. Eventually, the Hopf boundaries completely disappear from the inhibitory region of the diagram. A numerical estimation of the critical value of δ at which the diagram disappears gives $\delta_c = 0.577\ldots$ for both $\tau = 0.5,\ 5$. Thus, oscillations are fragile against heterogeneity in inhibitory networks consistently across the three forms of synaptic coupling considered in this thesis.

As in the previous section, we also show the phase diagram of the system in a parameter space with physical dimensions. The diagram is shown in Fig. 4.4; the parameters chosen are the same as in the right panel of Fig. 4.2. In this range of delays, oscillations appears for both excitatory and inhibitory coupling. While for excitatory coupling, sufficiently increasing the synaptic strength may lead to oscillations, the oscillations rapidly disappear from the inhibitory region of the diagram.

In the next section, we analyse the dynamics of traditional firing rate

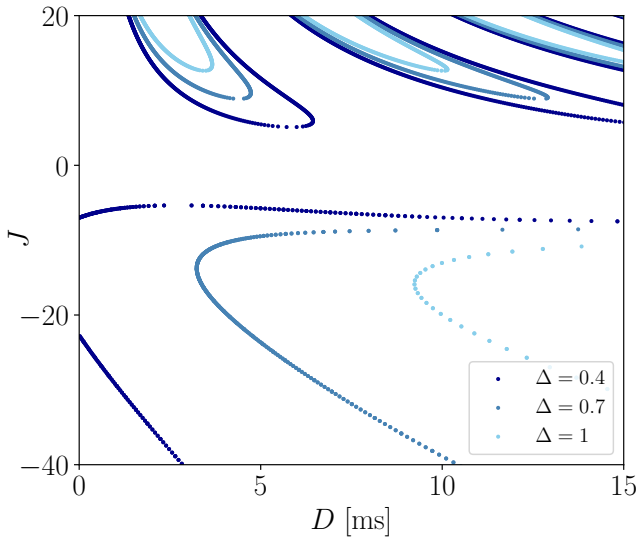

Figure 4.4: Phase diagrams of the QIF-FRE Eqs. (4.1) for different values of the heterogeneity Δ and fast synaptic kinetics $\tau_d = 5$ ms. The scatter points are the Hopf boundaries. Different colors correspond to different values of Δ. All other parameters are as in right panel of Fig. 4.2.

equations with fixed delays and first order synaptic kinetics, to compare it with the results obtained with the QIF-FRE.

4.2 Wilson-Cowan equations with fixed delays and synaptic kinetics

A Wilson-Cowan-type equation with both synaptic kinetics and a fixed delay takes the form:

$$\tau_m \dot{R} = -R + \Phi(J\tau_m S + \bar{\eta}), \tag{4.7a}$$

$$\tau_d \dot{S} = -S + R(t - D), \tag{4.7b}$$

where, as in previous chapters, we choose the function Φ to be the transfer function for QIF neurons Eq. (2.3). The fixed points of Eq. (4.7), determined by the conditions $R_* = \Phi(R_*)$ and $S_* = R_*$, clearly are the same of Eqs. (4.1). Here, we analyse the model without rescaling parameters, even though the same rescaling adopted for the QIF-FRE can be employed.

This model, with fixed delays and synaptic kinetics, also display oscillations, which are induced by the time delay D. Linearizing around the fixed point and imposing the condition of marginal stability $\lambda = i\Omega$, we obtain the following conditions for the emergence of oscillations:

$$\frac{(\tau_m + \tau_d)\Omega}{1 - \tau_m \tau_d \Omega^2} = -\tan(\Omega D), \tag{4.8a}$$

$$(\tau_d + \tau_m)\Omega = -\tau_m J \Phi' \sin(\Omega D), \tag{4.8b}$$

where Φ' is the derivative of the transfer function evaluated at the fixed point. Eqs. (4.8) clearly reduce to Eqs. (1.9) when $\tau_d \to 0$.
Solving for D and Ω, we find:

$$D_H^{(n)} = \frac{\arctan\left[\frac{(\tau_m + \tau_d)\,\Omega}{\tau_m \tau_d \Omega^2 - 1}\right] + n\pi}{\Omega}, \tag{4.9a}$$

$$\Omega = \frac{\sqrt{-\tau_m^2 - \tau_d^2 + \sqrt{\left(\tau_m^2 - \tau_d^2\right)^2 + 4J^2\tau_d^2\left(\Phi'\right)^2}}}{\sqrt{2}\tau_m \tau_d}, \tag{4.9b}$$

where $n \in \mathbb{Z}$.
Hence Eqs. (4.9) together with the fixed point condition $\Phi(R_*) = R_*$, permit to plot the Hopf boundaries in the (D, J) plane for several values of the heterogeneity Δ. The resulting diagram is shown in Fig. 4.5. In contrast to the QIF-FRE, here only the first Hopf line $n = 1$ is relevant for the dynamics of the system, as the subsequent Hopfs destabilize already unstable solutions. Moreover, this line exists only for negative values of the coupling J, in contrast with the QIF-FRE, where oscillatory instabilities exist also for excitatory coupling.
For identical neurons ($\Delta = 0$), the difference between the H-FRE and the QIF-FRE is pronounced also for negative couplings: for short delays, the QIF-FRE display oscillatory behaviour, in contrast to the H-FRE where incoherence is always stable. This result agrees with the fact that the H-FRE with first order synaptic kinetics do not show oscillations, unless some delay is explicitly considered into the equations (Keeley et al., 2017; Devalle et al., 2017). We note that, if second order kinetics is considered (e.g. alpha synapses), then the H-FRE do have an oscillatory instability for vanishing delay– not shown.

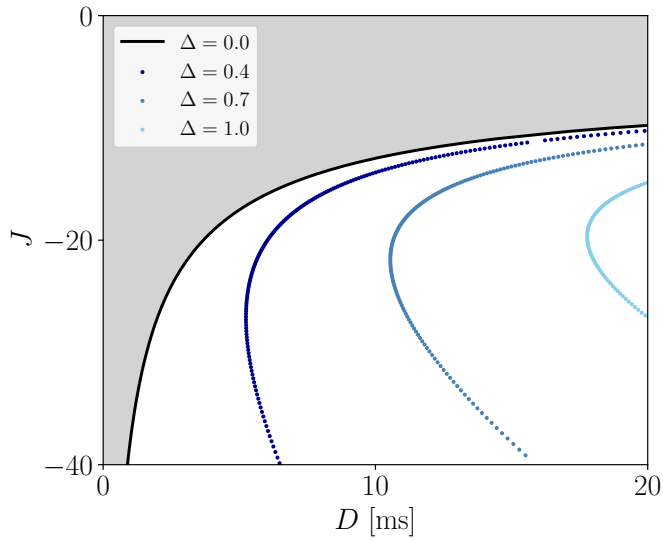

Figure 4.5: Phase diagrams of the Wilson Cowan model Eqs. (4.7) for different values of the heterogeneity Δ. The black line corresponds to the Hopf bifurcation for identical neurons. Gray shading indicates stability of incoherence for identical neurons. The scatter points are the Hopf boundaries obtained varying r_* in Eqs. (4.9). Incoherence is stable left to the Hopf boundaries. All other parameters are as in right panel of Fig. 4.2.

4.2.1 Disappearance of oscillations for large heterogeneity

Increasing heterogeneity, the Hopf lines shift toward larger values of D, as in the QIF-FRE. It is possible to compute the critical value of Δ at which the boundaries disappear. Indeed, imposing that the solutions of Eq. (4.9b) must be real (positive argument of the square root), we find the critical value:

$$\left(\frac{\Delta}{\bar{\eta}}\right)_c = \frac{1}{\sqrt{3}} = \delta_c. \tag{4.10}$$

Note how the relevant parameter for the existence of inhibition-driven oscillation is the previously defined dimensionless quantity δ. At this value of δ, the Hopf frequency Ω vanishes and the boundaries tend to $D \to \infty$, as it can be easily verified by computing the limit $\omega \to 0$ in Eq. (4.9a).
Interestingly, this critical value δ_c coincides with the critical value we

numerically estimated for the QIF-FRE. The value does not depend on the synaptic time constant τ; in fact, it holds also for infinitely fast synapses. In Fig. 3.6 of *Chapter* 3, it corresponds to a vertical line tangent to the Hopf boundary, due to the different variables' rescaling.
In the QIF-FRE, the ratio $\Delta/\bar{\eta}$ establishes the fraction of excitable vs oscillatory neurons. The cumulative distribution of the Lorentzian density of frequencies is:

$$F(\eta) = \frac{1}{\pi}\text{arccot}\left(\frac{\bar{\eta}-\eta}{\Delta}\right),$$

which, for $\eta = 0$, gives:

$$F(0) = \frac{1}{\pi}\arctan\left(\frac{\Delta}{\bar{\eta}}\right).$$

The critical value of the fraction of excitable (non-oscillatory) neurons is then

$$F_c = \frac{1}{\pi}\arctan\delta_c = \frac{1}{6}.$$

Hence, when the fraction of excitable or inactive neurons is above $\sim$16%, both the QIF-FRE and the H-FRE with delays and first order synaptic kinetics do not display oscillations for any (D, J) values. Note that this value does not depend on the decay time constant of the synapses τ_d. On the other hand, we saw in the previous chapter that, when $D = 0$ in Eqs. (4.1), such critical value reduces to $\sim$5 % (see section (2.5.3.1) of chapter 2). This further indicates the importance of the time delay for generating oscillatory behavior.

4.3 Discussion

Presynaptic and dendritic processing unavoidably produce some delay in action potential transmission (Markram et al., 1997). Together with postsynaptic filtering, they contribute to shape the collective dynamics of neuronal populations. In this chapter, we analyzed the combined effect that fixed delays and synaptic kinetics have on the QIF-FRE.
We showed that a fixed time delay is greatly determining the dynamics of the network. In fact, even short delays of the order of a few milliseconds, generate oscillatory instabilities in networks of excitatory neurons.

Oscillatory states cannot be achieved on the other hand in excitatory networks with only first or second order synaptic kinetics. In fact, the effect of introducing a finite time constant in the interaction is mainly quantitative. It certainly favors the emergence of oscillatory behaviours in physiological ranges of the synaptic latency, but does not qualitatively alters the model dynamics.
Moreover, we conducted a similar analysis in the Wilson-Cowan equations for one recurrently coupled population with fixed delays and first order synaptic kinetics. At variance with the QIF-FRE, the H-FRE do not capture the excitation-driven oscillations observed in presence of delays, neither for identical, or heterogeneous neuronal populations. The two models, QIF-FRE and H-FRE, qualitatively agree only for inhibitory coupling, and large heterogeneity.

Conclusions and discussion

In this dissertation, we investigated the emerge of synchrony-driven oscillations in networks of spiking neurons with synaptic delays. For this purpose, we employed a recently derived firing rate model for networks of QIF neurons, the QIF-FRE. We were able to analyze the bifurcation structure of the model to a large extent analytically for different forms of synaptic delays. In parallel to the analysis of the reduced model, we conducted extensive numerical simulations of the underlying network of spiking neurons, which confirm the presence of several synchrony-based oscillatory states. Moreover, we systematically compared the dynamics of the novel QIF-FRE, to that of traditional rate equations of Wilson-Cowan type. In the following we discuss the most relevant results that emerged from the analysis conducted.

Synchrony-driven oscillations and heterogeneity. Synaptic delays favor the emergence of synchronization in networks of spiking neurons (Wang and Buzsáki, 1996; Van Vreeswijk et al., 1994; White et al., 1998). Synchronous neuronal firing is reflected at the macroscopic level by collective rate oscillations. Traditional firing rate equations cannot describe such oscillations, as they generally capture the dynamics of highly asynchronous networks' states (Wilson and Cowan, 1972; Abbott and van Vreeswijk, 1993).

The firing rate equations employed in this dissertation faithfully capture synchronous neuronal firing, and hence correctly display the macroscopic self-sustained oscillations that synaptic delays generate in networks of spiking neurons. It is well known that such synchrony-driven oscilla-

tions are fragile against heterogeneity for inhibitory networks (Wang and Buzsáki, 1996; White et al., 1998; Tiesinga and José, 2000). In contrast to the Kuramoto model with time delays, where increasing (either excitatory or inhibitory) coupling, may always result in a synchronization transition (Yeung and Strogatz, 1999; Montbrió et al., 2006), networks of inhibitory neurons cease to oscillate when heterogeneity is too strong (Wang and Buzsáki, 1996; White et al., 1998; Tiesinga and José, 2000). We have shown that this phenomenon is well captured and predicted by the QIF-FRE. For all three forms of synaptic delays considered in this thesis, oscillations in inhibitory networks are suppressed beyond a critical value of the heterogeneity, no matter the strength of recurrent connections.

The relation of the QIF-FRE with traditional firing rate models. As previously discussed, traditional firing rate models, at variance with the QIF-FRE, do not describe synchronous states. The fundamental reason for this discrepancy resides in the fact that, while traditional rate rate models only keep track of the mean firing rate of the neuronal population, the firing rate equations employed in this dissertation track both the mean firing rate *and* the mean membrane voltage (Montbrió et al., 2015). This difference produces important effects on the network dynamics, particularly concerning oscillatory behavior. Already a comparison of the QIF-FRE and traditional rate models in the simple setting of one excitatory recurrently coupled population with instantaneous synapses, reveals a simple but essential discrepancy. While the steady bifurcations of the two models are the same, the high activity stable fixed point of the QIF-FRE is a focus rather than a node (i.e. perturbations decay oscillating to the fixed point) (Montbrió et al., 2015). This feature is what constitutes the substrate in the QIF-FRE for the presence of the self-sustained oscillatory states shown in *Chapters* 2 and 3 when synaptic kinetics, or time delays, are considered.
The dynamical regimes that traditional rate models show are also captured by the QIF-FRE. The bistability among high and low activity fixed points is inherent to the fixed point structure of the two models. The oscillations that emerge when explicit delays are introduced in the traditional rate equations for inhibitory networks are also captured by the QIF-FRE (*Chapter* 3). Interestingly, traditional rate equations are generally considered to describe highly asynchronous network states, in the noise-dominated regime. Using the QIF-FRE however, the microstates of the network can be directly observed, and it can be appreciated that

the neuronal dynamics is purely deterministic, and that the network state underlying the collective oscillations is partially synchronous (*Chapter* 3). This consideration further underlines the non-trivial relation among the microscopic state of a network, and its macroscopic or collective dynamics.
When the voltage-dependent spike synchronization mechanism is suppressed the QIF-FRE and the H-FRE become formally equivalent, and have the same dynamical behaviour (*Chapter* 2). This is what occurs when synaptic kinetics is assumed to be much slower than neuronal dynamics (and external inputs are also slow). In this limit, the neuronal variables (firing rate and membrane potential in the QIF-FRE, only the firing rate in the H-FRE), rapidly converge to their fixed points, suppressing the rate-voltage interplay of the QIF-FRE and therefore the spike-synchronization mechanism.
In the case of fixed delays (*Chapter* 3), no formal equivalence among the two models is found. Still, for inhibitory coupling, the phase diagrams of the QIF-FRE and the corresponding H-FRE become increasingly similar as heterogeneity is increased. The tendency of the QIF-FRE and H-FRE to agree as heterogeneity is increased holds also when both synaptic kinetics and fixed delays are simultaneously considered (*Chapter* 4). Also in the latter case, a reduction of the QIF-FRE to a Wilson-Cowan type equation is hard to achieve and requires further investigations, as more time scales are involved in the system dynamics (the fixed delay, the time constant of the synaptic dynamics, and the neuronal time constant).

Dichotomy among macroscopic and microscopic dynamics. A great advantage of the Ott-Antonsen theory is that it offers a description at two different scales: the microscopic (single neurons) dynamics, and the macroscopic (mean-field) dynamics. This allows to explore the relation among the two spatial scales. From a theoretical perspective, this fact represents a novelty in the field: typically, firing rate descriptions are not exactly derived from the underlying network of spiking neurons, and hence do not establish a precise relationship among the microscopic and the macroscopic scale.
For Kuramoto-like synchronous states (e.g. the oscillations shown in Chapter 2) the relation among neuronal and mean-field dynamics is transparent. The neurons that contribute to the mean-field oscillations are frequency-locked and regularly fire at the same frequency as the mean field. On the other hand, for the partially synchronous states illustrated

in Chapter 3, such as the QPS and the M-QPS, the micro-macro relation is far more intricate: in the QPS, a periodic mean field is produced self-consistently by a population of quasiperiodic neuronal oscillators. The neurons ”feel” a periodic mean-field, with incommensurable frequency to their own: therefore they behave quasiperiodically. Intriguingly, the mean-field is produced by the population itself. The neurons contributing to the peaks of the mean field change over time, at variance with the Kuramoto-like synchronous states.
In the M-QPS, a similar reasoning can be carried out, with the difference that here the mean-field is quasiperiodic: single neuron dynamics is then also quasiperiodic, but with three, rather than two, frequencies. The microscopic-macroscopic dichotomy emerges also in the chaotic states: here, the collective dynamics is chaotic, while the single neurons have either zero (if they are identical) or negative Lyapunov exponents (*Chapter* 3 and (Pazó and Montbrió, 2016)).
Remarkably, the presence of complex partially synchronous states as the QPS is revealed by the QIF-FRE. This fact shows the utility of low-dimensional descriptions as the QIF-FRE to analyze and investigate the dynamics of large neuronal networks. Thanks to their simplicity, such firing rate descriptions allow to uncover and thoroughly analyze complex dynamical regimes.

Open questions and perspectives for future work

The firing rate equations employed in this dissertation have shown to be a valuable tool to investigate the dynamics of networks of spiking neurons. Specifically, at variance with traditional firing rate equations the QIF-FRE correctly account for synchrony-driven oscillations generated by the interplay between recurrent network connections and synaptic delays. Yet, the QIF-FRE also suffer some limitations, mainly due to the assumptions made to obtain the low-dimensional description (Ott and Antonsen, 2008, 2009; Ott et al., 2011).
Specifically:

- The connectivity structure of the network of spiking neurons is assumed to be all-to-all. However, local cortical circuits have complex synaptic connectivity structures, see e.g. (Song et al., 2005);

- The shape of the distribution of heterogeneity is Lorentzian;
- The dynamics of the single neurons is purely deterministic.

On the connectivity structure, a certain progress has been recently made to account for more complex topologies in networks of theta neurons (Chandra et al., 2017) and phase oscillators (Restrepo and Ott, 2014). Additionally, mean-field approximations allow to rephrase a random structure of the synaptic connectivity into quenched heterogeneity of the synaptic weights (di Volo et al., 2014). This approach has been recently employed using the QIF-FRE to investigate the dynamics of random networks of spiking neurons (di Volo and Torcini, 2018).
Concerning the type of distribution assumed for the heterogeneity, the QIF-FRE were shown to qualitatively capture the dynamics of the system also for Gaussian distributed heterogeneity (Montbrió et al., 2015). However, further studies are needed to extend the Ott-Antonsen ansatz, and hence the QIF-FRE, to more general shapes of synaptic connectivity and forms of heterogeneity. In the following, we discuss the role of noise, which is probably the more compelling issue, as experimental evidence indicates that spike train statistics of single neurons is often stochastic.

The presence of noise. Strictly speaking, the Ott-Antonsen approach, on which the derivation of the QIF-FRE is based, holds only for deterministic networks of oscillators. Still, it can be expected to capture the qualitative dynamics of the systems as long as the noise is small, i.e. the oscillator's dynamics is mainly governed by the deterministic contribution (Vlasov et al., 2016). In networks of neurons, this regime is usually called *mean-driven* regime. In the mean-driven regime, neuronal spiking is substantially regular. The mean-driven regime is opposed to the *noise-driven* regime, where spiking (driven by noisy inputs) is highly irregular. Irregular spike trains are often observed both in *in vivo* and *in vitro* experiments. A vast literature exists on the dynamics of noise-driven excitable system, see (Lindner et al., 2004) for a review. A relevant example closely related to the topics of this dissertation are the stochastic oscillations that arise in networks of spiking neurons with recurrent delayed inhibition and strong noise (Brunel and Hakim, 1999, 2008; Brunel and Wang, 2003). In this regime, also known as sparsely synchronized state (SPS), the mean field oscillates with a period of about twice the delay, while the neurons fire stochastically, with a rate much lower than the collective oscillation. The origin of these oscillations can be intuitively understood

as follows: strong noise guarantees the irregular microscopic firing, while strong recurrent delayed inhibition produces windows where firing is less likely to occur. This, in turn, induces (after a delay) windows of lower inhibition, and therefore higher activity. The period of the collective oscillation is then about twice the delay. Macroscopically, the SPS is closely related to the QPS state reported in Chapter 3. In the QPS, the collective period is also about twice the delay (or exactly twice the delay for populations of identical neurons), and the collective oscillation can be understood intuitively exactly in the same way as the SPS. However, the single neurons dynamics in the two regimes is very different. In the QPS, neurons fire quasiperiodically, with an average firing rate higher than the mean-field; in the SPS, neurons fire irregularly at low rate. Intuitively speaking, the QPS appears to be the "mean-driven" correspondent regime of the SPS: it preserves the same macroscopic collective dynamics, yet with a strikingly different microscopic counterpart.
Some progress has been recently made to obtain low dimensional descriptions for populations of noisy oscillators. A strategy to tackle the problem has been developed in (Tyulkina et al., 2018; Goldobin et al., 2018), based on a perturbative approach on top of the Ott-Antonsen reduction. The approach is perturbative on the order of magnitudes of the noise, and could then in principle account for high noise intensities. As noise is increased, extra equations are added to the mean-field description. Could this approach bridge among states, and regimes, like the QPS and the SPS? Is it actually possible to describe with macroscopic laws highly stochastic regimes as the SPS? Could a mean-field model account both the *mean-driven* and the *noise-driven* regimes, and be sufficiently simple to be of practical utility? These are important questions which need to be further explored.

Modelling perspectives. A great challenge of theoretical neuroscience is to understand possible functional roles and underlying mechanisms of the wide range of rhythms that are constantly observed in electrical recordings of brain activity (Dipoppa and Gutkin, 2013; Deco et al., 2013; Cabral et al., 2011, 2014; Freyer et al., 2011; Daffertshofer et al., 2018). Are brain oscillations a mere epiphenomenon, or do they play a functional role? What are the neuronal mechanisms that generate such large-scale rhythms? Theoretical modelling should address and provide insights into these questions.
The spike-synchronization mechanism inherent in networks of spiking

neurons has been proposed to play a functional role in working memory (Dipoppa and Gutkin, 2013) and inter-areal brain communication (Fries, 2005). The firing rate equations employed in this dissertation, the QIF-FRE, readily account for a large variety of synchrony-driven dynamical regimes, ranging from Kuramoto-like synchronous states, to the non-trivial partially synchronous states reported in *Chapter* 3. Faithfully accounting for the spike-synchronization mechanism inherent in networks of spiking neurons, the QIF-FRE constitute an ideal candidate to investigate oscillations-driven brain functions. Specifically, mean-field descriptions as the QIF-FRE have been employed to model working memory computations (Schmidt et al., 2018), motor control (Byrne et al., 2017), and inter-areal neuronal communication (Dumont and Gutkin, 2018).

We expect the firing rate equations studied in this dissertation to serve as a valuable modeling tool for the neuroscience community, helping to unravel the fundamental principles that underlie the relation between oscillations and cognitive functions. cognitive functions.

APPENDIX A

Numerical simulations of Chapter 1

In this Appendix, we describe the models and methods used to perform the numerical simulations of networks of spiking neurons of *Chapter* 1. The model neurons used throughout Chapter 1 are the Wang-Buzsáki (WB) neuron (Wang and Buzsáki, 1996), and the quadratic integrate-and-fire (QIF) neuron (Ermentrout and Kopell, 1986; Izhikevich, 2007). In the following, we describe the equations of the model neurons employed.

A.1 Spiking neuron models

Wang-Buzsáki neuron. We numerically simulated a network of N all-to-all coupled WB neurons, where the dynamics of each neuron is described by the time evolution of its membrane potential:

$$C_m \dot{V}_i = -I_{\text{Na},i} - I_{\text{K},i} - I_{\text{L},i} - I_{\text{syn}} + I_{\text{app},i} + I_0.$$

The cell capacitance is $C_m = 1\ \mu\text{F/cm}^2$. The inputs I_{app} (in $\mu\text{A/cm}^2$) are distributed according to a Lorentzian distribution with half width σ and center $\bar{I}$. In numerical simulations these currents were selected deterministically to represent the Lorentzian distribution as $I_{\text{app},i} = \bar{I} + \sigma \tan(\pi/2(2i - N - 1)/(N + 1))$, for $i = 1, \ldots, N$. The constant input

$I_0 = 0.1601\ \mu\text{A/cm}^2$ sets the neuron at the SNIC bifurcation when $I_{app} = 0$. The leak current is

$$I_{\text{L},i} = g_{\text{L}} \left(V_i - E_{\text{L}}\right),$$

with $g_{\text{L}} = 0.1\ \text{mS/cm}^2$, so that the passive time constant $\tau_m = C_m/g_{\text{L}} = 10$ ms. The sodium current is

$$I_{\text{Na},i} = g_{\text{Na}} m_\infty^3 h \left(V_i - E_{\text{Na}}\right),$$

where $g_{\text{Na}} = 35\ \text{mS/cm}^2$, $E_{\text{Na}} = 55$ mV, $m_\infty = \alpha_m/\left(\alpha_m + \beta_m\right)$ with $\alpha_m\left(V_i\right) = -0.1\left(V_i + 35\right)/\left(\exp\left(-0.1\left(V_i + 35\right) - 1\right)\right)$, $\beta_m\left(V_i\right) = 4\exp\left(-\left(V_i + 60\right)/18\right)$. The inactivation variable h obeys the differential equation

$$\dot{h} = \phi\left(\alpha_h\left(1 - h\right) - \beta_h h\right),$$

with $\phi = 5$, $\alpha_h\left(V_i\right) = 0.07\exp\left(-\left(V_i + 58\right)/20\right)$ and $\beta_h\left(V_i\right) = 1/\left(\exp\left(-0.1\left(V_i + 28\right)\right) + 1\right)$. The potassium current follows

$$I_{\text{K},i} = g_{\text{K}} n^4 \left(V_i - E_{\text{K}}\right),$$

with $g_{\text{K}} = 9\ \text{mS/cm}^2$, $E_{\text{K}} = -90$ mV. The activation variable n obeys

$$\dot{n} = \phi\left(\alpha_n\left(1 - n\right) - \beta_n n\right),$$

where $\alpha_n\left(V_i\right) = -0.01\left(V_i + 34\right)/\left(\exp\left(-0.1\left(V_i + 34\right)\right) - 1\right)$ and $\beta_n\left(V_i\right) = 0.125\exp\left(-\left(V_i + 44\right)/80\right)$.

The synaptic current is $I_{\text{syn}} = k_{\{E,I\}} C_m S$, where S is the synaptic activation variable and $k_{\{E,I\}}$ is the excitatory or inhibitory coupling strength (expressed in mV). The factor C_m ensures that the effect of an incoming spike to the neuron is independent from its passive time constant. The neuron is defined to emit a spike when its membrane potential crosses 0 mV.

Quadratic integrate-and-fire neuron model. In the numerical simulations of *Chapter* 1 we considered a population of N QIF neurons, where each neuron is described by the differential equation:

$$\tau_m \dot{V}_j = V_j^2 + \eta_j + J\tau_m S(t) + I(t) \tag{A.1.1}$$

where $j = 1, \ldots, N$, η_j represents the quenched heterogeneity, S is the synaptic activity, J the coupling or synaptic strength, and $I(t)$ an

external time varying input. The membrane time constant τ_m is set to 10 ms. The inputs η_j are distributed according to a Lorentzian distribution with half width Δ and center Θ. In numerical simulations these currents were selected deterministically to represent the Lorentzian distribution as $\eta_j = \Theta + \Delta \tan(\pi/2(2j - N - 1)/(N + 1))$, for $j = 1, \ldots, N$. Eq. (A.1.1) is accompanied by the resetting condition:

$$\text{If} \quad V_j \geq V_{\text{th}} \quad \text{then} \quad -V_j \leftarrow V_j. \tag{A.1.2}$$

According to the theoretical analysis presented in section 1.5 of *Chapter* 1, the resetting rule is applied as follows: when $V_j \geq V_{\text{th}}$, the membrane voltage is held at V_j for a time interval τ_m/V_j. Then, a spike is emitted, and the voltage is reset and hold at $-V_j$ for another interval τ/V_j.

Numerical simulations

In the numerical simulations carried out in *Chapter* 1 we considered populations of $N = 1000$ WB neurons and $N = 1000$ QIF neurons. To integrate the evolution equations for both the WB and the QIF spiking model we used the Euler method. For WB neurons, we used a time step $dt = 0.001$ ms, while for QIF neurons we used $dt = 5 \times 10^{-5}$ ms. From all the simulations, an initial transient is discarded.
In Figs. 1.3, 1.4 and 1.5 the synaptic variable is defined as $S(t) = R(t - D)$, where $D = 3$ ms and the firing rate is defined according to

$$R(t) = \frac{1}{N\tau_s} \sum_{j=1}^{N} \sum_{k \backslash t_j^k < t} \int_{t-\tau_s}^{t} dt' \delta(t' - t_j^k), \tag{A.1.3}$$

with $\tau_s = 10^{-2}$ ms.
In Figs. 1.7 and 1.8 the synaptic variable follows the first order kinetics:

$$\tau_d \dot{S} = -S + R, \tag{A.1.4}$$

where R is defined according to Eq. (A.1.3) with $\tau_s = 10^{-2}$ ms.

References

Abbott, L. F. and van Vreeswijk, C. (1993). Asynchronous states in networks of pulse-coupled oscillators. *Phys. Rev. E*, 48:1483–1490.

Acebrón, J. A., Bonilla, L. L., Pérez-Vicente, C. J., Ritort, F., and Spigler, R. (2005). The Kuramoto model: A simple paradigm for synchronization phenomena. *Rev. Mod. Phys.*, 77:137–185.

Achuthan, S., Butera, R. J., and Canavier, C. C. (2011). Synaptic and intrinsic determinants of the phase resetting curve for weak coupling. *Journal of computational neuroscience*, 30(2):373–390.

Amari, S.-I. (1971). Characteristics of randomly connected threshold-element networks and network systems. *Proceedings of the IEEE*, 59(1):35–47.

Amari, S. I. (1972). Characteristics of Random Nets of Analog Neuron-Like Elements. *IEEE Transactions on Systems, Man and Cybernetics*, 2(5):643–657.

Angulo, M. C., Rossier, J., and Audinat, E. (1999). Postsynaptic glutamate receptors and integrative properties of fast-spiking interneurons in the rat neocortex. *Journal of Neurophysiology*, 82(3):1295–1302.

Anninos, P. A., Beek, B., Csermely, T. J., Harth, E. M., and Pertile, G. (1970). Dynamics of neural structure. *Journal of theoretical biology*, 26:121–148.

Ashwin, P., Coombes, S., and Nicks, R. (2016). Mathematical frameworks for oscillatory network dynamics in neuroscience. *The Journal of Mathematical Neuroscience*, 6(1):2.

Axmacher, N., Mormann, F., Fernández, G., Elger, C. E., and Fell, J. (2006). Memory formation by neuronal synchronization. *Brain research reviews*, 52(1):170–182.

Bartos, M., Vida, I., Frotscher, M., Geiger, J. R. P., and Jonas, P. (2001). Rapid signaling at inhibitory synapses in a dentate gyrus interneuron network. *The Journal of neuroscience : the official journal of the Society for Neuroscience*, 21(8):2687–2698.

Bartos, M., Vida, I., and Jonas, P. (2007). Synaptic mechanisms of synchronized gamma oscillations in inhibitory interneuron networks. *Nature reviews neuroscience*, 8(1):45–56.

Battaglia, D., Brunel, N., and Hansel, D. (2007). Temporal decorrelation of collective oscillations in neural networks with local inhibition and long-range excitation. *Phys. Rev. Lett.*, 99:238106.

Ben-Yishai, R., Bar-Or, R. L., and Sompolinsky, H. (1995). Theory of orientation tuning in visual cortex. *Proc. Nat. Acad. Sci.*, 92(9):3844–3848.

Berger, H. (1929). Über das elektrenkephalogramm des menschen. *Archiv für psychiatrie und nervenkrankheiten*, 87(1):527–570.

Beurle, R. L. (1956). Properties of a mass of cells capable of regenerating pulses. *Philosophical Transactions of the Royal Society of London. Series B, Biological Sciences*, 240(669):55–94.

Breakspear, M., Heitmann, S., and Daffertshofer, A. (2010). Generative models of cortical oscillations: neurobiological implications of the kuramoto model. *Frontiers in human neuroscience*, 4:190.

Bressloff, P. C. and Kilpatrick, Z. P. (2008). Nonlocal ginzburg-landau equation for cortical pattern formation. *Phys. Rev. E*, 78:041916.

Brunel, N. and Hakim, V. (1999). Fast global oscillations in networks of integrate-and-fire neurons with low firing rates. *Neural Comput.*, 11(7):1621–1671.

Brunel, N. and Hakim, V. (2008). Sparsely synchronized neuronal oscillations. *Chaos: An Interdisciplinary Journal of Nonlinear Science*, 18(1):015113.

Brunel, N. and Hansel, D. (2006). How noise affects the synchronization properties of recurrent networks of inhibitory neurons. *Neural Comput.*, 18(5):1066–1110.

Brunel, N. and Wang, X.-J. (2003). What determines the frequency of fast network oscillations with irregular neural discharges? i. synaptic dynamics and excitation-inhibition balance. *Journal of neurophysiology*, 90(1):415–430.

Buzsáki, G. (2006). *Rhythms of the Brain*. Oxford University Press.

Buzsáki, G. and Draguhn, A. (2004). Neuronal oscillations in cortical networks. *Science*, 304(5679):1926–1929.

Buzsáki, G. and Wang, X.-J. (2012). Mechanisms of gamma oscillations. *Annual Review of Neuroscience*, 35:203–225.

Byrne, Á., Brookes, M. J., and Coombes, S. (2017). A mean field model for movement induced changes in the beta rhythm. *Journal of computational neuroscience*, 43(2):143–158.

Cabral, J., Hugues, E., Sporns, O., and Deco, G. (2011). Role of local network oscillations in resting-state functional connectivity. *Neuroimage*, 57(1):130–139.

Cabral, J., Luckhoo, H., Woolrich, M., Joensson, M., Mohseni, H., Baker, A., Kringelbach, M. L., and Deco, G. (2014). Exploring mechanisms of spontaneous functional connectivity in meg: how delayed network interactions lead to structured amplitude envelopes of band-pass filtered oscillations. *Neuroimage*, 90:423–435.

Chandra, S., Hathcock, D., Crain, K., Antonsen, T. M., Girvan, M., and Ott, E. (2017). Modeling the network dynamics of pulse-coupled neurons. *Chaos: An Interdisciplinary Journal of Nonlinear Science*, 27(3):033102.

Choi, M. Y., Kim, H. J., Kim, D., and Hong, H. (2000). Synchronization in a system of globally coupled oscillators with time delay. *Phys. Rev. E*, 61:371–381.

Clusella, P. and Politi, A. (2018). From phase to amplitude oscillators. *arXiv preprint arXiv:1810.01281*.

Clusella, P., Politi, A., and Rosenblum, M. (2016). A minimal model of self-consistent partial synchrony. *New Journal of Physics*, 18(9):093037.

Coombes, S. (2005). Waves, bumps, and patterns in neural field theories. *Biol. Cybern.*, 93(2):91–108.

Coombes, S., beim Graben, P., Potthast, R., and Wright, J. (2014). *Neural fields: theory and applications*. Springer.

Coombes, S. and Byrne, Á. (2019). Next generation neural mass models. In Corinto, F. and Torcini, A., editors, *Nonlinear Dynamics in Computational Neuroscience*, pages 1–16. Springer International Publishing, Cham.

Coombes, S. and Laing, C. (2009). Delays in activity-based neural networks. *Philosophical Transactions of the Royal Society of London A: Mathematical, Physical and Engineering Sciences*, 367(1891):1117–1129.

Cowan, J. (2014). A personal account of the development of the field theory of large-scale brain activity from 1945 onward. In *Neural fields*, pages 47–96. Springer.

Curry, J. H. and Yorke, J. A. (1978). A transition from hopf bifurcation to chaos: computer experiments with maps on r^2. In *The structure of attractors in dynamical systems*, number 668 in Springer Notes in Mathematics, pages 48–56. Springer-Verlag, Berlin.

Daffertshofer, A., Ton, R., Pietras, B., Kringelbach, M. L., and Deco, G. (2018). Scale-freeness or partial synchronization in neural mass phase oscillator networks: Pick one of two? *NeuroImage*.

Dayan, P. and Abbott, L. F. (2001). *Theoretical neuroscience*. Cambridge, MA: MIT Press.

de Monte, S. and d'Ovidio, F. (2002). Dynamics of order parameters for globally coupled oscillators. *Europhys. Lett.*, 58(1):21.

Deco, G., Ponce-Alvarez, A., Mantini, D., Romani, G. L., Hagmann, P., and Corbetta, M. (2013). Resting-state functional connectivity emerges from structurally and dynamically shaped slow linear fluctuations. *Journal of Neuroscience*, 33(27):11239–11252.

Destexhe, A., Mainen, Z. F., and Sejnowski, T. J. (1998). Kinetic models of synaptic transmission. *Methods in neuronal modeling*, 2:1–25.

Devalle, F., Roxin, A., and Montbrió, E. (2017). Firing rate equations require a spike synchrony mechanism to correctly describe fast oscillations in inhibitory networks. *PLOS Computational Biology*, 13(12):1–21.

di Volo, M., Burioni, R., Casartelli, M., Livi, R., and Vezzani, A. (2014). Heterogeneous mean field for neural networks with short-term plasticity. *Physical Review E*, 90(2):022811.

di Volo, M. and Torcini, A. (2018). Transition from asynchronous to oscillatory dynamics in balanced spiking networks with instantaneous synapses. *Physical review letters*, 121(12):128301.

Dijkstra, K., van Gils, S. A., Janssens, S., Kuznetsov, Y. A., and Visser, S. (2015). Pitchfork–hopf bifurcations in 1d neural field models with transmission delays. *Physica D: Nonlinear Phenomena*, 297:88–101.

Dipoppa, M. and Gutkin, B. S. (2013). Flexible frequency control of cortical oscillations enables computations required for working memory. *Proceedings of the National Academy of Sciences*, 110(31):12828–12833.

Dumont, G., Ermentrout, G. B., and Gutkin, B. (2017). Macroscopic phase-resetting curves for spiking neural networks. *Phys. Rev. E*, 96:042311.

Dumont, G. and Gutkin, B. (2018). Macroscopic phase resetting-curves determine oscillatory coherence and signal transfer in inter-coupled neural circuits. *arXiv preprint arXiv:1812.03455*.

Dumont, G., Henry, J., and Tarniceriu, C. O. (2014). A density model for a population of theta neurons. *The Journal of Mathematical Neuroscience*, 4(1):2.

Durstewitz, D., Seamans, J. K., and Sejnowski, T. J. (2000). Neurocomputational models of working memory. *Nature neuroscience*, 3(11s):1184.

Earl, M. G. and Strogatz, S. H. (2003). Synchronization in oscillator networks with delayed coupling: A stability criterion. *Phys. Rev. E*, 67:036204.

Engel, A. K. and Singer, W. (2001). Temporal binding and the neural correlates of sensory awareness. *Trends in cognitive sciences*, 5(1):16–25.

Ermentrout, B. (1994). Reduction of conductance-based models with slow synapses to neural nets. *Neural Comput.*, 6(4):679–695.

Ermentrout, B. and Kopell, N. (1986). Parabolic bursting in an excitable system coupled with a slow oscillation. *SIAM J. Appl. Math.*, 46:233–253.

Ermentrout, G. B., Glass, L., and Oldeman, B. E. (2012). The shape of phase-resetting curves in oscillators with a saddle node on an invariant circle bifurcation. *Neural computation*, 24(12):3111–3125.

Ermentrout, G. B. and Terman, D. H. (2010). *Mathematical foundations of neuroscience*, volume 64. Springer.

Ernst, U., Pawelzik, K., and Geisel, T. (1995). Synchronization induced by temporal delays in pulse-coupled oscillators. *Phys. Rev. Lett.*, 74(9):1570.

Ernst, U., Pawelzik, K., and Geisel, T. (1998). Delay-induced multistable synchronization of biological oscillators. *Phys. Rev. E*, 57(2):2150.

Esnaola-Acebes, J. M., Roxin, A., Avitabile, D., and Montbrió, E. (2017). Synchrony-induced modes of oscillation of a neural field model. *Phys. Rev. E*, 96:052407.

Farmer, J. D. (1982). Chaotic attractors of an infinite-dimensional dynamical system. *Physica D*, 4:366–393.

Faye, G. and Faugeras, O. (2010). Some theoretical and numerical results for delayed neural field equations. *Physica D: Nonlinear Phenomena*, 239(9):561 – 578.

Faye, G. and Touboul, J. (2014). Pulsatile localized dynamics in delayed neural field equations in arbitrary dimension. *SIAM Journal on Applied Mathematics*, 74(5):1657–1690.

Fell, J. and Axmacher, N. (2011). The role of phase synchronization in memory processes. *Nature Reviews Neuroscience*, 12(2):105–118.

Fell, J., Klaver, P., Lehnertz, K., Grunwald, T., Schaller, C., Elger, C. E., and Fernández, G. (2001). Human memory formation is accompanied by rhinal–hippocampal coupling and decoupling. *Nature neuroscience*, 4(12):1259.

Freeman, W. J. (1975). *Mass action in the nervous system*. Academic Press, New York.

Freyer, F., Roberts, J. A., Becker, R., Robinson, P. A., Ritter, P., and Breakspear, M. (2011). Biophysical mechanisms of multistability in resting-state cortical rhythms. *Journal of Neuroscience*, 31(17):6353–6361.

Fries, P. (2005). A mechanism for cognitive dynamics: neuronal communication through neuronal coherence. *Trends in cognitive sciences*, 9(10):474–480.

Fries, P., Reynolds, J. H., Rorie, A. E., and Desimone, R. (2001). Modulation of oscillatory neuronal synchronization by selective visual attention. *Science*, 291(5508):1560–1563.

Gerstner, W. (1995). Time structure of the activity in neural network models. *Phys. Rev. E*, 51:738–758.

Gerstner, W. (2000). Population dynamics of spiking neurons: fast transients, asynchronous states, and locking. *Neural Comput.*, 12(1):43–89.

Gerstner, W. and Kistler, W. M. (2002). *Spiking neuron models: Single neurons, populations, plasticity*. Cambridge university press.

Gerstner, W. and van Hemmen, J. L. (1992). Associative memory in a network of 'spiking' neurons. *Network: Computation in Neural Systems*, 3(2):139–164.

Gerstner, W. and van Hemmen, J. L. (1993). Coherence and incoherence in a globally coupled ensemble of pulse-emitting units. *Physical review letters*, 71(3):312.

Gerstner, W., Van Hemmen, J. L., and Cowan, J. D. (1996). What matters in neuronal locking? *Neural computation*, 8(8):1653–1676.

Goldobin, D. S., Tyulkina, I. V., Klimenko, L. S., and Pikovsky, A. (2018). Collective mode reductions for populations of coupled noisy oscillators. *Chaos: An Interdisciplinary Journal of Nonlinear Science*, 28(10):101101.

Golomb, D., Donner, K., Shacham, L., Shlosberg, D., Amitai, Y., and Hansel, D. (2007). Mechanisms of firing patterns in fast-spiking cortical interneurons. *PLoS Computational Biology*, 3(8):e156.

Gray, C. M., König, P., Engel, A. K., and Singer, W. (1989). Oscillatory responses in cat visual cortex exhibit inter-columnar synchronization which reflects global stimulus properties. *Nature*, 338(6213):334.

Griffith, J. S. (1963). On the Stability of Brain-Like Structures. *Biophysical Journal*, 3(4):299–308.

Hansel, D. and Mato, G. (2003). Asynchronous states and the emergence of synchrony in large networks of interacting excitatory and inhibitory neurons. *Neural computation*, 15(1):1–56.

Hansel, D., Mato, G., and Meunier, C. (1993). Clustering and slow switching in globally coupled phase oscillators. *Physical Review E*, 48(5):3470.

Hansel, D., Mato, G., and Meunier, C. (1995). Synchrony in excitatory neural networks. *Neural Comput.*, 7:307–337.

Hodgkin, A. L. and Huxley, A. F. (1952). A quantitative description of membrane current and its application to conduction and excitation in nerve. *J Physiol.*, 117(4):500–544.

Hopfield, J. J. (1984). Neurons with graded response have collective computational properties like those of two-state neurons. *Proceedings of the national academy of sciences*, 81(10):3088–3092.

Hubel, D. H. and Wiesel, T. N. (1963). Receptive fields of cells in striate cortex of very young, visually inexperienced kittens. *J. Neurophysiol.*, 26(6):994–1002.

Hutt, A. and Atay, F. M. (2006). Effects of distributed transmission speeds on propagating activity in neural populations. *Phys. Rev. E*, 73:021906.

Izhikevich, E. M. (2007). *Dynamical Systems in Neuroscience*. The MIT Press, Cambridge, Massachusetts.

Jansen, B. H. and Rit, V. G. (1995). Electroencephalogram and visual evoked potential generation in a mathematical model of coupled cortical columns. *Biological cybernetics*, 73(4):357–366.

Kaplan, J. L. and Yorke, J. A. (1979). Chaotic behavior of multidimensional difference equations. In Walter, H. O. and Peitgen, H.-O., editors, *Functional Differential Equations and Approximation of Fixed Points*, volume 730 of *Lecture Notes in Mathematics*, pages 204–227. Springer-Verlag, Berlin.

Keeley, S., Fenton, A. A., and Rinzel, J. (2017). Modeling fast and slow gamma oscillations with interneurons of different subtype. *Journal of Neurophysiology*, 117(3):950–965. PMID: 27927782.

Kilpatrick, Z. P. (2015). Wilson-cowan model. *Encyclopedia of Computational Neuroscience*, pages 3159–3163.

Kilpatrick, Z. P. and Ermentrout, B. (2011). Sparse gamma rhythms arising through clustering in adapting neuronal networks. *PLoS computational biology*, 7(11):e1002281.

Kim, C., Egert, U., and Kumar, A. (2018). Dynamics of multiple interacting excitatory and inhibitory populations with delays. *bioRxiv*, page 360479.

Kim, S., Park, S. H., and Ryu, C. S. (1997). Multistability in coupled oscillator systems with time delay. *Phys. Rev. Lett.*, 79:2911–2914.

Knight, B. W., Manin, D., and Sirovich, L. (1996). Dynamical models of interacting neuron populations in visual cortex. *Robot Cybern*, 54:4–8.

Knight, B. W., Omurtag, A., and Sirovich, L. (2000). The approach of a neuron population firing rate to a new equilibrium: an exact theoretical result. *Neural computation*, 12(5):1045–1055.

Kori, H. (2003). Slow switching and broken cluster state in a population of neuronal oscillators. *Int. J. Mod. Phys. B*, 17:4238–4241.

Kori, H. and Kuramoto, Y. (2001). Slow switching in globally coupled oscillators: robustness and occurrence through delayed coupling. *Physical Review E*, 63(4):046214.

Kuramoto, Y. (1975). Self-entrainment of a population of coupled nonlinear oscillators. In Araki, H., editor, *International Symposium on Mathematical Problems in Theoretical Physics*, volume 39 of *Lecture Notes in Physics*, pages 420–422. Springer, Berlin.

Kuramoto, Y. (1984). *Chemical Oscillations, Waves, and Turbulence*. Springer-Verlag, Berlin.

La Camera, G., Rauch, A., Thurbon, D., Luscher, H.-R., Senn, W., and Fusi, S. (2006). Multiple time scales of temporal response in pyramidal and fast spiking cortical neurons. *Journal of neurophysiology*, 96(6):3448–3464.

Laing, C. R. (2014). Derivation of a neural field model from a network of theta neurons. *Phys. Rev. E*, 90:010901.

Laing, C. R. (2015). Exact neural fields incorporating gap junctions. *SIAM Journal on Applied Dynamical Systems*, 14(4):1899–1929.

Laing, C. R. (2018). The dynamics of networks of identical theta neurons. *The Journal of Mathematical Neuroscience*, 8(1):4.

Lapique, L. (1907). Recherches quantitatives sur l'excitation electrique des nerfs traitee comme une polarization. *Journal of Physiology and Pathololgy*, 9:620–635.

Latham, P., Richmond, B., Nelson, P., and Nirenberg, S. (2000). Intrinsic dynamics in neuronal networks. i. theory. *Journal of Neurophysiology*, 83(2):808–827.

Ledoux, E. and Brunel, N. (2011). Dynamics of networks of excitatory and inhibitory neurons in response to time-dependent inputs. *Frontiers in Computational Neuroscience*, 5:25.

Lee, W. S., Ott, E., and Antonsen, T. M. (2009). Large coupled oscillator systems with heterogeneous interaction delays. *Phys. Rev. Lett.*, 103(4):044101.

Lindner, B., Garcıa-Ojalvo, J., Neiman, A., and Schimansky-Geier, L. (2004). Effects of noise in excitable systems. *Physics reports*, 392(6):321–424.

Luke, T. B., Barreto, E., and So, P. (2013). Complete classification of the macroscopic behavior of a heterogeneous network of theta neurons. *Neural Comput.*, 25(12):3207–3234.

MacDonald, N. (1989). *Biological Delay Systems: Linear Stability Theory*, volume 8. Cambridge University Press.

Mancilla, J. G., Lewis, T. J., Pinto, D. J., Rinzel, J., and Connors, B. W. (2007). Synchronization of electrically coupled pairs of inhibitory interneurons in neocortex. *Journal of Neuroscience*, 27(8):2058–2073.

Markram, H., Lübke, J., Frotscher, M., Roth, A., and Sakmann, B. (1997). Physiology and anatomy of synaptic connections between thick tufted pyramidal neurones in the developing rat neocortex. *The Journal of physiology*, 500(2):409–440.

Mattia, M. and Del Giudice, P. (2002). Population dynamics of interacting spiking neurons. *Physical Review E*, 66(5):051917.

Mongillo, G., Barak, O., and Tsodyks, M. (2008). Synaptic theory of working memory. *Science*, 319(5869):1543–1546.

Montbrió, E. and Pazó, D. (2018). Kuramoto model for excitation-inhibition-based oscillations. *Phys. Rev. Lett.*, 120:244101.

Montbrió, E., Pazó, D., and Roxin, A. (2015). Macroscopic description for networks of spiking neurons. *Phys. Rev. X*, 5:021028.

Montbrió, E., Pazó, D., and Schmidt, J. (2006). Time delay in the Kuramoto model with bimodal frequency distribution. *Phys. Rev. E*, 74(5):056201.

Moreno-Bote, R., Rinzel, J., and Rubin, N. (2007). Noise-induced alternations in an attractor network model of perceptual bistability. *J. Neurophysiol.*, 98(3):1125–1139.

Morris, C. and Lecar, H. (1981). Voltage oscillations in the barnacle giant muscle fiber. *Biophysical Journal*, 35(1):193–213.

Nakagawa, N. and Kuramoto, Y. (1995). Anomalous lyapunov spectrum in globally coupled oscillators. *Physica D*, 80(3):307–316.

Niebur, E., Schuster, H. G., and Kammen, D. M. (1991). Collective frequencies and metastability in networks of limit-cycle oscillators with time delay. *Phys. Rev. Lett.*, 67:2753.

Nischwitz, A. and Glünder, H. (1995). Local lateral inhibition: a key to spike synchronization? *Biological Cybernetics*, 73(5):389–400.

Nykamp, D. Q. and Tranchina, D. (2000). A population density approach that facilitates large-scale modeling of neural networks: Analysis and an application to orientation tuning. *Journal of computational neuroscience*, 8(1):19–50.

Okuda, K. (1993). Variety and generality of clustering in globally coupled oscillators. *Physica D: Nonlinear Phenomena*, 63(3-4):424–436.

Olmi, S., Politi, A., and Torcini, A. (2014). Linear stability in networks of pulse-coupled neurons. *Frontiers in Computational Neuroscience*, 8:8.

Ostojic, S. and Brunel, N. (2011). From spiking neuron models to linear-nonlinear models. *PLoS Comput. Biol.*, 7(1):e1001056.

Ott, E. and Antonsen, T. M. (2008). Low dimensional behavior of large systems of globally coupled oscillators. *Chaos*, 18(3):037113.

Ott, E. and Antonsen, T. M. (2009). Long time evolution of phase oscillator systems. *Chaos*, 19(2):023117.

Ott, E., Hunt, B. R., and Antonsen, T. M. (2011). Comment on "long time evolution of phase oscillators systems". *Chaos*, 21:025112.

Palmigiano, A., Geisel, T., Wolf, F., and Battaglia, D. (2017). Flexible information routing by transient synchrony. *Nature neuroscience*, 20(7):1014.

Pazó, D. and Montbrió, E. (2014). Low-dimensional dynamics of populations of pulse-coupled oscillators. *Phys. Rev. X*, 4:011009.

Pazó, D. and Montbrió, E. (2016). From quasiperiodic partial synchronization to collective chaos in populations of inhibitory neurons with delay. *Phys. Rev. Lett.*, 116:238101.

Petkoski, S., Spiegler, A., Proix, T., Aram, P., Temprado, J.-J., and Jirsa, V. K. (2016). Heterogeneity of time delays determines synchronization of coupled oscillators. *Physical Review E*, 94(1):012209.

Pietras, B. and Daffertshofer, A. (2016). Ott-antonsen attractiveness for parameter-dependent oscillatory systems. *Chaos*, 26(10):103101.

Pietras, B., Devalle, F., Daffertshofer, A., Roxin, A., and Montbrió, E. (In preparation, 2019). Neuronal firing rate models with electrical and chemical synapses.

Pikovsky, A. and Rosenblum, M. (2011). Dynamics of heterogeneous oscillator ensembles in terms of collective variables. *Physica D*, 240(9-10):872 – 881.

Pikovsky, A. S., Rosenblum, M. G., and Kurths, J. (2001). *Synchronization, a Universal Concept in Nonlinear Sciences*. Cambridge University Press, Cambridge.

Politi, A. and Rosenblum, M. (2015). Equivalence of phase-oscillator and integrate-and-fire models. *Phys. Rev. E*, 91:042916.

Press, W. H., Teukolsky, S. A., Vetterling, W. T., and Flannery, B. P. (1992). *Numerical Recipes in FORTRAN (2nd Ed.): The Art of Scientific Computing*. Cambridge University Press, New York, NY, USA.

Rabinovich, M., Huerta, R., and Laurent, G. (2008a). Transient dynamics for neural processing. *Science*, pages 48–50.

Rabinovich, M. I., Huerta, R., Varona, P., and Afraimovich, V. S. (2008b). Transient cognitive dynamics, metastability, and decision making. *PLoS computational biology*, 4(5):e1000072.

Rankin, J., Meso, A. I., Masson, G. S., Faugeras, O., and Kornprobst, P. (2014). Bifurcation study of a neural field competition model with an application to perceptual switching in motion integration. *Journal of Computational Neuroscience*, 36(2):193–213.

Rankin, J., Sussman, E., and Rinzel, J. (2015). Neuromechanistic model of auditory bistability. *PLoS computational biology*, 11(11):e1004555.

Ratas, I. and Pyragas, K. (2016). Macroscopic self-oscillations and aging transition in a network of synaptically coupled quadratic integrate-and-fire neurons. *Phys. Rev. E*, 94:032215.

Ratas, I. and Pyragas, K. (2017). Symmetry breaking in two interacting populations of quadratic integrate-and-fire neurons. *Phys. Rev. E*, 96:042212.

Reddy, D. V. R., Sen, A., and Johston, G. (1999). Time delay effects on coupled limit cycle oscillators at hopf bifurcation. *Physica D*, 129:15–34.

Restrepo, J. G. and Ott, E. (2014). Mean-field theory of assortative networks of phase oscillators. *EPL (Europhysics Letters)*, 107(6):60006.

Rinzel, J. and Ermentrout, G. B. (1989). Analysis of neural excitability and oscillations, methods in neuronal modeling: From synapses to networks.

Robinson, P. A., Rennie, C. J., and Wright, J. J. (1997). Propagation and stability of waves of electrical activity in the cerebral cortex. *Physical Review E*, 56(1):826.

Rohenkohl, G., Bosman, C. A., and Fries, P. (2018). Gamma Synchronization between V1 and V4 Improves Behavioral Performance. *Neuron*, 100(4):953–963.e3.

Roth, A. and van Rossum, M. C. (2009). Modeling synapses. *Computational modeling methods for neuroscientists*, 6:139–160.

Roulet, J. and Mindlin, G. B. (2016). Average activity of excitatory and inhibitory neural populations. *Chaos: An Interdisciplinary Journal of Nonlinear Science*, 26(9):093104.

Roxin, A., Brunel, N., and Hansel, D. (2005). Role of delays in shaping spatiotemporal dynamics of neuronal activity in large networks. *Phys. Rev. Lett.*, 94(23):238103.

Roxin, A. and Montbrió, E. (2011). How effective delays shape oscillatory dynamics in neuronal networks. *Physica D*, 240(3):323–345.

Schaffer, E. S., Ostojic, S., and Abbott, L. (2013). A complex-valued firing-rate model that approximates the dynamics of spiking networks. *PLoS Comput. Biol.*, 9(10):e1003301.

Schmidt, H., Avitabile, D., Montbrió, E., and Roxin, A. (2018). Network mechanisms underlying the role of oscillations in cognitive tasks. *bioRxiv*, page 271973.

Schuster, H. and Wagner, P. (1990). A model for neuronal oscillations in the visual cortex. *Biological cybernetics*, 64(1):77–82.

Schuster, H. G. and Wagner, P. (1989). Mutual entrainment of two limit cycle oscillators with time delayed coupling. *Prog. Theor. Phys.*, 81:939–945.

Schwalger, T., Deger, M., and Gerstner, W. (2017). Towards a theory of cortical columns: From spiking neurons to interacting neural populations of finite size. *PLOS Computational Biology*, 13(4):1–63.

Senk, J., Korvasová, K., Schuecker, J., Hagen, E., Tetzlaff, T., Diesmann, M., and Helias, M. (2018). Conditions for traveling waves in spiking neural networks. *arXiv preprint arXiv:1801.06046*.

So, P., Luke, T. B., and Barreto, E. (2014). Networks of theta neurons with time-varying excitability: Macroscopic chaos, multistability, and final-state uncertainty. *Physica D*, 267(0):16–26.

Song, S., Sjöström, P. J., Reigl, M., Nelson, S., and Chklovskii, D. B. (2005). Highly nonrandom features of synaptic connectivity in local cortical circuits. *PLoS biology*, 3(3):e68.

Strogatz, S. H. (1994). Norbert wiener's brain waves. In *Frontiers in mathematical biology*, pages 122–138. Springer.

Strogatz, S. H. (2000). From Kuramoto to Crawford: exploring the onset of synchronization in populations of coupled oscillators. *Physica D*, 143:1–20.

Strogatz, S. H. (2003). *Sync: The emerging science of spontaneous order*. Hyperion Press, New York.

Tateno, T., Harsch, A., and Robinson, H. (2004). Threshold firing frequency–current relationships of neurons in rat somatosensory cortex: type 1 and type 2 dynamics. *Journal of neurophysiology*, 92(4):2283–2294.

Tateno, T. and Robinson, H. (2007). Phase resetting curves and oscillatory stability in interneurons of rat somatosensory cortex. *Biophysical Journal*, 92(2):683–695.

Tiesinga, P. and José, J. V. (2000). Robust gamma oscillations in networks of inhibitory hippocampal interneurons. *Network: Computation in Neural Systems*, 11(1):1–23.

Tikidji-Hamburyan, R. A., Martínez, J. J., White, J. A., and Canavier, C. C. (2015). Resonant interneurons can increase robustness of gamma oscillations. *Journal of Neuroscience*, 35(47):15682–15695.

Ton, R., Deco, G., and Daffertshofer, A. (2014). Structure-function discrepancy: inhomogeneity and delays in synchronized neural networks. *PLoS computational biology*, 10(7):e1003736.

Touboul, J. (2012). Mean-field equations for stochastic firing-rate neural fields with delays: Derivation and noise-induced transitions. *Physica D: Nonlinear Phenomena*, 241(15):1223 – 1244.

Traub, R., Whittington, M., Colling, S., Buzsaki, G., and Jefferys, J. (1996). Analysis of gamma rhythms in the rat hippocampus in vitro and in vivo. *The Journal of physiology*, 493(2):471–484.

Tyulkina, I. V., Goldobin, D. S., Klimenko, L. S., and Pikovsky, A. (2018). Dynamics of noisy oscillator populations beyond the ott-antonsen ansatz. *Phys. Rev. Lett.*, 120:264101.

Van Vreeswijk, C., Abbott, L., and Ermentrout, G. B. (1994). When inhibition not excitation synchronizes neural firing. *Journal of computational neuroscience*, 1(4):313–321.

Veltz, R. (2013). Interplay between synaptic delays and propagation delays in neural field equations. *SIAM Journal on Applied Dynamical Systems*, 12(3):1566–1612.

Veltz, R. and Faugeras, O. (2013). A center manifold result for delayed neural fields equations. *SIAM Journal on Mathematical Analysis*, 45(3):1527–1562.

Venkov, N., Coombes, S., and Matthews, P. (2007). Dynamic instabilities in scalar neural field equations with space-dependent delays. *Physica D: Nonlinear Phenomena*, 232(1):1 – 15.

Villegas, P., Moretti, P., and Munoz, M. A. (2014). Frustrated hierarchical synchronization and emergent complexity in the human connectome network. *Scientific reports*, 4:5990.

Vlasov, V., Rosenblum, M., and Pikovsky, A. (2016). Dynamics of weakly inhomogeneous oscillator populations: perturbation theory on top of watanabe–strogatz integrability. *Journal of Physics A: Mathematical and Theoretical*, 49(31):31LT02.

Von der Malsburg, C. and Schneider, W. (1986). A neural cocktail-party processor. *Biological cybernetics*, 54(1):29–40.

Wang, X.-J. (2010). Neurophysiological and computational principles of cortical rhythms in cognition. *Physiological reviews*, 90(3):1195–1268.

Wang, X.-J. and Buzsáki, G. (1996). Gamma oscillation by synaptic inhibition in a hippocampal interneuronal network model. *The journal of Neuroscience*, 16(20):6402–6413.

Wang, X.-J. and Rinzel, J. (1992). Alternating and synchronous rhythms in reciprocally inhibitory model neurons. *Neural computation*, 4(1):84–97.

Wang, X.-J. and Rinzel, J. (1993). Spindle rhythmicity in the reticularis thalami nucleus: synchronization among mutually inhibitory neurons. *Neuroscience*, 53(4):899–904.

Watanabe, S. and Strogatz, S. H. (1994). Constant of motion for superconducting Josephson arrays. *Physica D*, 74:197–253.

White, J. A., Chow, C. C., Rit, J., Soto-Treviño, C., and Kopell, N. (1998). Synchronization and oscillatory dynamics in heterogeneous, mutually inhibited neurons. *Journal of computational neuroscience*, 5(1):5–16.

Whittington, M., Traub, R., Kopell, N., Ermentrout, B., and Buhl, E. (2000). Inhibition-based rhythms: experimental and mathematical observations on network dynamics. *Int. Journal of Psychophysiol.*, 38(3):315 – 336.

Whittington, M. A., Traub, R. D., and Jefferys, J. G. (1995). Synchronized oscillations in interneuron networks driven by metabotropic glutamate receptor activation. *Nature*, 373:612–615.

Wiener, N. (1961). *Cybernetics or Control and Communication in the Animal and the Machine*, volume 25. MIT press.

Wilson, H. R. and Cowan, J. D. (1972). Excitatory and inhibitory interactions in localized populations of model neurons. *Biophys. J.*, 12(1):1–24.

Wilson, H. R. and Cowan, J. D. (1973). A mathematical theory of the functional dynamics of cortical and thalamic nervous tissue. *Kybernetik*, 13(2):55–80.

Wilson, M. T., Robinson, P. A., O'Neill, B., and Steyn-Ross, D. A. (2012). Complementarity of spike- and rate-based dynamics of neural systems. *PLOS Computational Biology*, 8(6):1–1.

Winfree, A. T. (1967). Biological rhythms and the behavior of populations of coupled oscillators. *J. Theor. Biol.*, 16:15–42.

Wong, K.-F. and Wang, X.-J. (2006). A recurrent network mechanism of time integration in perceptual decisions. *J. Neurosci.*, 26(4):1314–1328.

Yeung, M. K. S. and Strogatz, S. H. (1999). Time delay in the kuramoto model of coupled oscillators. *Phys. Rev. Lett.*, 82(3):648–651.

Zhang, K. (1996). Representation of spatial orientation by the intrinsic dynamics of the head-direction cell ensemble: a theory. *J. Neurosci.*, 16(6):2112–2126.